UNIVERSITY OF CALIFORNIA SAN DIEGO

Novel Studies in Acute Myeloid Leukemia

A dissertation submitted in partial satisfaction of the
requirements for the degree Doctor of Philosophy

in

Biology

by

Daniel Thomas Johnson

Committee in charge:

Professor Dong-Er Zhang, Chair
Professor Michael David
Professor Jens Lykke-Andersen
Professor Robert Signer
Professor Liangfang Zhang

2021

The Dissertation of Daniel Thomas Johnson is approved, and it is acceptable in quality and form for publication on microfilm and electronically.

University of California San Diego

2021

DEDICATION

This work is dedicated to my wife and children. For loving and supporting me through all the late nights, the vacations missed, and all other manner of nonsense that comes with Grad-school.

EPIGRAPH

“They say the secret of success is being at the right place at the right time, but since you never know when the right time is going to be, I figure the trick is to find the right place and just hang around.”

- Calvin/Bill Watterson

TABLE OF CONTENTS

LIST OF FIGURES

LIST OF TABLES

ACKNOWLEDGEMENTS

First and foremost, I would like to thank Dr. Dong-Er Zhang for her support and mentorship. I am also grateful for every member of the Zhang lab that I had the joy of working with over the years. I would also like to thank my committee members for their time, scientific insight, and advice. Dr. Michael David, Dr. Liangfang Zhang, Dr. Jens Lykke-Andersen, and Dr. Robert Signer, I am truly grateful.

Chapter 1 is a modified version of work that has been accepted for publication in *Leukemia* (Springer Nature Group) and authored by Daniel T. Johnson, Jiarong Zhou, Ashley V. Kroll, Ronnie H. Fang, Ming Yan, Crystal Xiao, Xiufen Chen, Justin Kline, Liangfang Zhang, and Dong-Er Zhang. The dissertation author is the primary investigator and writer of this manuscript. These studies were made possible because of a phenomenal collaboration with Dr. Liangfang Zhang's group at UCSD's Department of NanoEngineering.

Chapter 2 is a modified version work that was published in *Experimental Hematology & Oncology* (BioMed Central, Springer Nature Group) and authored by Daniel T. Johnson, Amanda G. Davis, Jie-Hua Zhou, Edward D. Ball, and Dong-Er Zhang. The dissertation author is the primary investigator and writer of this manuscript. I want to thank Drs. Zhou and Ball for their collaboration on this project. I would also like to thank Amanda for being so collaborative and giving despite some unusual difficulties (to say the least!).

VITA

2007 Bachelor of Science, University of California Davis

2021 Doctor of Philosophy, University of California San Diego

PUBLICATIONS

Johnson DT*, Zhou JR*, Zhou J, Kroll AV, Fang RH, Yan M, Xiao C, Chen X, Kline J, Zhang L, Zhang DE. Acute Myeloid Leukemia Cell Membrane-Coated Nanoparticles for Cancer Vaccination Immunotherapy. Leukemia. 2021. [In Press]. [*these authors contributed equally to this work]

Davis AG, **Johnson DT**, Zheng D, Wang R, Jayne ND, Liu M, Shin J, Wang L, Stoner SA, Zhou JH, Ball ED, Tian Bin, Zhang DE. Alternative polyadenylation dysregulation contributes to the differentiation block of acute myeloid leukemia. Blood. 2021. [In Press].

Johnson DT, Davis AG, Zhou JH, Ball ED, Zhang DE. MicroRNA let-7b downregulates AML1-ETO oncogene expression in t(8;21) AML by targeting its 3'UTR. Exp Hematol Oncol. 2021 Feb 2;10(1):8. PMID: 33531067.

Stoner SA, Yan M, Liu KTH, Arimoto KI, Shima T, Wang HY, **Johnson DT**, Bejar R, Jamieson C, Guan KL, Zhang DE. Hippo kinase loss contributes to del(20q) hematologic malignancies through chronic innate immune activation. Blood. 2019 Nov 14;134(20):1730-1744. PMID: 31434702.

He Y, **Johnson DT**, Yang JS, Wu H, You S, Yoon J, Lee DH, Kim WK, Aldahl J, Le V, Hooker E, Yu EJ, Geradts J, Cardiff RD, Sun Z. Loss of the tumor suppressor, Tp53, enhances the androgen receptor-mediated oncogenic transformation and tumor development in the mouse prostate. Oncogene. 2019 Sep;38(38):6507-6520. Epub 2019 Jul 29. PMID: 31358900.

Mi J, Hooker E, Balog S, Zeng H, **Johnson DT**, He Y, Yu EJ, Wu H, Le V, Lee DH, Aldahl J, Gonzalgo ML, Sun Z. Activation of hepatocyte growth factor/MET signaling initiates oncogenic transformation and enhances tumor aggressiveness in the murine prostate. J Biol Chem. 2018 Dec 28;293(52):20123-20136. Epub 2018 Nov 6. PMID: 30401749.

Maddamsetti R, **Johnson DT**, Spielman SJ, Petrie KL, Marks DS, Meyer JR. Gain-of-function experiments with bacteriophage lambda uncover residues under diversifying selection in nature. Evolution. 2018 Oct;72(10):2234-2243. Epub 2018 Sep 11. PMID: 30152871.

Petrie KL, Palmer ND, **Johnson DT**, Medina SJ, Yan SJ, Li V, Burmeister AR, Meyer JR. Destabilizing mutations encode nongenetic variation that drives evolutionary innovation. Science. 2018 Mar 30;359(6383):1542-1545. PMID: 29599247.

Yu EJ*, Hooker E*, **Johnson DT***, Kwak MK, Zou K, Luong R, He Y, Sun Z. LZTS2 and PTEN collaboratively regulate ß-catenin in prostatic tumorigenesis. PLoS One. 2017

Mar 21;12(3):e0174357. PMID:28323888. [*these authors contributed equally to this work]

Johnson DT*, Hooker E*, Luong R, Yu EJ, He Y, Gonzoalgo ML, Sun Z. Conditional Expression of the Androgen Receptor Increases Susceptibility of Bladder Cancer in Mice. PLoS One. 2016 Feb 10;11(2):e0148851. PMID: 26862755. [*these authors contributed equally to this work]

Lee SH, Luong R, **Johnson DT**, Cunha GR, Rivina L, Gonzalgo ML, Sun Z. Androgen signaling is a confounding factor for β-catenin-mediated prostate tumorigenesis. Oncogene. 2016 Feb 11;35(6):702-14. PMID:25893287

Lee SH, **Johnson DT**, Luong R, Yu EJ, Cunha GR, Nusse R, Sun Z. Wnt/β-Catenin-Responsive Cells in Prostatic Development and Regeneration. Stem Cells. 2015 Nov;33(11):3356-67. PMID:26220362

Lee SH, **Johnson D**, Luong R, Sun Z. Crosstalking between androgen and PI3K/AKT signaling pathways in prostate cancer cells. J Biol Chem. 2015 Jan 30;290(5):2759-68. PMID:25527506

Lee SH, Zhu C, Peng Y, **Johnson DT**, Lehmann L, Sun Z. Identification of a novel role of ZMIZ2 in regulating the activity of the Wnt/B-catenin signaling pathway. J Biol Chem. 2013 Dec 13;288(50):35913-24. PMID: 24174533

Johnson DT, Luong R, Lee SH, Peng Y, Shaltouki A, Lee JT, Lin D, Wang Y, Sun Z. Deletion of leucine zipper tumor suppressor 2 (Lzts2) increases susceptibility to tumor development. J Biol Chem. 2013 Feb 8;288(6):3727-38. PMID: 23275340.

Kwak MK*, **Johnson DT***, Zhu C, Lee SH, Ye DW, Luong R, Sun Z. Conditional deletion of the Pten gene in the mouse prostate induces prostatic intraepithelial neoplasms at early ages but a slow progression to prostate tumors. PLoS One. 2013;8(1):e53476. PMID: 23308230. [*these authors contributed equally to this work]

Peng Y, Clark C, Luong R, Tu WH, Lee J, **Johnson DT**, Das A, Carroll TJ, Sun Z. The leucine zipper putative tumor suppressor 2 protein LZTS2 regulates kidney development. J Biol Chem. 2011 Nov 18;286(46):40331-42. PMID: 21949185.

Zhu C, Luong R, Zhuo M, **Johnson DT**, McKenney JK, Cunha GR, Sun Z. Conditional expression of the androgen receptor induces oncogenic transformation of the mouse prostate. J Biol Chem. 2011 Sep 23;286(38):33478-88. PMID: 21795710.

FIELDS OF STUDY

Prostate Cancer
Professor Zijie Sun, PhD

Viral Evolution
Professor Justin Meyer, PhD

Hematology and myeloid malignancies
Professor Dong-Er Zhang, PhD

ABSTRACT OF THE DISSERTATION

Novel Studies in Acute Myeloid Leukemia

by

Daniel Thomas Johnson

Doctor of Philosophy in Biology

University of California San Diego, 2021

Professor Dong-Er Zhang, Chair

Acute myeloid leukemia (AML) is the most common and deadly leukemia in adults. Although most AML patients respond to first-line chemotherapy, relapse is common. Thus, the five-year overall survive rate remains under 50%. The high relapse rate of patients who achieve “complete remission” is largely due to the difficulties of eradicating minimal residual AML cells, using current therapeutic strategies. Thus, additional therapies to target and eradicate residual AML are greatly needed.

In the Chapter 1, we report the development of a novel nanoparticle-based AML vaccination immunotherapy for the treatment of AML. Our vaccine platform utilizes AML cell membrane-coated nanoparticles (AMCNPs), in which immune stimulatory adjuvant-loaded nanoparticles are coated with leukemic cell membrane material. The AMCNP

vaccine stimulates leukemia-specific immune responses by co-delivering membrane-associated antigens along with adjuvants to antigen-presenting cells. The AMCNP vaccines were efficiently acquired by antigen-presenting cells *in vitro* and *in vivo* and stimulate antigen cross-presentation. Vaccination with AMCNPs significantly enhanced antigen-specific T cell expansion and effector function. Furthermore, in an AML post-remission vaccination model, AMCNP vaccination significantly enhanced survival in comparison to control vaccination. Our AMCNP vaccination strategy is multi-antigenic, fully personalized, and obviates the need for neoantigen identification. Thus, AMCNPs are a promising platform that can be further developed as an AML vaccination immunotherapy.

In chapter 2, we examined the post-transcriptional regulation of the AML1-ETO oncofusion gene. The AML1-ETO oncofusion gene is created by the t(8;21)(q22;q22) chromosomal translocation, which characterizes a common AML subtype [t(8;21) AML]. Post-transcriptional regulation of gene expression is often mediated through interactions between *trans*-factors and *cis*-elements within transcript 3'-untranslated regions (UTR). *AML1-ETO* uses the 3’UTR of the *ETO* gene, which is not normally expressed in hematopoietic cells. Therefore, the mechanisms regulating AML1-ETO expression via the 3’UTR are attractive therapeutic targets. Here, we identify a negative regulatory element within the *AML1-ETO* 3’UTR and demonstrate that the let-7b microRNA directly represses AML1-ETO through this site, inhibits the proliferation of t(8;21) AML cell lines, rescues expression of AML1-ETO target genes, and promotes differentiation. We conclude that AML1-ETO is posttranscriptional regulated by let-7b, which contributes to the leukemic phenotype of t(8;21) AML.

Chapter 1. Acute Myeloid Leukemia Cell Membrane-Coated Nanoparticles for Cancer Vaccination Immunotherapy

Cancer vaccines are promising treatments to prevent relapse after chemotherapy in acute myeloid leukemia (AML) patients, particularly for those who cannot tolerate intensive consolidation therapies. Here, we report the development of an AML cell membrane-coated nanoparticle (AMCNP) vaccine platform, in which immune stimulatory adjuvant-loaded nanoparticles are coated with leukemic cell membrane material. This AMCNP vaccination strategy stimulates leukemia-specific immune responses by co-delivering membrane-associated antigens along with adjuvants to antigen-presenting cells. To demonstrate that this AMCNP vaccine enhances leukemia-specific antigen presentation and T cell responses, we modified a murine AML cell line to express membrane-bound chicken ovalbumin as a model antigen. AMCNPs were efficiently acquired by antigen-presenting cells *in vitro* and *in vivo* and stimulated antigen cross-presentation. Vaccination with AMCNPs significantly enhanced antigen-specific T cell expansion and effector function compared with control vaccines. Prophylactic vaccination with AMCNPs enhanced cellular immunity and protected against AML challenge. Moreover, in an AML post-remission vaccination model, AMCNP vaccination significantly enhanced survival in comparison to vaccination with whole leukemia cell lysates. Collectively, AMCNPs retained AML-specific antigens, elicited enhanced antigen-specific immune responses, and provided therapeutic benefit against AML challenge.

1.1 INTRODUCTION

Acute myeloid leukemia (AML) continues to be associated with a poor prognosis, with an overall 5-year survival of approximately 29%[1]. Although many patients achieve complete remission after initial induction chemotherapy[2], there remains a high rate of relapse due to the persistence of a small number of therapy-resistant leukemic cells, termed minimal residual disease (MRD)[3, 4]. The current standard treatment strategy to clear MRD is intensive consolidation therapy with allogeneic hematopoietic stem cell transplantation (HSCT)[5]. Unfortunately, HSCT carries significant morbidity and is unsuited for older or less healthy patients[5, 6]. While the recent approval of various targeted AML therapies has improved survival in certain patient subgroups, relapse after initial therapy remains a large problem[7, 8]. Thus, there is a great need for alternative tolerable consolidation therapies that target MRD to delay or prevent relapse.

Cancer immunotherapy has revolutionized the treatment of a growing number of human cancers. Although therapeutic cancer vaccines have not been successful in subjects with large tumor burden, they may be useful as consolidation therapy for AML in the MRD state[9, 10]. The underlying strategy of cancer vaccines is to enhance the presentation of cancer-specific or cancer-associated antigens by activated professional antigen-presenting cells (APCs) to induce effective and durable T cell immunity[10]. However, presentation of leukemia antigens by quiescent APCs is insufficient to stimulate functional leukemia-specific T cell responses, and rather can lead to a T cell tolerant state[11]. The efficient activation of APCs in the context of cancer vaccination requires the co-administration of antigens with immunostimulatory adjuvants[12-14]. Thus,

a key component of AML vaccination immunotherapies is the effective delivery of both AML-associated antigens and immunostimulatory adjuvants to APCs[9, 10].

Recent studies have highlighted the promise of “personalized” anticancer vaccination with identification of patient specific neoantigens[15-19]. Because AML is a heterogeneous disease, AML vaccination strategies should ideally induce a multi-antigenic immune response. Clinical trials have recently shown the feasibility and promise of personalized and multi-antigenic AML vaccines using various methods, including pulsing *ex vivo* antigen-presenting dendritic cells (DCs) with autologous apoptotic AML blasts/lysates as the antigen source[20-22], generating *ex-vivo* DCs differentiated directly from AML blasts[23-25], or fusing *ex vivo* DCs with autologous AML blasts[26]. These strategies have proven to be well tolerated[20-26], elicit AML-associated T cell responses[21-24, 26], and protect against disease relapse[25, 26]. While *ex vivo* strategies benefit from easily providing DCs with adjuvants and antigens, they face challenges associated with generating sufficient DCs, homing *ex vivo* vaccinated DCs to lymph nodes, and maintaining active DCs in culture[27]. These challenges may potentially be overcome by *in vivo* vaccination strategies. Indeed, *in vivo* administration of allogeneic or autologous AML whole cell vaccines induced leukemia-associated immunity and prolonged overall survival, although responses have varied among patients[28-30]. The promising results of these vaccines may be improved upon through the development of strategies to simultaneously deliver immunostimulatory adjuvants and a broad array of leukemic antigens to individual APCs *in vivo*.

Cell membrane coating nanotechnology is an emerging approach for developing multifunctional biomimetic nanoformulations consisting of a synthetic nanoparticle core

coated in a layer of natural cell membrane[31]. Leveraging this technology, it has been demonstrated there may be tremendous benefits in the nanodelivery of antigen-rich cancer cell membrane material for anticancer vaccination[32].A cancer cell membrane-coated nanovaccine employing an adjuvant-loaded polymeric core was recently developed to treat melanoma[33]. As a prophylaxis, the nanovaccine protected a majority of vaccinated mice from developing tumors in a lowly immunogenic B16F10 model. When used in combination with immune checkpoint inhibitors, effective control of tumor growth was also achieved in a therapeutic setting. This work highlighted the potential of leveraging a cell membrane-coated nanovaccine to generate systemic antitumor immunity, which is an even more important consideration for blood cell malignancies such as leukemia. AML is an attractive target for the application of this technology because suitable numbers of malignant blasts can be harvested and enriched from bone marrow aspirates or apheresis as a source of antigen-rich membrane material[22-24, 26, 28, 29].

Here, we developed an AML cell membrane-coated nanoparticle (AMCNP) vaccine to treat liquid tumors in a clinically relevant setting, targeting MRD and aiming to prevent relapse. AMCNPs are adjuvant-loaded nanoparticles wrapped with antigen-rich leukemic cell membrane material and were readily deliverable to APCs *in vitro* and *in vivo.* Upon AMCNP acquisition, APCs presented leukemia membrane-associated antigens. Furthermore, vaccination with AMCNPs led to enhanced leukemia specific and leukemia associated antigen-specific T cell responses compared to a control whole cell lysate (WCL)-based vaccine. Prophylactic AMCNP vaccination provided protection from AML cell challenge *in vivo*. In a model of consolidation therapy, vaccination with

AMCNPs after chemotherapy improved long-lasting immunity and significantly prolonged survival after AML re-challenge compared to WCL vaccination controls. These results demonstrate that AMCNPs are a novel and feasible approach for the development of effective AML vaccination immunotherapies.

1.2 RESULTS

1.2.1 Production of AMCNPs for vaccination immunotherapy.

To improve neoantigen vaccination strategies for AML, we examined a recently developed antigen presentation approach with AML cell membrane-coated nanoparticles (AMCNPs) containing immunostimulatory adjuvants[31-33]. The AMCNP strategy is designed to promote AML-specific immune responses by delivering nanoparticles (NPs) carrying multiple unidentified AML cell membrane-associated antigens and immunostimulatory adjuvants to APCs (**Fig. 1.1**). Through sonication, isolated membrane material is used to coat poly (lactic-*co*-glycolic acid) (PLGA) NP cores, which are synthesized using a double emulsion process. The final particles exhibit a core–shell structure uniformly coated with leukemia cell membrane[33]. A key advantage of AMCNPs is the capacity to package immune-stimulatory adjuvants within the NP core[33]. We used CpG oligodeoxynucleotide 1826, a Toll-like receptor 9 (TLR9) agonist, as a well-characterized and potent adjuvant in the current study (**Fig. 1.1B**). TLR agonists have been extensively used in vaccine immunotherapy due to their role in activating immune responses by stimulating APCs to upregulate co-stimulatory factors, secrete inflammatory cytokines, present antigens to T cells, and activate tumor-specific T cells[14].

To test the efficacy of the AMCNP vaccine platform, the syngeneic C1498 murine AML cell line was employed. C1498 cells are derived from an AML that developed spontaneously in a C57BL/6 (H-2^b) mouse[34]. The C1498 model has been used previously to examine various immunotherapeutic strategies[35-37]. We first used membrane-bound ovalbumin (OVA) as a model membrane-associated leukemic antigen for our study. To maximize OVA antigen expression on C1498 cells, sequences corresponding to the murine *Cadm1* signal peptide and transmembrane domain, along with full-length OVA, were cloned into the MSCV-IRES-puromycin^R (MIP) retroviral vector to generate MIP-OVA (**Fig. 1.2A**). MIP and MIP-OVA retrovirus-transduced C1498 cells are referred to as C1498-MIP and C1498-OVA cells, respectively. Presentation of OVA-derived peptides in the context of MHC class I molecules (H-$2K^b$:SIINFEKL) on C1498-OVA cells was confirmed by flow cytometry (**Fig. 1.2B**). OVA-specific presentation by the C1498-OVA cell line was also confirmed through beta-galactosidase (lacZ) B3Z T cell activation assays[38], in which an OVA-specific $CD8^+$ T cell activation lacZ reporter line (B3Z) was activated after co-culture with C1498-OVA cells but not C1498-MIP cells (**Fig. 1.2C**). Following intravenous inoculation of C1498-OVA cells, C57BL/6 mice uniformly succumbed, although at a later time point when compared to mice challenged with C1498 parental cells (C1498) (**Fig. S1.1**). The enhanced survival of mice challenged with C1498-OVA cells suggests that this cell line is more immunogenic than C1498 cells, likely due to the expression and presentation of the OVA antigen. Together, these results confirm that the C1498-OVA cell line expresses and presents OVA-derived antigens.

AMCNPs were generated using membrane material from C1498-OVA, C1498-MIP, and C1498 cells. AMCNPs were loaded with CpG at roughly 100 pmol CpG/mg NP. Dynamic light scattering measurements were used to assess the size and zeta potential of the PLGA NP cores, AMCNPs, and isolated membrane material. AMCNPs showed slightly increased size compared to uncoated PLGA NPs (~165 nm vs 133 nm), consistent with successful membrane coating (**Fig. 1.3A**). As expected, the size of AMCNPs was far smaller than the corresponding isolated membrane material (~165 nm vs 1 μm) (**Fig. 1.3A**). Zeta potential is an important measurement of the effective electric charge on the NP surface. AMCNPs demonstrated increased zeta potential compared to uncoated PLGA NPs (~-40 mV vs -58 mV), consistent with successful membrane coating, as membrane material is less negatively charged than the PLGA NP core (~-40 mV vs -58 mV) (**Fig. 1.3B**). C1498 AMCNPs displayed a core–shell structure with uniform coating when observed through transmission electron microscopy (**Fig. 1.3C**). Furthermore, AMCNPs retained a very similar composition of membrane proteins when assessed by polyacrylamide gel electrophoresis protein separation (**Fig. 1.3D**). Together, these results confirmed our ability to successfully generate AMCNPs coated with leukemia cell-derived membrane material.

1.2.2 APCs effectively acquire AMCNPs.

In order to stimulate effective immune responses, AMCNPs must first be acquired by APCs. Therefore, we examined the ability of AMCNPs to be captured by APCs by pulsing bone marrow-derived dendritic cells (BMDC) with either dye-labeled CpG at a final concentration of 100 nM or equivalent C1498-OVA AMCNPs encapsulated with dye-labeled CpG. We observed efficient acquisition of labeled

AMCNPs in BMDCs, where a detectable signal was initially observed after 30 min of pulsing (**Fig. 1.4A, S1.2**), which became readily visualized after 24 h (**Fig. S1.2**). In comparison to AMCNPs, BMDC acquisition of free CpG was far less detectable at both time points (**Fig. 1.4A, S1.2**). We also observed efficient acquisition of labeled C1498-OVA AMCNPs by the DC2.4 mouse DC cell line (**Fig. S1.3A**).

DC maturation is promoted through the engagement of pattern-recognition receptors, such as TLRs[39], with pathogen-associated molecular patterns, such as CpG[39, 40]. Thus, we next examined the ability of AMCNPs to promote BMDC maturation and antigen presentation by pulsing BMDCs for 2 h with 100 nM of either C1498-OVA AMCNPs, equivalent amounts (based on membrane material) of C1498-OVA WCL plus CpG (WCL vaccine), or CpG plus 1 μg/ml OVA SIINFEKL peptide (peptide vaccine). We observed enhanced maturation and activation of BMDCs pulsed with C1498-OVA AMCNPs as evidenced by the increased frequency of CD11c+ cells with high expression of the co-stimulatory molecules CD40, CD80, CD86, and MHC-II (**Fig. 1.4B**). Furthermore, the frequency of activated $CD11c^{+}CD40^{hi}$ BMDCs presenting the SIINFEKL peptide in the context of MHC-I ($H\text{-}2K^{b}$:SIINFEKL) was significantly greater when pulsed with C1498-OVA AMCNPs, versus pulsing with either the WCL vaccine or the peptide vaccine (**Fig. 1.4B**).

To test the delivery of AMCNPs to APCs *in vivo*, fluorescently labeled AMCNPs were inoculated subcutaneously via the hock[41] of C57BL/6 mice. Labeled AMCNPs could be detected within $CD11c^{+}$ DCs in the draining lymph node and spleen (**Fig. 1.4C**). To test the effect of the AMCNPs on *in vivo* DC maturation, C57BL/6 mice were inoculated subcutaneously into each hock[41] with 50 μL of 25 mg/ml of C1498-OVA

AMCNPs, equivalent C1498-OVA WCL vaccine, or mock treatment. After 24 h, C1498-OVA AMCNP vaccination significantly increased DC maturation within the draining lymph node compared to vaccination with the C1498-OVA WCL vaccine or the mock control, as evidenced by increased frequency of $CD11c^+$ cells with high expression of CD80, CD83, CD86, and MHC-II (**Fig. 1.4D**). Similar results were observed using C1498 AMCNP vaccination (**Fig. S1.3B**), suggesting that the promotion of DC maturation is not dependent upon the OVA antigen. Collectively, these results demonstrate that AMCNPs are efficiently delivered to APCs, induce maturation, and stimulate antigen presentation.

1.2.3 AMCNPs enhance T cell activation.

We next examined the ability of AMCNP-pulsed APCs to promote antigen-specific $CD8^+$ T cell activation. BMDCs and DC2.4 cells were pulsed with C1498-OVA AMCNPs or C1498-MIP AMCNPs, and OVA-specific T cell activation was measured using B3Z OVA T cell activation assays[38]. C1498-OVA AMCNPs significantly stimulated OVA-specific T cell activation, whereas the C1498-MIP AMCNPs did not (**Fig. 1.5A, S1.3C**). These results suggest that antigens contained within the AMCNP are presented by APCs to stimulate specific T cell responses.

To test the efficacy of AMCNPs *in vivo*, C57BL/6 mice were vaccinated on days 0, 2, and 4 via subcutaneous inoculation into each hock[41] with 50 µl of 25 mg/ml C1498-MIP AMCNPs, C1498-OVA AMCNPs, or equivalent C1498-OVA WCL vaccine; their splenocytes were collected on day 10 and re-stimulated *ex vivo* with OVA-derived peptide (SIINFEKL) until day 17 (**Fig. 1.5B**). A significantly higher frequency of *ex vivo*-stimulated splenic $CD8^+$ T cells from C1498-OVA AMCNP-vaccinated mice were

labeled by H-2K^{b}:SIINFEKL tetramers, compared to C1498-OVA or C1498-MIP AMCNP-vaccinated mice, suggesting that C1498-OVA AMCNP vaccination drives the expansion of antigen-specific CD8^{+} T cells (**Fig. 1.5C**). Furthermore, *ex vivo*-stimulated splenocytes from C1498-OVA AMCNP-vaccinated mice secreted significantly higher concentrations of interferon-γ (IFN-γ) compared to those vaccinated with C1498-MIP AMCNPs or C1498-OVA WCL vaccines (**Fig. 1.5D**).

We next sought to directly examine activation and OVA specific T cell expansion *in vivo*. Mice were vaccinated with C1498-OVA AMCNPs or equivalent C1498-OVA WCL vaccine on days 0, 7, and 14 **(Fig. 1.5E, F)**. On day 17, we observed significantly increased numbers of CD8^{+}CD69^{+} and CD8^{+}CD25^{+} T cells among the PB mononuclear cells of AMCNP-vaccinated mice compared with WCL-vaccinated or control mice (**Fig. 1.5F**); suggesting that AMCNP vaccination stimulates activation of CD8^{+} T cells. OVA-specific T cell expansion was then assessed by H-2K^{b}:SIINFEKL dextramer (OVA dextramer) staining on day 21 (**Fig. 1.5G-I**). Significantly higher numbers of CD3^{+}CD8^{+} OVA dextramer^{+} T cells were found in AMCNP-vaccinated mice compared with WCL-vaccinated mice (**Fig. 1.5H**). To examine OVA specific memory CD8^{+} T cells, splenocytes were collected from the mice on day 57 (**Fig. 1.5H, J**). Significantly higher numbers of OVA-specific central memory (CD62L^{hi}CD44^{hi}CD8^{+}OVA dextramer^{+}) and effector memory (CD62L^{low}CD44^{hi}CD8^{+}OVA dextramer^{+}) CD8^{+} T cells were observed in AMCNP-vaccinated mice compared with WCL-vaccinated mice (**Fig. 1.5J**).

We next sought to demonstrate AMCNP mediated immune responses against a known leukemia associated antigen, Wilms' tumor 1 (WT1). WT1 is a well characterized leukemia associated antigen that has been targeted in various AML vaccination

therapies[30, 42]. Because C1498 cells do not express WT1[43], we generated a WT1 expressing C1498 cell line (C1498-WT1)(**Fig. S1.4A**). WT1 expression in the C1498-WT1 line was confirmed by western blotting (**Fig. S1.4B**). To examine WT1 specific T cell expansion *in vivo*, mice were vaccinated with C1498-WT1 AMCNPs or equivalent C1498-WT1 WCL vaccine on days 0, 7, and 14 (**Fig. S1.4C**). Using H-2D^{b}:RMFPNAPYL dextramer (WT1 dextramer) staining of PB mononuclear cells on day 21, we observed significantly higher numbers of $CD3^{+}CD8^{+}$ WT1 $dextramer^{+}$ T cells in the AMCNP-vaccinated mice compared with WCL-vaccinated mice (**Fig. S1.4C**). Additionally, splenocytes from AMCNP-vaccinated mice secreted significantly higher concentrations of IFN-γ compared to WCL-vaccinated mice, after *ex vivo*-stimulation with WT1 peptide (**Fig. S1.4D**). Collectively, these data suggest that *in vivo* vaccination with AMCNPs mediates potent $CD8^{+}$ T cell immunity against leukemia-specific and leukemia-associated antigens.

1.2.4 AMCNP vaccination protects against AML cell challenge

We next sought to determine if immune responses elicited by AMCNPs provided protective anti-leukemic immunity. To first confirm that AMCNP vaccination could elicit anti-leukemic immunity against AML cells which expressed a known antigen, we prophylactically vaccinated C57BL/6 mice with three rounds of 50 µl of 25 mg/ml C1498-OVA AMCNPs (n = 5) or mock treatment with equivalent CpG (n = 5) before challenging them with 1×10^{5} C1498-OVA cells (**Fig. S1.5A**). All C1498-OVA AMCNP-treated mice survived more than 21 weeks after challenge with C1498-OVA cells, whereas none of the control mice survived past 19 weeks (median survival 8.7 weeks) (**Fig. S1.5B**). These results suggested that AMCNP vaccination provides prophylactic

anti-leukemic immunity in a context in which AML-specific antigens are being expressed.

We further sought to test C1498 AMCNPs in a more therapeutically relevant remission model, in which vaccination occurs after initial induction therapy with conventional chemotherapeutic drugs. C57BL/6 mice challenged with 1×10^5 C1498 cells were subsequently treated with clinically-relevant AML chemotherapy drugs[5], cytarabine and doxorubicin, prior to vaccination (**Fig. 1.6A**). Cytarabine and doxorubicin treatment significantly prolonged survival in unvaccinated, “chemotherapy only” mice (n = 5, median survival 8.7 weeks) compared to mock chemotherapy controls (n = 7, median survival 4.3 weeks) (**Fig. 1.6B**). Mice were vaccinated with C1498 AMCNPs (n = 13) or C1498 WCL vaccine (n = 15) at 4-, 5-, and 6-weeks post-chemotherapy (**Fig. 1.6A**). Both AMCNP and WCL vaccine groups had significantly prolonged survival compared to the chemotherapy only group (median survival 8.7 weeks) by week 21 (**Fig. 1.6B**). The AMCNP vaccinated group had a higher survival rate (85%) than the WCL vaccine group (60%) at 21 weeks post-C1498 challenge. However, this difference was not significantly greater due to the high survivability of both groups (**Fig. 1.6B**). To observe the longer-term effect of AMCNPs, we re-challenged surviving mice with 2×10^6 C1498 cells 21 weeks after the initial challenge. After re-challenge, the AMCNP-vaccinated group showed significant survival benefit (median survival 4.4 weeks post-re-challenge) compared to the WCL-vaccinated mice (median survival 2.7 weeks post-re-challenge) (**Fig. 1.6C**). To further examine the anti-leukemic effect of AMCNPs in our remission model, additional C1498 AMCNP-vaccinated (n = 4) and C1498 WCL-vaccinated (n = 4) mice underwent the same course of C1498 cell challenge,

chemotherapy, and vaccination; however, these mice were re-challenged with 2×10^6 C1498 cells that stably expressed enhanced GFP (C1498-eGFP) 32 days after the final vaccination (**Fig. 1.6D**). The AMCNP-vaccinated mice had a significantly lower percentage of C1498-eGFP cells in the bone marrow and liver compared to WCL-vaccinated mice at 21 days post-re-challenge (**Fig. 1.6E, S1.6**). The WCL vaccination mice had significantly higher expression levels of the programmed cell death protein 1 (PD-1) inhibitory receptor within both BM and liver $CD3^+$ T lymphocyte populations, compared to AMCNP vaccinated mice (**Fig. 1.6F**). Interestingly, the AMCNP-vaccinated mice showed a significant decrease in the frequency of naïve $CD8^+$ T cells ($CD62L^{hi}$ $CD44^{low}$) (**Fig. 1.6G, S1.7**), suggesting that AMCNP-vaccinated mice have an increased proportion of antigen-exposed $CD8^+$ T cells. Taken together, these results suggest that AMCNP vaccination during remission improves long-lasting immunity and significantly delays disease progression upon re-challenge, compared to WCL vaccination.

1.3 DISCUSSION

The lack of well-tolerated and effective consolidation therapy strategies is a major gap in the current AML standard of care, due to the significant morbidity and imperfect prevention of relapse associated with allogeneic hematopoietic stem cell transplantation[5, 6, 44]. This gap remains despite recent progress in benefiting patients with various subtypes of AML through targeted therapies, such as hypomethylating agents, immune checkpoint inhibitors, FLT3 inhibitors, and isocitrate dehydrogenase inhibitors[7, 8]. AML vaccination therapies have proven to be generally tolerable and to consistently promote leukemia antigen-associated T cell immunity; thus, displaying their therapeutic potential[10, 42]. Additionally, the efficacy of AML vaccination may be further

improved when combined with targeted therapies, such as hypomethylating agents[45] and immune checkpoint inhibitors[17, 46]. We developed an AMCNP vaccination therapy that is personalized, multi-antigenic, and can deliver both membrane-associated leukemic antigens as well as immunostimulatory adjuvants to professional APCs *in vivo*.

In our C1498 AML relapse model, consolidation therapy using AMCNPs provided a significant benefit to overall survival compared to WCL vaccines. Importantly, this benefit was observed after re-challenge 4 months post-vaccination using a 20-fold increase in the number of C1498 leukemia cells than in the initial challenge. Thus, AMCNPs induced a long-term benefit, even without additional therapeutic interventions, such as immune checkpoint inhibitors. We observed far fewer leukemic cells in the bone marrow and liver of AMCNP-vaccinated versus WCL-vaccinated mice in our C1498-eGFP re-challenge model. Correspondingly, we observed increased expression levels of PD-1 in the T cells of WCL-vaccinated mice, which is associated with AML immune-suppression[47, 48] and is a mechanism of immune evasion in C1498 cells[49], suggesting that AMCNP vaccination might be beneficial in preventing immune evasion during AML relapse. AMCNP vaccination was also associated with a significant decrease in naïve $CD8^+$ T lymphocytes within the spleen, suggesting that an increased proportion of $CD8^+$ T cells in the AMCNP vaccinated mice have been exposed to leukemic antigens. Collectively, we demonstrate that AMCNP vaccination enhanced anti-leukemic immunity.

AML is a heterogeneous disease, in which individual patients often have varying leukemic clonal populations. A single suitable protein target that is present in all AMLs has yet to be identified and likely does not exist. AML blasts between and within

patients may present clonal AML specific neoantigens, due to random mutation[50]. Thus, there is great need for AML immunotherapies that are both fully personalized and multi-antigenic to overcome these challenges. Indeed, the feasibility of recurrent neoantigen immunotherapy in AML has recently been demonstrated[15, 16]. However, personalized vaccines that rely on identifying patient-specific neoantigens are technically challenging, time-consuming, and expensive. Our AMCNP vaccination strategy is multi-antigenic, fully personalized, and obviates the need for neoantigen identification. Therefore, AMCNP vaccination therapy is suitable for AML.

The AMCNP vaccine strategy is amenable to further development and refinement for potential clinical applications. A key advantage of the AMCNP strategy is the colocalization of both antigen and adjuvant, ensuring that individual APCs receive both, which promotes enhanced antigen-specific immune responses[12, 51, 52]. We show that CpG-encapsulated AMCNPs are efficiently acquired by APCs, increase co-stimulatory signal expression (CD80, CD86, CD83, CD40, and MHC-II), and promote leukemic antigen presentation. Of note, empty PLGA particles themselves are unable to induce APC activation and cytotoxic T cell responses[33, 52, 53]. Furthermore, PLGA particles are widely used[54] and have already been approved by the US FDA for drug delivery. While CpG has often been used as an adjuvant in preclinical models[14], there are many additional immunostimulatory adjuvants[55]. Indeed, great efforts have been made to identify which adjuvants, or combinations of adjuvants, are best in clinical settings[55]. AMCNPs can potentially be packaged with a variety of different adjuvants; thus, this strategy is adaptable to future advances in clinical adjuvant use.

In summary, our AMCNP vaccine is multi-antigenic, personalized, co-localizes adjuvant with antigens, and is efficiently delivered to APCs. We demonstrate the successful development of the AMCNPs. We further show that AMCNPs outperform a control WCL vaccine in activating AML-specific immune responses and providing long-term anti-leukemic survival benefit when used as a consolidation therapy. Thus, AMCNPs are a promising platform that can be further developed and refined as an AML vaccination immunotherapy.

1.4 MATERIALS & METHODS

Plasmids

The MIP-OVA plasmid was created using overlap PCR; the murine *Cadm1* signaling peptide was cloned upstream of the mouse *Cadm1* trans-membrane domain followed by a fusion with the full-length chicken *OVA* cDNA, which was then cloned into the MSCV-IRES- puromycin^R (MIP) plasmid[56] using bglll restriction enzyme sites. The *Cadm1* and *OVA* cDNA templates were from the pcDNA3-HA-*Cadm1* and the pODpCAGGS plasmid[57]. The MIP-WT1 plasmid was created using PCR; the full-length murine *Wt1* cDNA was cloned into the MSCV-IRES- puromycin^R (MIP) plasmid[56] using bglll restriction enzyme sites. The murine *Wt1* MGC premier full length cDNA clone (transOMIC, Huntsville, AL) was used as the template for cloning.

Equalization of WCL vaccines

Whole cell lysate was prepared by five freeze-thaw cycles of liquid nitrogen followed by 10 min at 37°C. The amount of WCL used was normalized by the amount of Na+/K+-ATPase protein, a characteristic membrane protein, compared with AMCNPs

as determined by dot blotting (anti-ATP1A1 rabbit antibody, GenScript Biotech, Piscataway, NJ). Equivalent concentrations of CpG ODN 1826 (Integrated DNA Technologies, Coralville, IA) was added compared to AMCNP-encapsulated CpG.

Dendritic cell maturation

For *in vitro* experiments, 1.5×10^6 BMDCs were plated into 12-well suspension plates in BMDC growth media. Cells were pulsed for 2 h at a concentration of 1.4 mg/ml with C1498-OVA AMCNPs, equivalent C1498-OVA WCL vaccine, or equivalent CpG plus 1 μg/ml OVA SIINFEKL peptide (InvivoGen, San Diego, CA), then washed twice with fresh media. After 48 h of additional culture, cells were then collected in PBS with 1 mM EDTA and washed twice in PBS with 1% bovine serum albumin (Thermo Fisher Scientific). Cells were stained as indicated in Supplementary Table 1.1 For *in vivo* experiments, 50 μL of 25 mg/ml of AMCNPs, equivalent WCL vaccine, or mock treatment, were inoculated subcutaneously into each hock[41] of 8- to 12-week-old C57BL/6J mice (The Jackson Laboratory, Bar Harbor, ME). After 24 h, the popliteal lymph nodes of the mice were collected and manually dissociated in 500 μl dissociation buffer [Dulbecco's PBS with calcium and magnesium (Gibco, Waltham, MA), 1 mg/ml collagenase D (Roche, Basel, Switzerland), and 1 mg/ml DNase I grade II (Roche)]. Cells were stained as indicated in Supplementary Table 1.1.

B3Z OVA presentation assays

The B3Z $CD8^+$ T cell hybridoma cell line is specific for OVA and expresses β-galactosidase under control of the IL-2 promoter[38]. For presentation assays, 1×10^4 C1498-MIP or C1498-OVA cells were co-incubated with either 5×10^4 (high) or 1×10^4 (low) B3Z cells for 16 h at 37°C, 5% CO_2. For cross-presentation assays, 1×10^4 DC2.4

cells or 5×10^4 BMDCs were seeded into each well of a 96-well plate overnight. Serial dilutions beginning with 20 µl per well of 50 mg/ml AMCNPs or equivalent WCL vaccine were added for up to 4 h at 37°C, 5% CO_2. The cells were washed twice with PBS, fixed in 100 µl of cold PBS + 1% formaldehyde (Thermo Fisher Scientific) for 5 min, and then washed three times with 37°C RPMI. B3Z cells (5×10^3 per well) were incubated with the fixed APCs for 16 h at 37°C, 5% CO_2. Plates were washed twice with PBS, and 100 µl LacZ lysis buffer [0.13% NP-40, 9 mM $MgCl_2$, 0.3 mM chlorophenol red-β-d-galactopyranoside (Roche) in PBS] was added for up to 4 h at 37°C. Absorbance was measured at 570 - 650 nm.

Ex vivo T cell functional assay

8- to 12-week-old C57BL/6J mice (The Jackson Laboratory) were vaccinated with 50 µl of 25 mg/ml of AMCNPs or equivalent WCL vaccine subcutaneously via the hock on days 0, 2, and 4. On day 10, spleens were extracted and mechanically dissociated into single cell suspensions. Red blood cell lysis was performed by resuspending the cell mixture in ice cold ACK buffer (0.1 mM Na_2EDTA, 10 mM $KHCO_3$, 150 mM NH_4Cl) for 5 min followed by washing with ice cold PBS and passage through a 40-µM cell strainer (Thermo Fisher Scientific). 5×10^6 splenocytes were then plated and cultured in 6-well suspension plates in BMDC growth media with 20 ng/ml GM-CSF and 1 µg/ml of either OVA SIINFEKL (InvivoGen) or WT1 RMFPNAPYL (MBL international, Woburn, MA) peptide. After 5 or 7 days of *ex vivo* culture, respectively, the supernatant was collected and analyzed for IFN-γ using ELISA kits (Biolegend, San Diego, CA). At 7 days of *ex vivo* culture, the splenocytes were stained as indicated in Supplementary Table 1.1 and used for flow cytometry analysis.

AMCNP consolidation vaccination

8- to 12-week-old C57BL/6J mice (The Jackson Laboratory) were challenged with 1×10^5 C1498 cells via intravenous inoculation. 100 µl of 20 mg/ml cytarabine was administered via intraperitoneal injection on days 1, 2, 3, 4, and 5. Additionally, 30 µL of 2 mg/ml doxorubicin was administered via intraperitoneal injection on days 2, 3, and 4. The mice were housed with water containing 125 mg/l of ciprofloxacin and 20 g/l sucrose for the first two weeks of the experiment. The mice were vaccinated on days 26, 33, and 40 subcutaneously in both hocks with 50 µl of 25 mg/ml C1498 AMCNPs, equivalent amounts of C1498 WCL vaccine, or mock treatment. Mice were monitored with signs of morbidity as the endpoint. For the overall survival experiment, surviving mice were re-challenged on day 163 with 2×10^6 C1498 cells and monitored for signs of morbidity. For the C1498-eGFP experiment, the surviving mice were re-challenged on day 72 with 2×10^6 C1498-eGFP cells and all mice were euthanized, once the first mouse reached the endpoint, on day 93.

Flow cytometry

Flow cytometry and cell sorting was performed as previously described[58]. The antibody staining schemes are indicated in Supplementary Table 1.1. Analysis were performed using FlowJo software version 7.6.5. For calculating total events, flow cytometry samples containing either a known amount of peripheral blood (PB) or 3×10^6 live splenocytes were run in their entirety and observed events were then normalized to 1 ml of PB or the total number of live splenocytes collected from each spleen.

Statistical analyses

All statistical analyses were performed using GraphPad Prism Software (Version 8.4.2). The specific tests used are documented in the corresponding figure legend. The number of independent experiments is indicated in the figures, data is presented as mean values, and error bars represent standard deviation. All *t*-tests were two-tailed. P values are denoted as follows: ns $p > 0.05$, * $p < 0.05$, ** $p < 0.01$, *** $p < 0.001$.

Cell culture

HEK293T cells were purchased from ATCC. C1498 cells were a kind gift from Dr. Shujun Liu (The Hormel Institute, University of Minnesota). B3Z T-cell hybridoma cells were a kind gift from Dr. Nilabh Shastri (University of California, Berkeley). HEK293T, C1498, and associated lines were cultured in DMEM media supplemented with 10% FBS (HyClone, Logan, UT) and 100 U/ml penicillin-streptomycin (Gibco, Waltham, MA). C1498-MIP, C1498-OVA, and C1498-WT1 cells were maintained in 0.5 µg/ml puromycin (InvivoGen, San Diego, CA). B3Z and DC2.4 cells were cultured in RPMI media supplemented with 10% FBS and 100 U/ml penicillin-streptomycin. BMDCs were cultured in BMDC culture media consisting of RPMI media supplemented with 10% FBS, 50 µM β-mercaptoethanol (Gibco), 100 U/ml penicillin-streptomycin, and 20 ng/ml murine GM-CSF (Peprotech, Rocky Hill, NJ). All cells were maintained in a 37°C incubator with 5% CO_2.

Viral transduction

For retroviral transduction experiments, retrovirus was produced in HEK293T cells. Transfections of HEK293T cells were conducted by combining 5 µg of MSCV-IRES-Puro[56] (MIP), MIP-OVA (OVA), MIP-WT1 (WT1), or MSCV-IRES-eGFP[59] (MIGR1) vectors with 5 µg of packaging vector (EcoPak) and 40 µl of 1 mg/ml polyethylenimine

(Polysciences Inc, Warrington, PA) in 1 ml of Opti-MEM reduced serum medium (Gibco). Approximately 16 h post-transfection, the media was aspirated, cells were washed once in PBS, and 7 ml of fresh DMEM media supplemented with 10% fetal bovine serum and 100 U/ml penicillin-streptomycin was added to each plate. At 24 h after the media change, DMEM media containing retroviral particles was collected, passed through a 0.45-μm syringe filter, pooled, and supplemented with 4 μg/ml polybrene (Millipore Sigma, Burlington, MA). C1498 cells were resuspended in retroviral media at a concentration of approximately 0.5×10^6 cells/ml and were transduced in 6-well plates by centrifugation (2,000 *g*) for 3 h at 32°C in an Allegra X-12R centrifuge (Beckman Coulter, Brea, CA) on two consecutive days. At 24 h following the second transduction, C1498-MIP, C1498-WT1, and C1498-OVA cells were resuspended in fresh DMEM media supplemented with 10% fetal bovine serum, 100 U/ml penicillin-streptomycin (Gibco), and 1 μg/ml puromycin (Millipore Sigma). After 48 h of puromycin selection, cells were diluted and maintained at 0.5 μg/ml puromycin until future analysis. C1498-eGFP (C1498-MIGR1) cells were sorted for the top 25% of eGFP fluorescence and maintained in DMEM media supplemented with 10% fetal bovine serum and 100 U/ml penicillin-streptomycin.

Membrane derivation

C1498 cells and associated variants were grown in T175 suspension flasks (Genesee Scientific, El Cajon, CA) and harvested every 3 to 4 days. For cell harvesting, the cell suspension media was collected, and any loosely adherent cells were detached with 1 mM EDTA (Corning, Corning, NY) in PBS (Corning). Cells were spun down at 700 *g* for 5 min and the packed pellet was resuspended in complete medium mixed 1:1

with cryopreservation media (Hyclone). The cells were stored in -20°C until enough harvests were accumulated. To derive the membrane, cell harvests were washed three times with a buffered solution containing 30 mM Tris-HCl pH 7.5 (Quality Biological, Gaithersburg, MD), 2.6% (w/v) sucrose (Millipore Sigma), and 4.1% (w/v) D-mannitol (Millipore Sigma) and then mechanically lysed twice with a Kinematica Polytron PT 10/35 probe homogenizer at 70% power for 15 s in a solution containing protease inhibitor (Millipore Sigma), phosphatase inhibitor (Millipore Sigma), and 500 µM ethylene glycol-bis(β-aminoethyl ether)-N,N,N′,N′-tetraacetic acid (Millipore Sigma). Intracellular contents were purified out by centrifuging the resulting homogenate at 10,000 *g* for 25 min in an Optima XPN-80 ultracentrifuge (SW32 Ti, Beckman Coulter). The membrane in the supernatant was pelleted at 150,000 *g* for 35 min and then buffer exchanged into a storage solution containing 200 µM ethylenediaminetetraacetic acid (EDTA, MP Biomedicals, Santa Ana, CA) in DNase free/RNase free water (Invitrogen, Carlsbad, CA). Finally, the membrane was resuspended, and the protein content was determined with a BCA protein assay kit (Pierce Biotechnology, Waltham, MA) according to manufacturer's instructions. All membrane derivation procedures were performed on ice or at 4°C and the resulting membrane was stored at -20°C until use.

Nanoparticle fabrication

The nanoparticles were synthesized with a double emulsion technique as previously reported[33]. Briefly, 25 nmol of CpG ODN 1826 with a full phosphorothioate backbone and sequence 5′-TCCATGACGTTCCTGACGTT-3 (Integrated DNA Technologies, Coralville, IA) was dissolved in 200 mM Tris-HCl pH 8.0 (Corning) and mixed with 25 mg of 0.18 dl/g carboxyl-terminated 50:50 poly(lactic-*co*-glycolic) acid

(PLGA, LACTEL Absorbable Polymers) dissolved in dichloromethane (Thermo Fisher Scientific, Waltham, MA) to form the inner phase. The mixture was probe sonicated with a 150E sonic dismembrator (Thermo Fisher Scientific) at 70% power with a 2 s on/1 s off pulse for 1 min. Then an emulsified solution containing 100 µl of dichloromethane and 5 ml of 10 mM Tris-HCl pH 8.0 was added into the CpG–polymer mixture as the outer phase and sonicated with the same settings for 2 min. The final emulsion was added into 10 ml of 10 mM Tris-HCl pH 8.0 and magnetically stirred (Thermo Fisher Scientific) at 700 rpm for at least 2.5 h to evaporate the dichloromethane. The NPs were spun down at 21,100 *g* for 8 min, consolidated into a single tube, and washed three times with 10 mM Tris-HCl pH 8.0 to remove free CpG. At the last wash, different types of membrane (C1498, C1498-MIP, C1498-WT1, or C1498-OVA) were used to resuspend the nanoparticles at a 1:10 membrane to polymer ratio, and the mixture was sonicated for 2 min with a FS30D bath sonicator (Thermo Fisher Scientific) in macro disposable cuvettes (BrandTech Scientific, Essex, CT). Excessive membrane was similarly washed out three times with 10 mM Tris-HCl pH 8.0 as before and the NPs were resuspended in 10% sucrose (Millipore Sigma, Burlington, MA) buffered with 5 mM Tris-HCl pH 7.5 and 200 µM EDTA in DNase free/RNase free water at a final concentration of 25 mg/ml. NPs were frozen in -20°C if they were not used on the same day. Fluorescently labeled NPs were prepared similarly by incorporating either 5’6-FAM-modified CpG (ex/em = 495/520 nm, Integrated DNA Technologies) or 1,1′-dioctadecyl-3,3,3′,3′-tetramethylindodicarbocyanine, 4-chlorobenzenesulfonate salt (DiD, ex/em = 644/663 nm, Biotium, Fremont, CA) at a 0.1% (w/w) ratio in the inner phase.

Nanoparticle characterization

Characterization of the nanoformulation was performed on particles resuspended at a final concentration of 5 mg/ml in DNase/RNase free water instead of the sucrose solution. The size and zeta potential of the nanoparticles were measured in a folded capillary zeta cell (Malvern Panalytical, Malvern, United Kingdom) using a Malvern ZEN3600 Zetasizer. Measurements for the membrane was similarly determined but at a final concentration of 500 µg/ml to reflect the coating ratio. The morphology of the nanoparticles was visualized via transmission electron microscope using a JEOL 1200 EX II transmission electron microscope. To prepare the imaging samples, the nanoparticle suspension was adsorbed onto a 400-mesh carbon film grid (Electron Microscopy Sciences, Hatfield, PA) for 10 min followed by three washes with distilled water for 2 min each. The grid was then negatively stained with 1% (w/v) uranyl acetate for 15 s and allowed to dry prior to imaging.

Protein characterization

C1498, C1498-MIP, and C1498-OVA whole cell lysates (WCL) were prepared by five freeze-thaw cycles in liquid nitrogen followed by 10 min at 37°C. The protein concentration of the WCL, membrane, and AMCNP samples were determined in tube format with a BCA protein assay kit. All samples were diluted to a final concentration of 500 µg/ml and mixed with NuPAGE LDS sample buffer (Novex, Waltham, MA) at a 3 to 1 ratio. Protein samples were denatured at 70°C for 10 min in a Isotemp digital dry bath (Thermo Fisher Scientific) and loaded into a 12-well Bolt 4-12% bis-tris gel (Novex) along with the SeeBlue Plus2 pre-stained protein standard (Invitrogen, Waltham, MA). The proteins were separated at 165 V for 45 min in Bolt MOPS SDS running buffer (Novex) in the mini blot module system and the gel was stained with Instant Blue

(Expedeon, Heidelberg, Germany) at room temperature for 1 h. Excessive dye was washed off in distilled water and images were taken the following morning.

Western blot

Primary antibodies used were anti-α-tubulin (1:10,000) antibody (12G10, Developmental Studies Hybridoma Bank, University of Iowa, Iowa City, IA) and anti-WT1 (1:1000) antibody (12609-1-AP, Protein Tech Group, Rosemont, IL). Licor (Lincoln, NE) IRDye 680RD goat anti-mouse IgG and IRDye 800CW goat anti-rabbit IgG secondary antibodies (1:10,000) were used for visualization on a LI-COR Odyssey Classic imager. Image analysis was performed using the LI-COR Application Software Version 3.0.

Animals

All animal protocols were approved by the UCSD Institutional Animal Care and Use Committee. Mice were housed and monitored in accordance with institutional guidelines.

Leukocyte cell collection and isolation

Peripheral blood was collected via submandibular vein bleeding[60]. Bone marrow cells were harvested by flushing two femurs per mouse with ice cold PBS using disposable syringes with 21-gauge needles. Spleen and liver leukocytes were harvested by physical tissue disruption and repeated pipetting in ice cold PBS. Red cell lysis was performed by resuspending cell mixture in ice cold ACK buffer (0.1 mM Na_2EDTA, 10 mM $KHCO_3$, 150 mM NH_4Cl) for 5 min, followed by washing with ice cold PBS and passage through a 40-μM cell strainer (Thermo Fisher Scientific) to eliminate large

tissue/cell clumps and debris. Live leukocytes were enriched via ficoll (Cytiva, Amersham, United Kingdom) gradient centrifugation. Viable cells were counted via trypan blue exclusion using a TC20 Automated Cell Counter (Bio-Rad Laboratories, Hercules, CA) to infer total cell numbers.

Multimer Staining

Prior to multimer staining, isolated cells were treated with 50 nM dasatanib[61] (R&D Systems, Minneapolis, MN) for 30 min at 37°C and then Fc receptors were blocked for 10 minutes on ice. Tetramer (MBL international, Woburn, MA) or Dextramer (immudex, Copenhagen, Denmark) staining was performed according to manufacturer's protocols. For tetramer staining, cells were washed twice prior to additional of cell surface antibody staining.

Generating BMDCs

Bone marrow cells were harvested by flushing two femurs per C57BL/6J mice (The Jackson Laboratory, Bar Harbor, ME) with ice cold PBS using disposable syringes with 21-gauge needles. Live cells were cultured in BMDC culture medium in untreated petri dishes at a density of 2×10^6 cells per plate. After 3 days, an additional 10 ml of BMDC culture medium was added to each dish. On day 7, non-adherent and loosely adherent cells were removed. Purified mouse BMDCs were analyzed for purity by flow cytometry (Supplementary Table 1.1.) before use in associated experiments.

AMCNP acquisition by BMDCs

BMDCs were seeded into 4-well Nunc chamber slides (Thermo Fisher Scientific) at a density of 1×10^5 cells/well and allowed to adhere overnight. FAM-labeled CpG-

encapsulated AMCNPs (C1498 or C1498-OVA) or equivalent amounts of free FAM-labeled CpG were added into each well at a final CpG concentration of 100 nM, either 24 h or 30 min before imaging. The media was discarded, and cells were washed three times with PBS to remove any free nanoparticles or FAM-labeled CpG. BMDCs were then fixed for 15 min at room temperature in 10% buffered formalin (Thermo Fisher Scientific) and washed three times as before. The chamber was finally removed, and the slide was mounted with VECTASHIELD mounting media with DAPI (Vector Laboratories, Burlingame, CA). Images were acquired with a Keyence BZ-X710 fluorescence microscope using a 40× objective lens equipped with the DAPI and GFP filters (UCSD Specialized Cancer Center Support P30 Grant 2P30CA023100).

AMCNP acquisition by DC2.4 murine DC cell line

DC2.4 were seeded into 24-well suspension plates (Genesee Scientific) at a density of 2.5×10^4 cells/well and allowed to adhere overnight. At various times before analysis (24 h, 12 h, 6 h, 2 h, 1 h, 30 min, 15 min, and 0 min), DiD-labeled CpG-AMCNPs (C1498-MIP) were added into each well at a final CpG concentration of 250 nM. The media was collected, and any adhered cells were detached with 0.25% Trypsin-EDTA (Gibco). The cells were spun at 700 *g* for 5 min and free nanoparticles were washed three times with 1% (w/v) bovine serum albumin (BSA, Millipore Sigma, Burlington, MA) in PBS. FITC-labeled Annexin V (Biolegend) was used to stain the cells at room temperature for 15 min as a viability dye and data was acquired with a BD FACSCanto II flow cytometer (BD Biosciences, San Jose, CA).

In vivo delivery

To monitor nanoparticle trafficking *in vivo*, 50 µl of each nanoformulation was injected subcutaneously through the right hock of six-week-old C57BL/6NHsd mice (Envigo, Indianapolis, IN). Mice were euthanized 24 h later via carbon dioxide asphyxiation followed by cervical dislocation, and the organs were excised. All organs were mechanically homogenized with a pipette and processed into a single cell suspension. The spleens were filtered with a 70-µm mesh cell strainer (Thermo Fisher Scientific) and the draining lymph nodes were filtered with a 40-µm Flowmi cell strainer (Bel Art Products, Wayne, NJ). Red blood cells were lysed using a commercial RBC lysis buffer (Biolegend, San Diego, CA) before the cells were blocked with 1% BSA (Millipore Sigma) in PBS on ice for 15 min and with TruStain FcX PLUS anti-mouse CD16/32 antibody (Biolegend) for 10 min. Cells were stained as indicated (Supplementary Table 1.1) and analyzed by flow-cytometry.

AMCNP prophylactic vaccination

8- to 12-week-old C57BL/6J mice (The Jackson Laboratory) were vaccinated via subcutaneous hock injection with 50 µL of 25 mg/ml of C1498-OVA AMCNPs, or mock treatment with equivalent CpG, on days 0, 7, and 14. On day 21, mice were challenged with 5×10^5 C1498-OVA cells via intravenous inoculation. Mice were monitored for signs of morbidity as an endpoint.

Figure 1.1. Schematic of AML membrane-coated nanoparticles (AMCNPs) production and anti-leukemic vaccination. (**A**) The immunostimulatory adjuvant, CpG oligodeoxynucleotide 1826, was encapsulated into biodegradable poly (lactic-*co*-glycolic acid) (PLGA) polymer nanoparticle cores (small grey spheres) via a double emulsion process. Through sonication, CpG-loaded nanoparticle cores were coated with isolated AML cell membrane (red circle), including membrane associated MHC-I-presented antigens (blue, green, purple, and yellow dots), to form AMCNPs. (**B**) Delivery of AMCNPs to immature APCs (blue cell) stimulates maturation and AML-associated antigen presentation. The mature APCs (blue cell) present AML antigens and co-stimulatory molecules to naïve T cells (green cells), resulting in activation and proliferation of T cells specific for different AML antigens (blue, green). Activated T cells (green cells) can initiate AML cell death, after detecting the MHC-I-presented antigens on AML cells (red cells).

A **AMCNP Vaccine Production:**

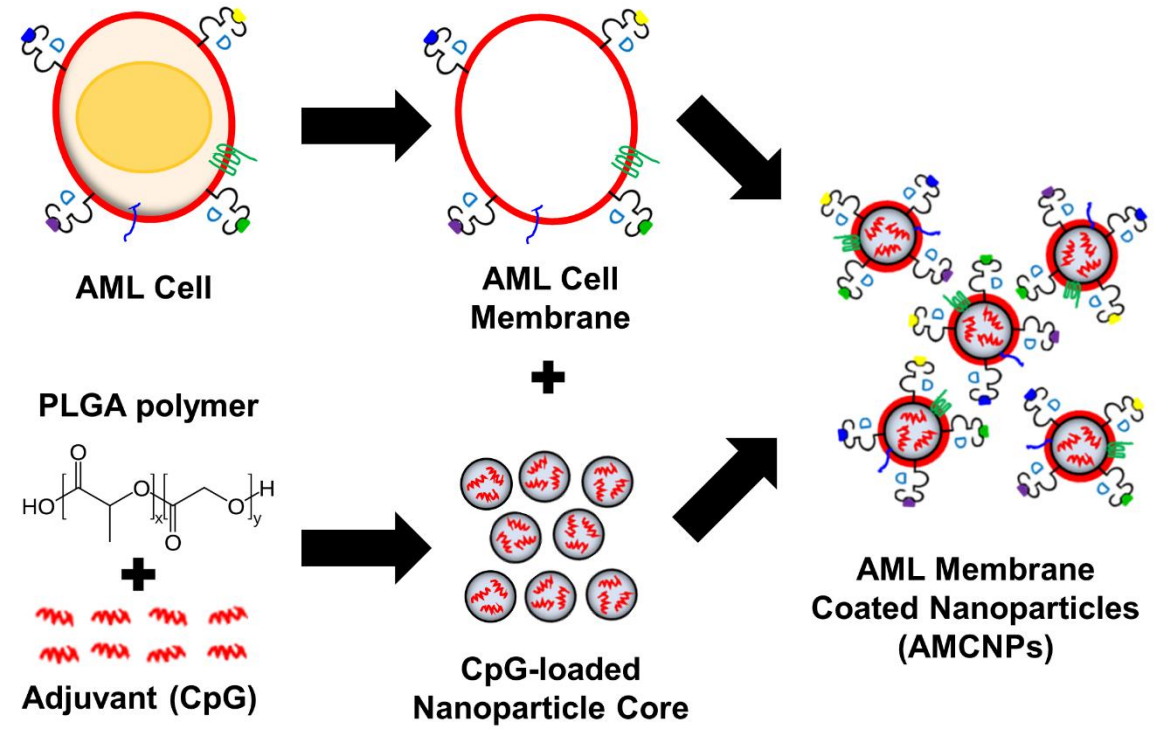

B **AMCNP Anti-AML Immune Activation:**

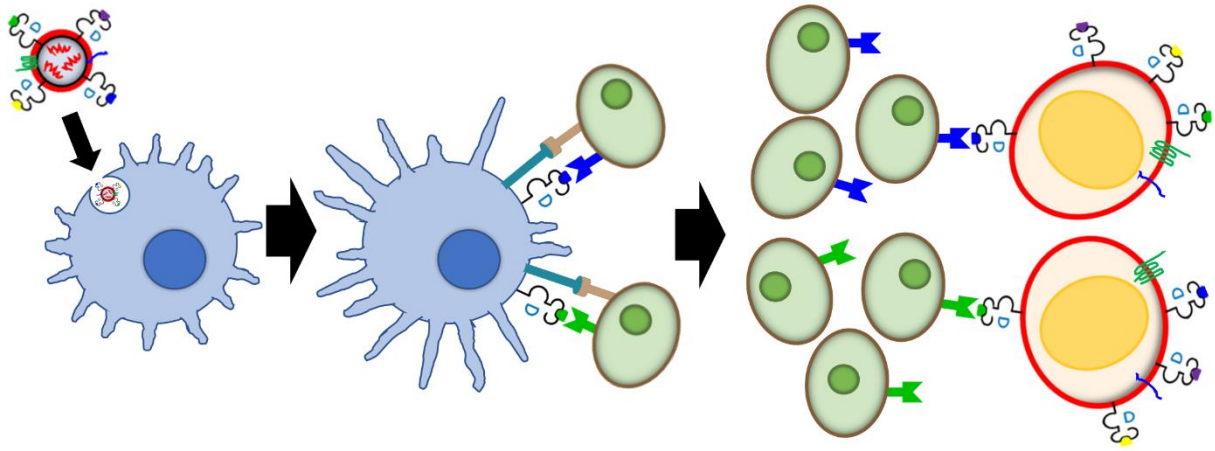

Figure 1.2. Characterization of C1498-OVA cell line. (**A**) MIP vector and MIP-OVA retrovirus constructs used in generation of C1498-MIP and C1498-OVA cell lines. The murine *Cadm1* signal peptide (SP) and transmembrane domain (TMD) were cloned 5' to full length chicken ovalbumin into the MIP vector. (**B**) Representative flow cytometry plots and histogram of C1498-MIP and C1498-OVA cell lines stained with antibodies against MHC class I-presented OVA peptide 257-264 (H-2K^{b}:SIINFEKL), which demonstrate OVA antigen presentation in C1498-OVA cells compared to C1498-MIP or fluorescence minus one (FMO) negative control staining. (**C**) OVA-specific T cell (B3Z) lacZ activation assay. C1498-MIP or C1498-OVA cells were incubated with B3Z T cell hybridoma reporter cells, in which OVA-specific T cell receptor activation drives lacZ expression. Representative image demonstrating OVA-specific T cell activation (red color) in B3Z lysates, as assayed with the β-gal substrate chlorophenol red-β-galactoside (CPRG).

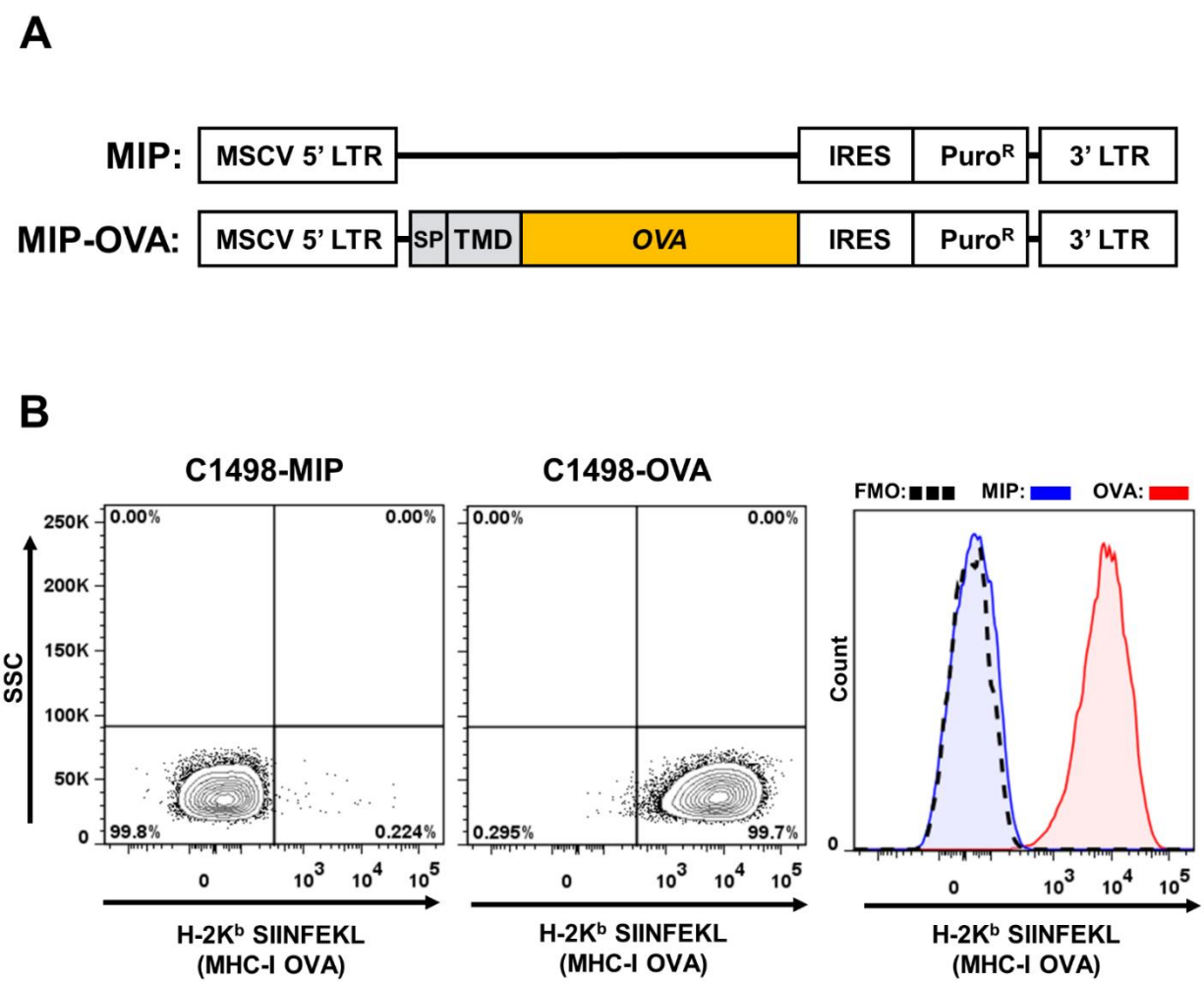
A
MIP:
MSCV 5' LTR
IRES
Puro^R
3' LTR
MIP-OVA:
MSCV 5' LTR
SP
TMD
OVA
IRES
Puro^R
3' LTR
B
C1498-MIP
C1498-OVA
FMO:
MIP:
OVA:
SSC
Count
250K
200K
150K
100K
50K
0
0.00%
0.00%
99.8%
0.224%
0.295%
99.7%
H-2K^b SIINFEKL
(MHC-I OVA)
C
B3Z (High)
B3Z (Low)
No APC
No B3Z
C1498 -MIP
C1498 -OVA

Figure 1.3. Characterization of AMCNPs. (**A, B**) Uncoated nanoparticles (CpG NP), AMCNPs (C1498, C1498-MIP, and C1498-OVA), and isolated membrane material (C1498, C1498-MIP, and C1498-OVA) were analyzed for size (A) and zeta potential (B) through dynamic light scattering analysis. (**C**) Representative transmission electron microscopy images of C1498, C1498-MIP, and C1498-OVA AMCNPs. (**D**) Coomassie blue staining of whole cell lysates, isolated membrane material, and AMCNPs from C1498, C1498-MIP, and C1498-OVA cells.

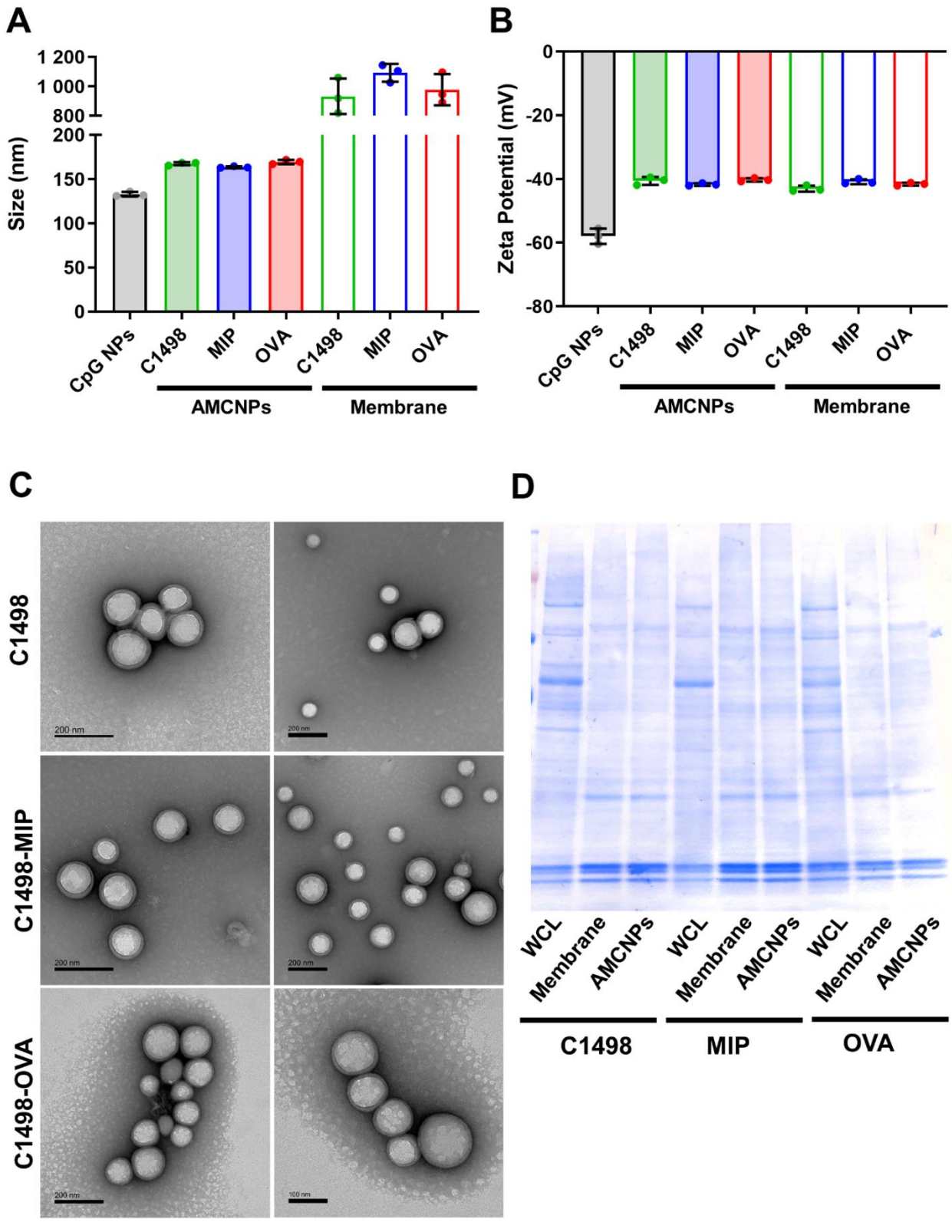
A
Size (nm)
1 200
1 000
800
200
150
100
50
0
CpG NPs
C1498
MIP
OVA
C1498
MIP
OVA
AMCNPs
Membrane
B
Zeta Potential (mV)
0
-20
-40
-60
-80
CpG NPs
C1498
MIP
OVA
C1498
MIP
OVA
AMCNPs
Membrane
C
C1498
C1498-MIP
C1498-OVA
200 nm
100 nm
D
WCL
Membrane
AMCNPs
C1498
MIP
OVA

Figure 1.4: AMCNPs are taken up by APCs efficiently, stimulate maturation, and promote antigen presentation. (**A**) BMDCs were pulsed for 30 min with free dye-labeled CpG or equivalent C1498-OVA AMCNPs with encapsulated dye-labeled CpG. Representative images show cellular DNA staining by DAPI (blue), labeled CpG (green), and merged. (**B**) BMDCs were pulsed for 2 h with C1498-OVA AMCNPs, equivalent C1498-OVA whole cell lysate (WCL) vaccine, or OVA SIINFEKL peptide with CpG. 48 h post-pulsing, $CD11c^+$ BMDCs were gated for high expression of the activation markers CD40, CD80, CD86, and MHC-II. Activated $CD11c^+CD40^{hi}$ BMDCs were further gated for MHC-I presentation of OVA ($H\text{-}2K^b$:SIINFEKL). Data is presented as the mean percentage of total live BMDCs. (**C**) Labeled C1498 AMCNPs or mock controls were injected into C57BL/6 mice via the hock. 24 h post-injection, $CD11c^+$ cells in the draining lymph node (dLN) and spleen were examined for presence of labeled C1498 AMCNPs. Representative flow cytometry plots are shown. (**D**) Mice received mock, C1498-OVA WCL, or equivalent C1498-OVA AMCNP vaccination. 24 h post-vaccination, $CD11c^+$ cells in the dLN were gated for high expression of CD80, CD83, CD86, and MHC-II. Data is presented as mean percentage of total live cells. Significance was determined using one-way ANOVA with a post-hoc test using the Holm-Šídák method.

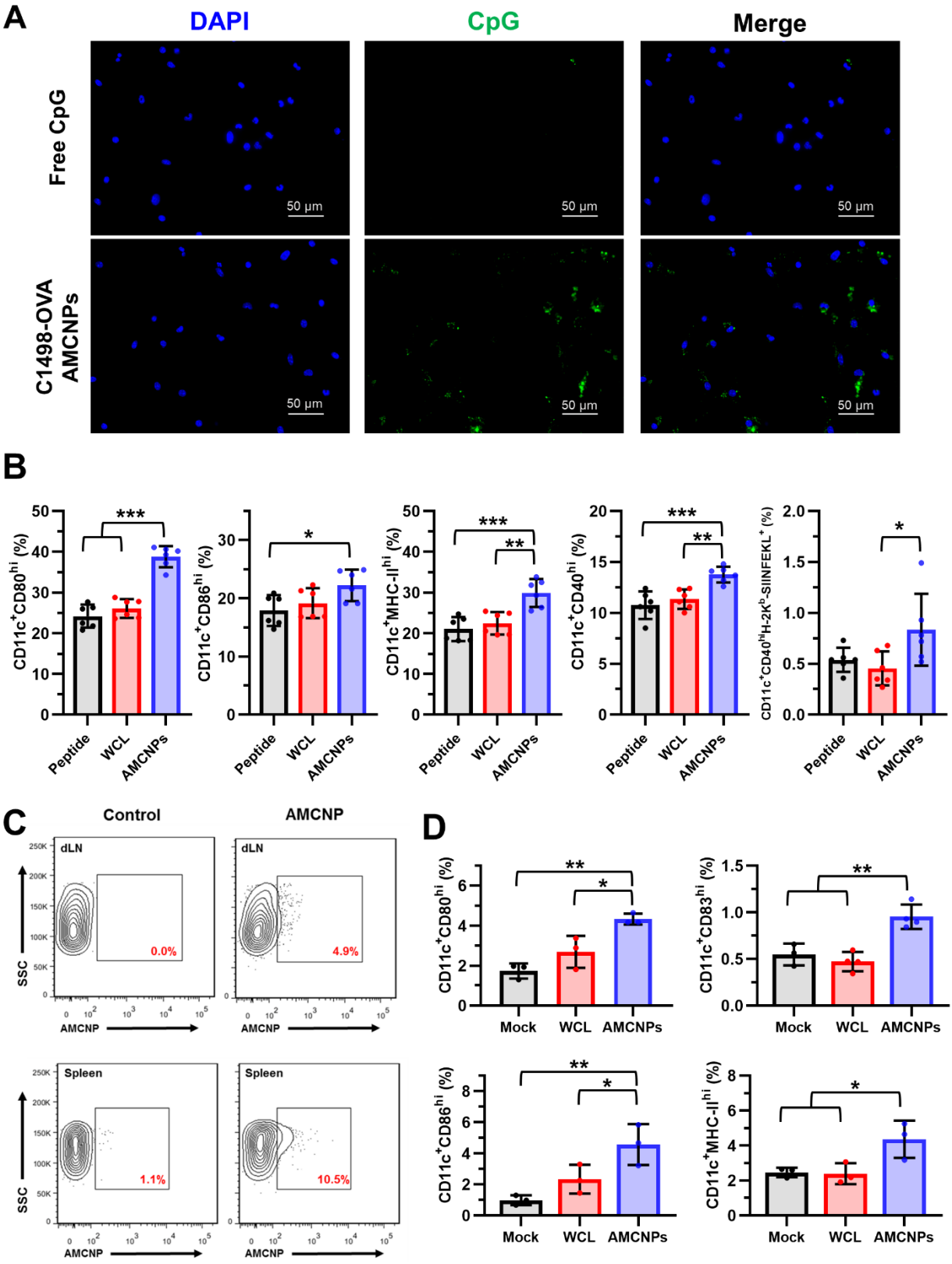
A
DAPI
CpG
Merge
Free CpG
C1498-OVA AMCNPs
50 μm
B
CD11c+CD80hi (%)
CD11c+CD86hi (%)
CD11c+MHC-IIhi (%)
CD11c+CD40hi (%)
CD11c+CD40hiH-2Kb-SIINFEKL+ (%)
Peptide
WCL
AMCNPs
C
Control
AMCNP
dLN
Spleen
SSC
AMCNP
0.0%
4.9%
1.1%
10.5%
D
CD11c+CD80hi (%)
CD11c+CD83hi (%)
CD11c+CD86hi (%)
CD11c+MHC-IIhi (%)
Mock
WCL
AMCNPs

Figure 1.5. AMCNPs enhance antigen-specific T cell activation. (**A**) BMDCs were pulsed with C1498-MIP AMCNPs or C1498-OVA AMCNPs before co-culture with B3Z T cells. OVA-specific B3Z T cell activation was measured by a CPRG assay. Data shown as mean optical density at 570 - 650 nm from 3 experiments. Significance was determined by unpaired *t*-test. (**B-D**) Mice were vaccinated 3 times as indicated, with C1498-MIP AMCNPs, equivalent C1498-OVA WCL vaccine, or C1498-OVA AMCNPs; splenocytes were collected and re-stimulated *ex vivo* with OVA SIINFEKL peptide for 7 days (n = 3). (**C**) OVA-specific T cell expansion was measured by H-2K^{b}:SIINFEKL tetramer staining of CD3^{+}CD8^{+} T cells. Data is presented as the mean frequency of CD3^{+}CD8^{+}OVA tetramer^{+} cells among CD3^{+} cells. (**D**) The concentration of secreted IFN-γ was measured by ELISA. (**C,D**) Significance was determined using one-way ANOVA with a post-hoc test using the Holm-Šídák method. (**E,F**) Mice were vaccinated 3 times, as indicated, with C1498-OVA AMCNPs (n = 3), equivalent C1498-OVA WCL vaccine (n = 3), or mock vaccination control (n = 3). Total number of CD69^{+} or CD25^{+} CD8^{+} T cells among peripheral blood (PB) mononuclear cells was determined by flow cytometry on day 17 and normalized to 1 ml of PB. Significance was determined using one-way ANOVA with a post-hoc test using the Holm-Šídák method. (**G-J**) Mice were vaccinated 3 times, as indicated, with C1498-OVA AMCNPs (n = 9) or equivalent C1498-OVA WCL vaccines (n = 8). (**H,I**) OVA-specific T cell expansion was determined through staining with H-2K^{b}:SIINFEKL dextramer (OVA-dextramer) of PB mononuclear cells on day 21. (**H**) Total CD3^{+}CD8^{+}OVA dextramer^{+} events observed were normalized to 1 ml of PB and adjusted for background staining by subtracting the average number of events in unvaccinated controls (n = 5). Significance was determined using one-way ANOVA with a post-hoc test using the Holm-Šídák method. (**I**) Representative flow cytometry plots of CD3^{+} gated live cells used to quantify CD3^{+}CD8^{+}OVA dextramer^{+} events are shown. (**J**) OVA-specific central memory (CM, CD62L^{hi}CD44^{hi}CD8^{+}OVA dextramer^{+}) and effector memory (EM, CD62L^{low}CD44^{hi}CD8^{+}OVA dextramer^{+}) expansion was determined through flow cytometry of live splenocytes on day 57. Total events observed were normalized to the total number of live splenocytes collected and adjusted for background staining by subtracting the average number of events in unvaccinated controls (n = 5). Significance was determined using one-way ANOVA with a post-hoc test using the Holm-Šídák method.

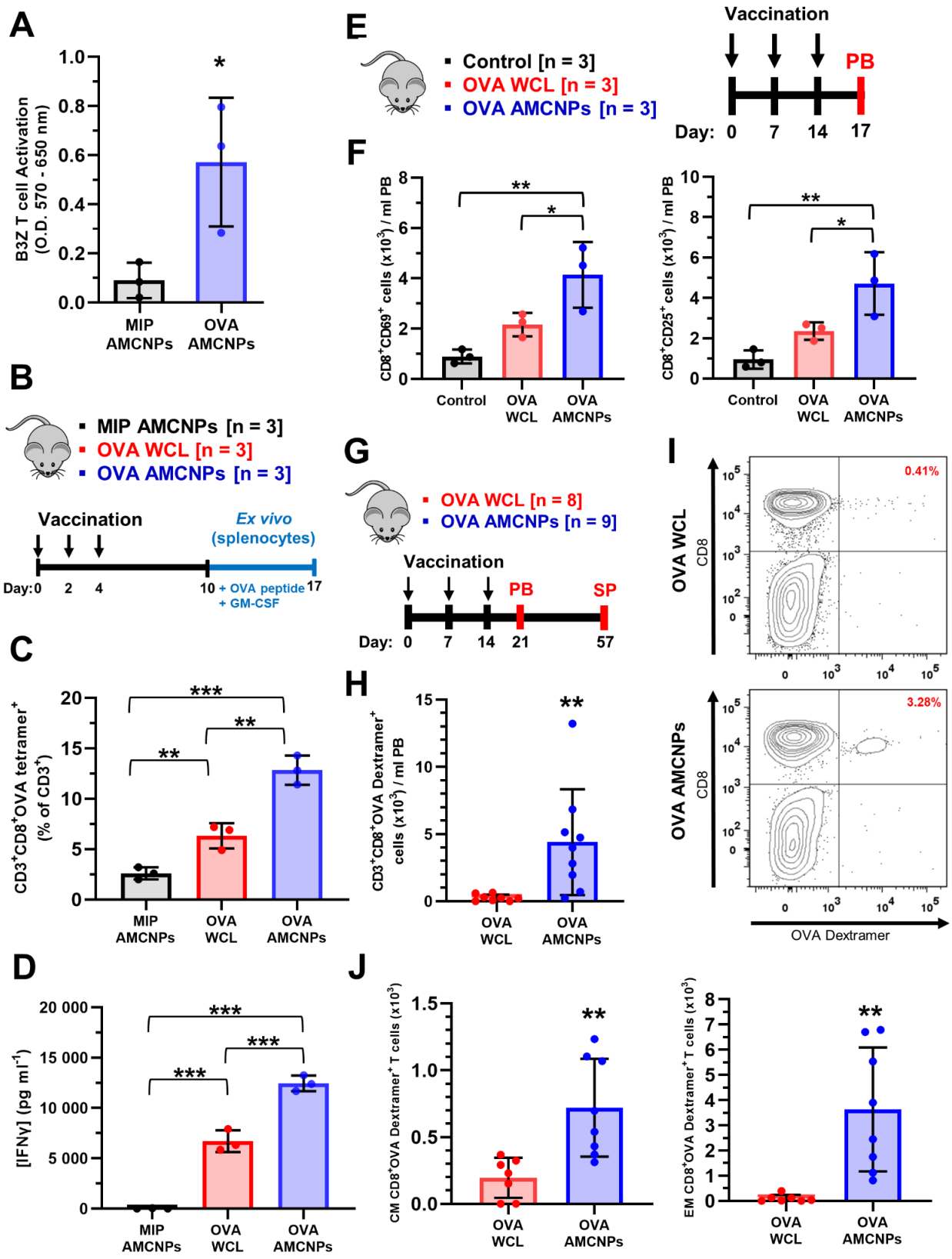
A
B3Z T cell Activation (O.D. 570 - 650 nm)
MIP AMCNPs
OVA AMCNPs
B
MIP AMCNPs [n = 3]
OVA WCL [n = 3]
OVA AMCNPs [n = 3]
Vaccination
Ex vivo (splenocytes)
Day: 0 2 4 10 17
+ OVA peptide + GM-CSF
C
CD3+CD8+OVA tetramer+ (% of CD3+)
D
[IFNγ] (pg ml-1)
E
Control [n = 3]
OVA WCL [n = 3]
OVA AMCNPs [n = 3]
Vaccination
PB
Day: 0 7 14 17
F
CD8+CD69+ cells (x10³) / ml PB
CD8+CD25+ cells (x10³) / ml PB
Control
OVA WCL
OVA AMCNPs
G
OVA WCL [n = 8]
OVA AMCNPs [n = 9]
Vaccination
PB
SP
Day: 0 7 14 21 57
H
CD3+CD8+OVA Dextramer+ cells (x10³) / ml PB
I
OVA WCL
OVA AMCNPs
CD8
OVA Dextramer
0.41%
3.28%
J
CM CD8+OVA Dextramer+ T cells (x10³)
EM CD8+OVA Dextramer+ T cells (x10³)

Figure 1.6. Post-remission AMCNP vaccination promotes long-lasting anti-leukemic immunity and survival benefit. (**A**) Mice were challenged with 1×10^5 C1498 cells, followed by either cytarabine and doxorubicin chemotherapy or mock chemotherapy (n = 7). (**B**) Mice were then vaccinated at 26-, 33-, and 40-days post-challenge with C1498 AMCNPs (n = 13) or equivalent C1498 whole cell lysate vaccine (WCL) (n = 15). Unvaccinated "chemotherapy only" mice were used as controls (n = 5). (**C**) Surviving mice were re-challenged at day 163 with 2×10^6 C1498 cells. Kaplan–Meier survival plots are shown with significance determined by the Mantel-Cox test. (**D-G**) Mice were challenged with 1×10^5 C1498 cells, followed by cytarabine and doxorubicin chemotherapy. Mice were then vaccinated at 26-, 33-, and 40-days post-challenge with C1498 AMCNPs (n = 4) or equivalent C1498 WCL vaccine (n = 4). Mice were re-challenged at day 72 with 2×10^6 C1498-eGFP cells and analyzed at day 93. (**E**) Frequency of $eGFP^+$ cells among mononuclear cells isolated from the bone marrow (BM) or liver of vaccinated mice. Representative flow plots are shown. (**F**) MFI of PD-1 expression among BM and liver $CD3^+$ T cells from AMCNP-vaccinated and WCL-vaccinated mice. (**G**) Splenic $CD3^+CD8^+$ T cells from AMCNP-vaccinated and WCL-vaccinated mice were analyzed for the frequency of naïve T cells ($CD62L^{hi}CD44^{low}$). Significance was determined using unpaired *t*-tests.

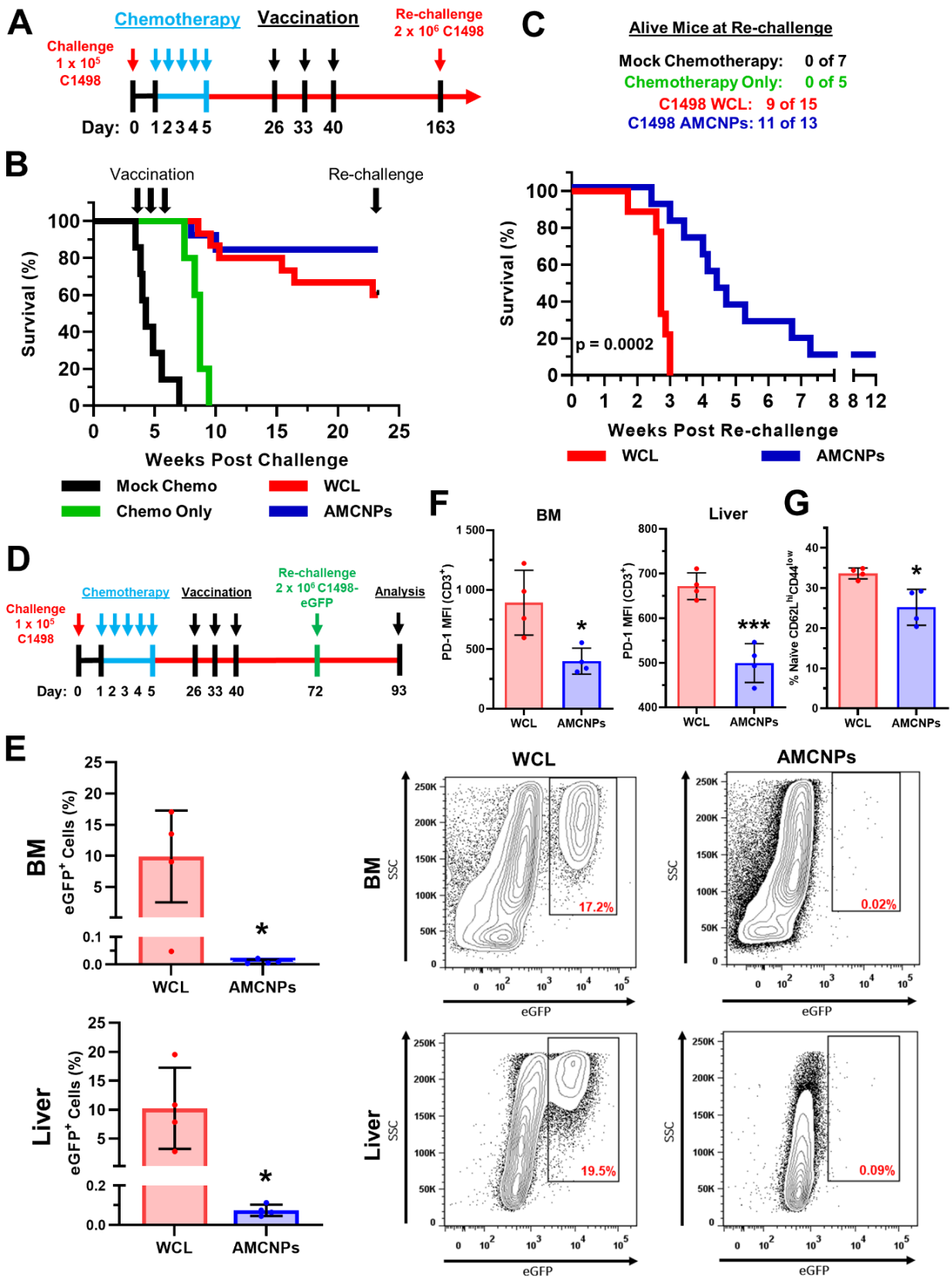
A
Chemotherapy
Vaccination
Re-challenge
2 x 10⁶ C1498
Challenge
1 x 10⁵
C1498
Day: 0 1 2 3 4 5 26 33 40 163
C
Alive Mice at Re-challenge
Mock Chemotherapy: 0 of 7
Chemotherapy Only: 0 of 5
C1498 WCL: 9 of 15
C1498 AMCNPs: 11 of 13
B
Vaccination
Re-challenge
Survival (%)
Weeks Post Challenge
Mock Chemo
Chemo Only
WCL
AMCNPs
Survival (%)
p = 0.0002
Weeks Post Re-challenge
WCL
AMCNPs
D
Challenge
1 x 10⁵
C1498
Chemotherapy
Vaccination
Re-challenge
2 x 10⁶ C1498-
eGFP
Analysis
Day: 0 1 2 3 4 5 26 33 40 72 93
F
BM
Liver
PD-1 MFI (CD3⁺)
WCL
AMCNPs
G
% Naive CD62L^hiCD44^low
E
BM
Liver
eGFP⁺ Cells (%)
WCL
AMCNPs
SSC
eGFP
17.2%
0.02%
19.5%
0.09%

Supplementary Table 1.1. Flow-cytometry staining schemes.

Experiment	Antibody/Viability Stain	Manufacturer	Clone	Catalog#
C1498-OVA MHC-I presentation	H-2K^{b} bound to SIINFEKL PE	Biolegend	25-D1.16	141604
	7-AAD	Biolegend		420404
BMDC maturation stain #1	CD80 PE	Biolegend	16-10A1	104707
	CD86 APC	eBioscience	GL1	17-0862-82
	CD11c APC-Cy7	Biolegend	N418	117324
	I-A/I-E (MHCII) FITC	Biolegend	MF5/114.15.2	107606
	F4/80 PerCP-Cy5.5	eBioscience	BM8	15-4801-82
	7-AAD	Biolegend		420404
BMDC maturation stain #2	H-2K^{b} bound to SIINFEKL PE	Biolegend	25-D1.16	141604
	CD40 APC	eBioscience	1C10	17-0401-82
	CD11c APC-Cy7	Biolegend	N418	117324
	F4/80 PerCP-Cy5.5	eBioscience	BM8	15-4801-82
	7-AAD	Biolegend		420404
In vivo DC maturation stain #1	CD80 PE	Biolegend	16-10A1	104707
	CD86 APC	eBioscience	GL1	17-0862-82
	CD11c APC-Cy7	Biolegend	N418	117324
	I-A/I-E (MHCII) FITC	Biolegend	MF5/114.15.2	107606
	F4/80 PerCP-Cy5.5	eBioscience	BM8	15-4801-82
	7-AAD	Biolegend		420404
In vivo DC maturation stain #2	H-2K^{b} bound to SIINFEKL PE	Biolegend	25-D1.16	141604
	CD40 APC	eBioscience	1C10	17-0401-82
	CD11c APC-Cy7	Biolegend	N418	117324
	F4/80 PerCP-Cy5.5	eBioscience	BM8	15-4801-82
	7-AAD	Biolegend		420404
In vivo DC maturation stain #3	CD83 FITC	Biolegend	Michel-19	121506
	CD11c APC-Cy7	Biolegend	N418	117324
	7-AAD	Biolegend		420404
Ex vivo OVA Tetramer	CD3 APC	eBioscience	145-2C11	17-0031-82
	CD8a FITC	Biolegend	53-6.7	100706
	iTAg Tetramer-H-2K^{b} OVA (SIINFEKL) PE	MBL International		TB-5001-1
	7-AAD	Biolegend		420404
In vivo OVA Dextramer (PB)	CD8a PE	Biolegend	53-6.7	100708
	CD3 FITC	Biolegend	17A2	100204
	H-2Kb OVA (SIINFEKL) MHC I Dextramer APC	immudex		JD2163
	7-AAD	Biolegend		420404
In vivo memory T cell OVA Dextramer (Spleen)	CD44 PE	Biolegend	IM7	103007
	CD62L FITC	Biolegend	MEL-14	104405
	H-2Kb OVA (SIINFEKL) MHC I Dextramer APC	immudex		JD2163
	CD8a PE-Cy7	Biolegend	53-6.7	100722
	7-AAD	Biolegend		420404
CD8^{+} T Cell activation	CD8a PE-Cy7	Biolegend	53-6.7	100722
	CD4 APC-Cy7	Biolegend	GK1.5	100414
	CD69 PE	Biolegend	H1.2F3	104507
	CD25 APC	Biolegend	PC61	102012
	7-AAD	Biolegend		420404
In vivo WT1 dextramer (PB)	CD8a PE	Biolegend	53-6.7	100708
	CD3 PE-Cy7	Biolegend	17A2	100220
	H-2 D^{b} WT1 (RMFPNAPYL) MHC I Dextramer APC	immudex		JA-2177
	7-AAD	Biolegend		420404
C1498-eGFP re-challenge BM, Liver, Stain #1	CD8a PerCP-Cy5.5	Biolegend	53-6.7	100734
	PD-1 FITC	Biolegend	29F.1A12	135214
	CD3 PE-Cy7	Biolegend	17A2	100220
C1498-eGFP re-challenge BM, Liver, Spleen Stain #2	CD44 PE	Biolegend	IM7	103007
	CD62L APC	Biolegend	MEL-14	104412
	CD4 FITC	Biolegend	RM4-5	100510
	CD8a PerCP-Cy5.5	Biolegend	53-6.7	100734
	CD3 PE-Cy7	Biolegend	17A2	100220
Checking BMDC purity	CD11c FITC	Biolegend	N418	117306
	F4/80 PerCP-Cy5.5	eBioscience	BM8	15-4801-82
	7-AAD	Biolegend		420404
Fc Block	(CD16/32)	Biolegend	93	101320

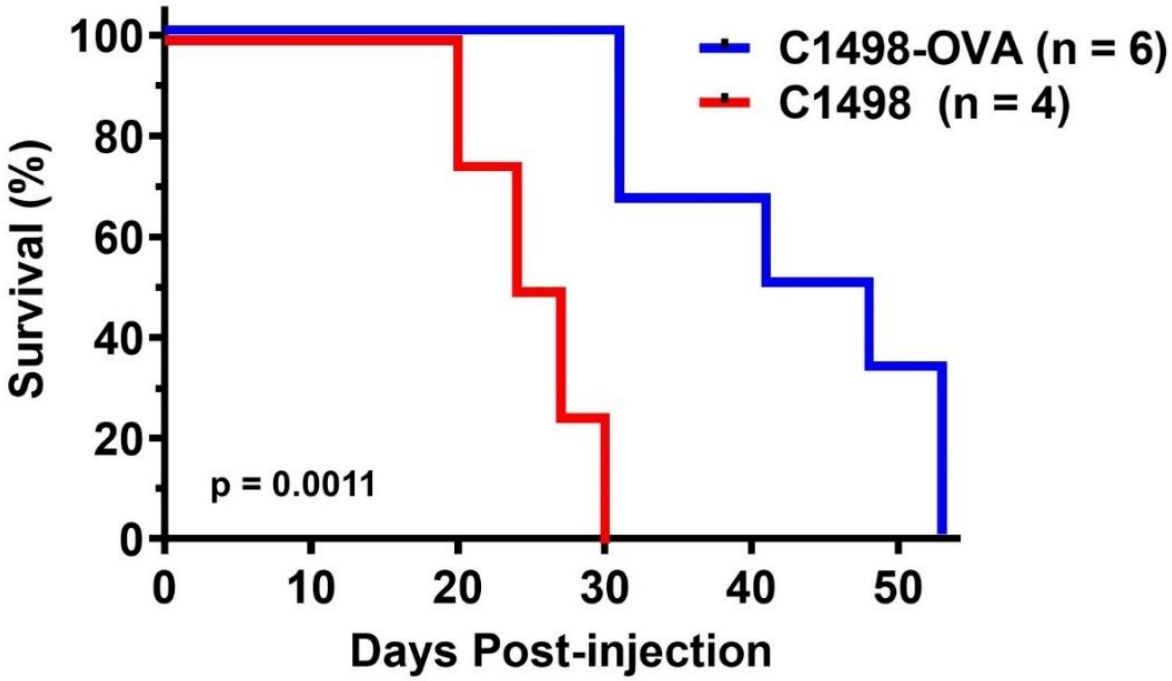

Supplementary Figure 1.1. C1498-OVA cells are leukemogenic. Kaplan-Meier survival plot for C57BL/6 mice injected with 5×10^5 C1498 (n = 4) or C1498-OVA cells (n = 6). Significance determined by the Mantel-Cox test.

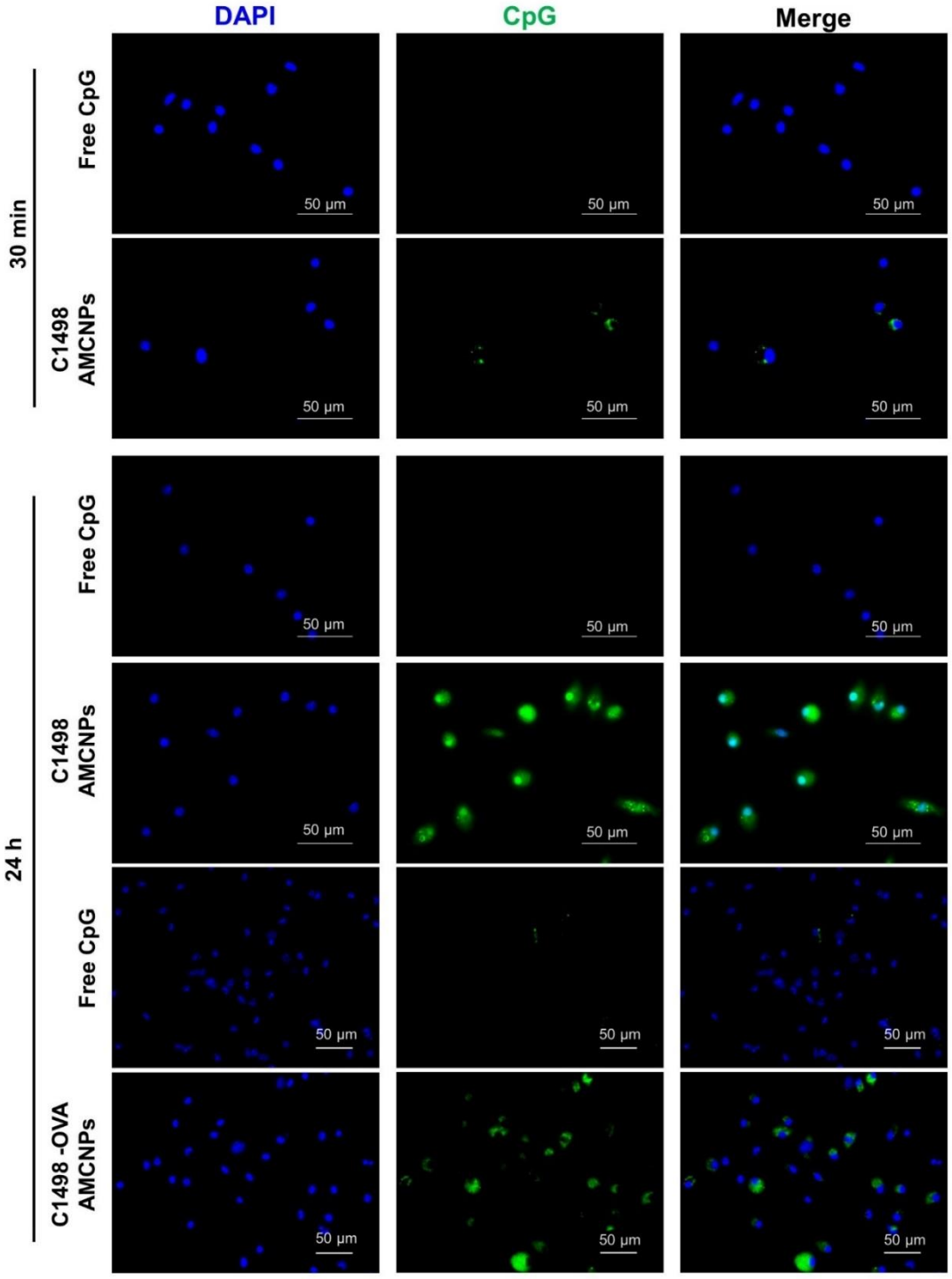

Supplementary Figure 1.2. *In vitro* AMCNP acquisition by BMDCs. BMDCs were pulsed for 30 min or 24 h with free dye-labeled CpG, or equivalent C1498-OVA or C1498 AMCNPs with encapsulated dye-labeled CpG. Representative images show cellular DNA staining by DAPI (blue), dye-labeled CpG (green), and merged.

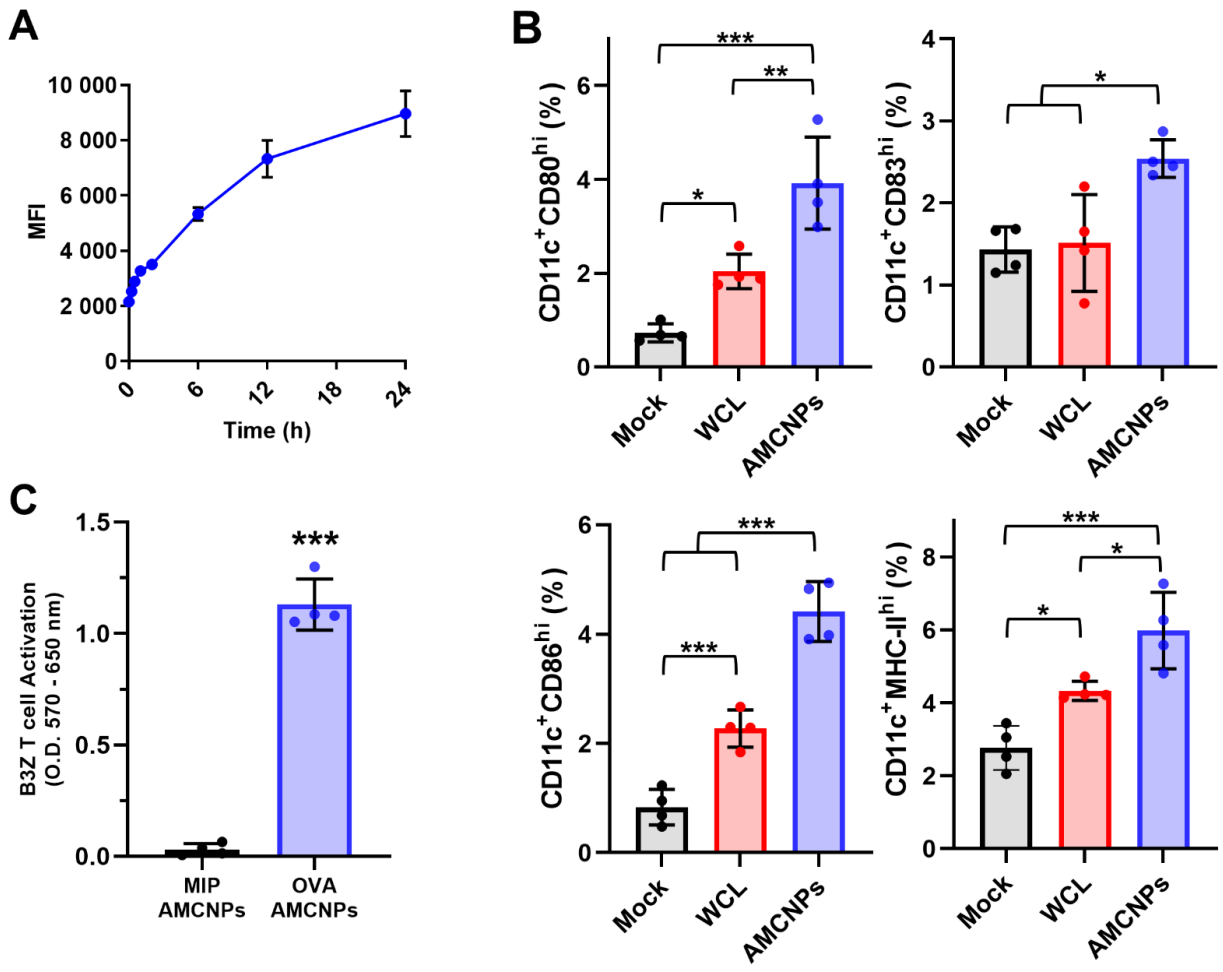

Supplementary Figure 1.3. Additional AMCNP acquisition, antigen presentation, and maturation data. (**A**) DC2.4 cells were pulsed with C1498-OVA AMCNPs with encapsulated dye-labeled CpG. AMCNP acquisition was detected through fluorescence over time. Data shown as mean fluorescence intensity (arbitrary units) from n = 3 biological replicates. (**B**) Mice received mock, C1498 WCL, or equivalent C1498 AMCNP vaccination. 24 h post-vaccination, $CD11c^+$ cells in the dLN were gated for high expression of CD80, CD83, CD86, and MHC-II. Data is presented as mean percentage of total live cells. Significance was determined using one-way ANOVA with a post-hoc test using the Holm- Šídák method. (**C**) DC2.4 cells were pulsed with C1498-MIP AMCNPs or C1498-OVA AMCNPs before co-culture with B3Z T cells. OVA-specific B3Z T cell activation was measured by CPRG assay. Data shown as mean optical density at 570 - 650 nm. Significance was determined by unpaired t-test.

Supplementary Figure 1.4. AMCNPs enhance AML associated antigen T cell response. (A) MIP-WT1 retrovirus constructs used in generation of the C1498-WT1 cell line. The full length murine *Wt1* cDNA was cloned into the MIP vector. (**B**) WT1 expression was confirmed in C1498-WT1 cells by western blot. (**C**) Mice were vaccinated 3 times, as indicated, with C1498-WT1 AMCNPs (n = 7) or equivalent C1498-WT1 WCL vaccines (n = 7). WT1-specific T cell expansion was determined through staining with H-2D^{b}: RMFPNAPYL dextramer (WT1-dextramer) on peripheral blood (PB) mononuclear cells on day 21. Total CD3^{+}CD8^{+}WT1-dextramer^{+} events observed were normalized to 1 ml of PB and adjusted for background staining by subtracting the average number of events in unvaccinated controls (n = 5). Significance was determined by unpaired t-test. (**D**) Mice were vaccinated 3 times as indicated, with C1498-WT1 AMCNPs or equivalent C1498-WT1 WCL vaccine; splenocytes were collected and re-stimulated *ex vivo* with WT1 RMFPNAPYL peptide for 7 days (n = 3), the concentration of secreted IFN-γ was measured by ELISA. Significance was determined by unpaired t-test.

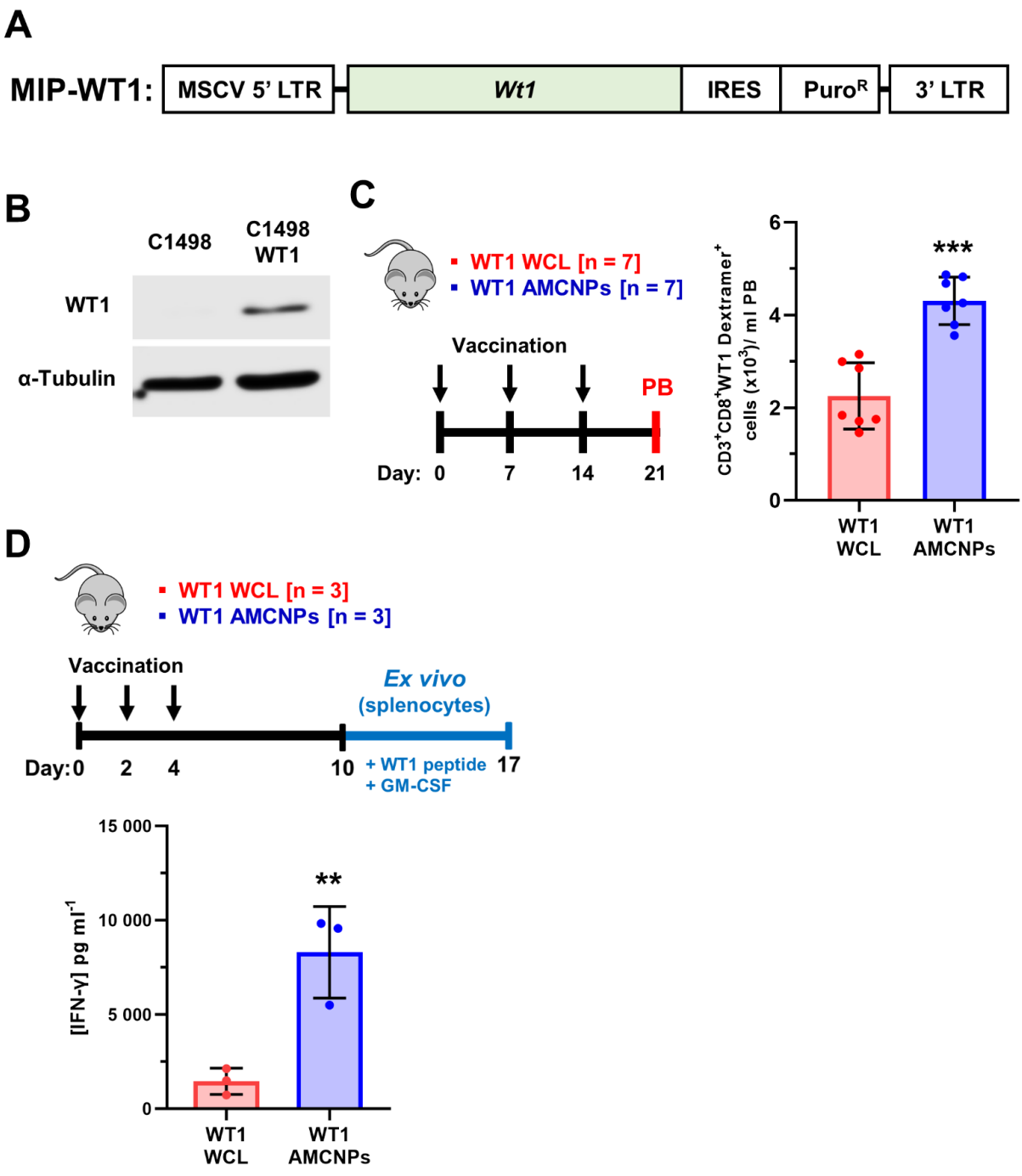
A
MIP-WT1:
MSCV 5' LTR
Wt1
IRES
PuroR
3' LTR
B
C1498
C1498 WT1
WT1
α-Tubulin
C
WT1 WCL [n = 7]
WT1 AMCNPs [n = 7]
Vaccination
PB
Day: 0 7 14 21
CD3+CD8+WT1 Dextramer+ cells (x10³)/ ml PB
***
WT1 WCL
WT1 AMCNPs
D
WT1 WCL [n = 3]
WT1 AMCNPs [n = 3]
Vaccination
Ex vivo (splenocytes)
Day: 0 2 4 10 + WT1 peptide + GM-CSF 17
[IFN-γ] pg ml-1
**
WT1 WCL
WT1 AMCNPs

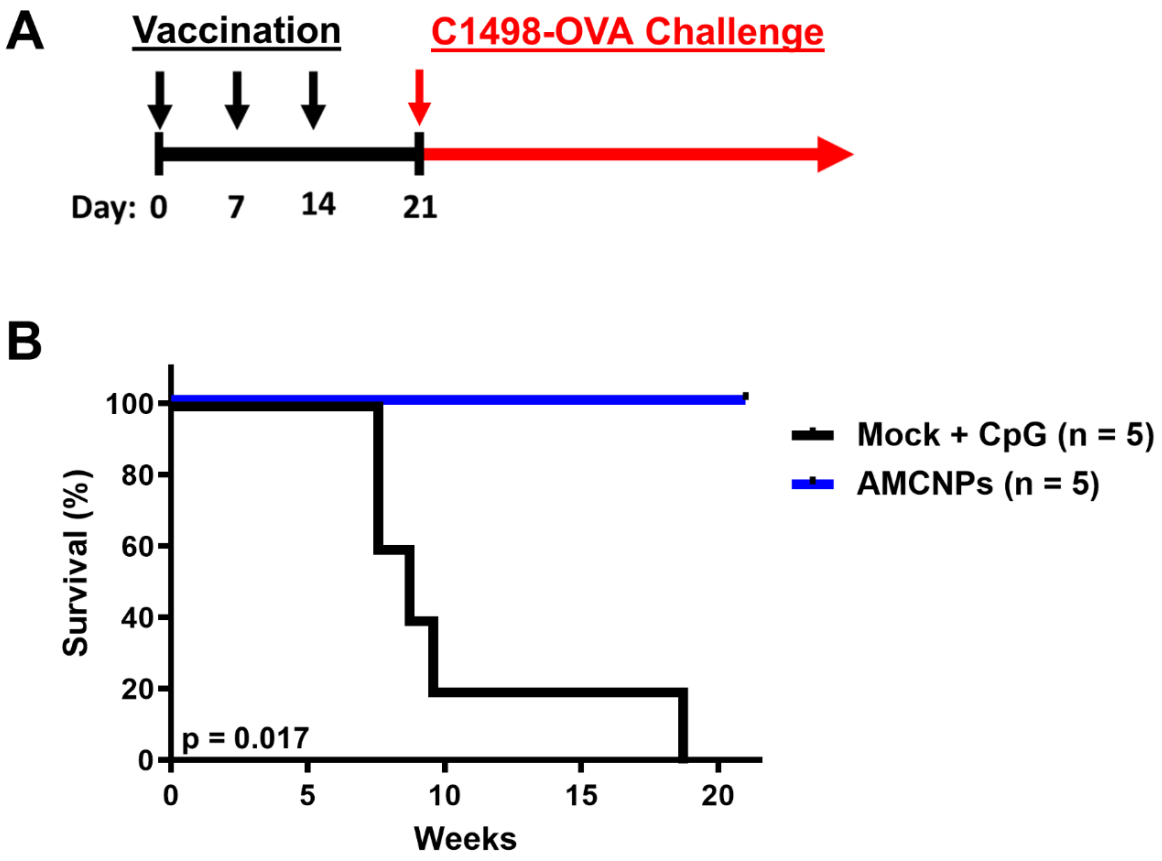

Supplementary Figure 1.5. Prophylactic AMCNP vaccination protects against C1498-OVA AML challenge. Supplementary Figure 1.5. Prophylactic AMCNP vaccination protects against C1498-OVA AML challenge. (A) Mice were vaccinated on days 0, 7, and 14 with 50 µl of 25 mg/ml C1498-OVA AMCNPs (n = 5) or mock with equivalent CpG (n = 5). At day 21, mice were challenged with 1×10^5 C1498-OVA cells. (B) Kaplan–Meier survival plot is shown with significance determined by the Mantel-Cox test.

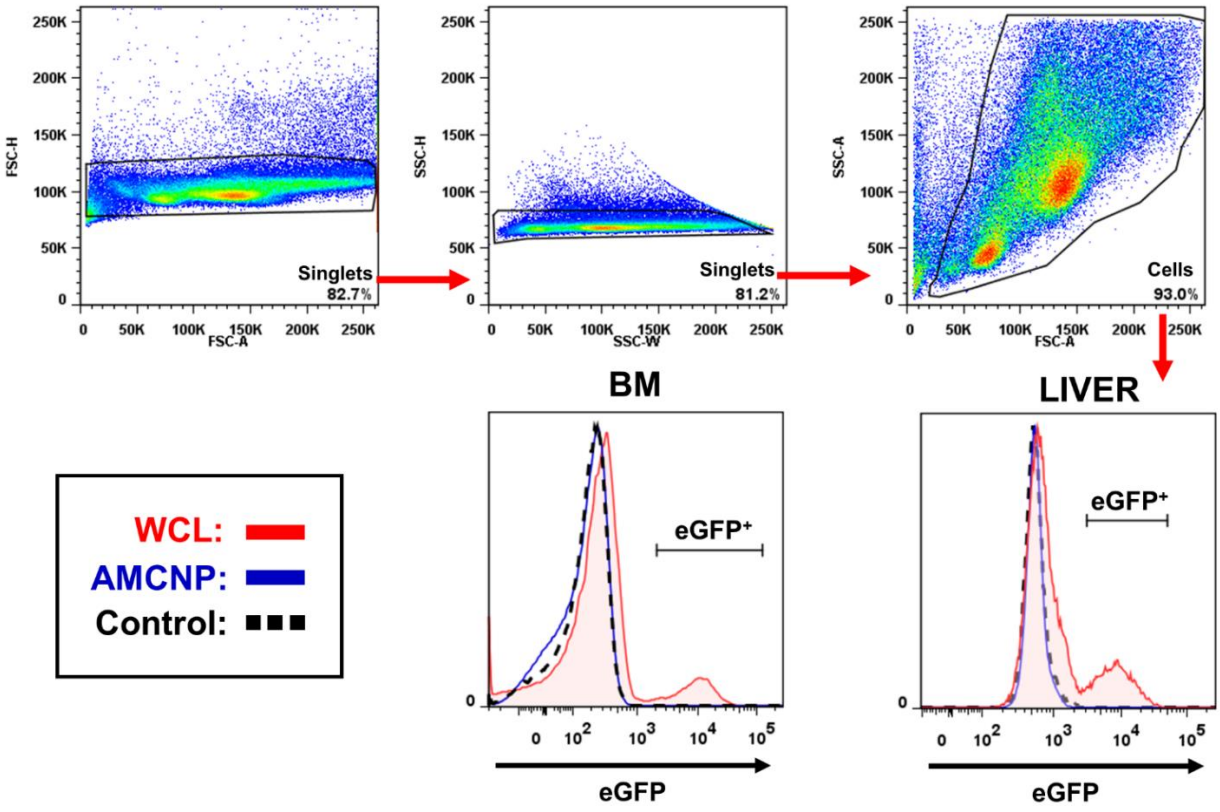

Supplementary Figure 1.6. Flow cytometry gating of C1498-eGFP re-challenge cells. Bone marrow and liver mononuclear leukocytes were isolated from the mice used in Figure 1.6D. Representative flow plots and histograms showing gating strategy used to examine live eGFP$^+$ cells from mice vaccinated with C1498 AMCNPs, C1498 whole cell lysate control vaccine (WCL), or healthy control mice (Control).

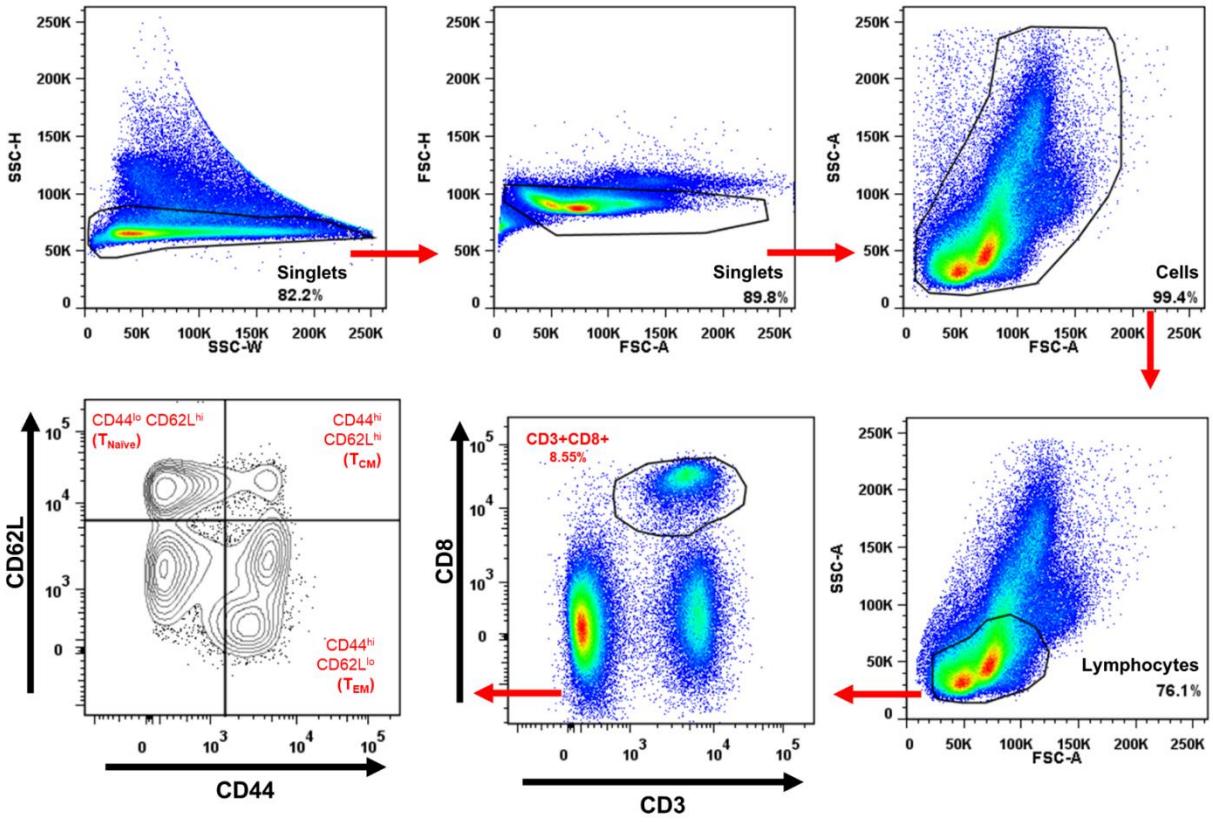

Supplementary Figure 1.7. Flow cytometry for splenic $CD3^{+}CD8^{+}$ memory T cell subsets. Splenic mononuclear cells were isolated from the mice used in Figure 6D. Representative gating of $CD3^{+}CD8^{+}$ $CD62L^{hi}$ $CD44^{low}$ naïve T cells used in Figure 6D.

ACKNOWLEDGMENTS

This chapter is a modified version of a paper that has been accepted for publication in *Leukemia* (Springer Nature Group) and authored by Daniel T. Johnson, Jiarong Zhou, Ashley V. Kroll, Ronnie H. Fang, Ming Yan, Crystal Xiao, Xiufen Chen, Justin Kline, Liangfang Zhang, and Dong-Er Zhang. The dissertation author is the primary investigator and writer of this manuscript. This work was supported by National Institutes of Health, National Cancer Institute grants R01CA104509 (D.E.Z), R01CA200574 (L.Z.), F31CA228324 (D.T.J), and T32CA009523 (D.T.J).

Chapter 2. MicroRNA let-7b downregulates AML1-ETO oncogene expression in t(8;21) AML by targeting its 3'UTR.

Acute myeloid leukemia (AML) with the t(8;21)(q22;q22) chromosomal translocation is among the most common subtypes of AML and produces the *AML1-ETO* (*RUNX1-ETO*, *RUNX1-RUNX1T1*) oncogenic fusion gene. AML1-ETO functions as an aberrant transcription factor which plays a key role in blocking normal hematopoiesis. Thus, the expression of AML1-ETO is critical to t(8;21) AML leukemogenesis and maintenance. Post-transcriptional regulation of gene expression is often mediated through interactions between *trans*-factors and *cis*-elements within transcript 3'-untranslated regions (UTR). *AML1-ETO* uses the 3'UTR of the *ETO* gene, which is not normally expressed in hematopoietic cells. Therefore, the mechanisms regulating AML1-ETO expression via the 3'UTR are attractive therapeutic targets. We used RNA-sequencing of t(8;21) patients and cell lines to examine the 3'UTR isoforms used by AML1-ETO transcripts. Using luciferase assay approaches, we test the relative contribution of 3'UTR *cis* elements to AML1-ETO expression. We further use let-7b microRNA mimics and anti-let-7b sponges for functional studies of t(8;21) AML cell lines. In this study, we examine the regulation of AML1-ETO via the 3'UTR. We demonstrate that *AML1-ETO* transcripts primarily use a 3.7 kb isoform of the *ETO* 3'UTR in both t(8;21) patients and cell lines. We identify a negative regulatory element within the *AML1-ETO* 3'UTR. We further demonstrate that the let-7b microRNA directly represses AML1-ETO through this site. Finally, we find that let-7b-5p inhibits the proliferation of t(8;21) AML cell lines, rescues expression of AML1-ETO target genes, and promotes differentiation. AML1-ETO is posttranscriptional regulated by let-7b,

which contributes to the leukemic phenotype of t(8;21) AML and may be important for t(8;21) leukemogenesis and maintenance.

2.1 INTRODUCTION

The t(8;21)(q22;q22) translocation is among the most common chromosomal abnormalities in AML[5]. Although t(8;21) AML is categorized as a favorable-risk AML, there remains a high incidence of relapse (up to 56% in some studies) and the median overall survival is only 5 years, highlighting the need for further studies and additional therapies[5, 62-65]. The t(8;21) translocation results in a fusion of the *AML1* (*RUNX1*) locus on chromosome 21 with the *ETO* (*MTG8*, *RUNX1T1*) locus on chromosome 8, creating the *AML1-ETO* (*RUNX1-ETO, RUNX1-RUNX1T1*) fusion gene[66]. AML1 is an essential transcription factor for healthy hematopoiesis[67]. The N-terminal runt homology domain (RHD) of *AML1* mediates sequence-specific DNA-binding whereas the C-terminal transcriptional regulatory domain controls target gene transcription through the recruitment of essential co-factors[67]. ETO (RUNX1T1) is not normally expressed in hematopoietic progenitor cells[68-70], does not have DNA binding activity [71], and interacts with transcriptional co-repressors and co-activators[66, 71-76]. The *AML1-ETO* chimeric transcript contains the N-terminal RHD of *AML1* and nearly the entire *ETO* gene, including its 3'UTR[66]. Thus, the AML1-ETO fusion transcription factor impairs normal AML1-mediated myeloid differentiation through the transcriptional dysregulation of critical hematopoietic genes[66, 77-85], although additional mutations are also required for leukemogenesis[86, 87].

Stable expression of the *AML1-ETO* fusion gene is critical for both the initiation and maintenance of t(8;21) AML[88-94]. Transient knockdown of *AML1-ETO* induces

differentiation [88, 90], inhibits proliferation[89, 90], and reduces leukemic burden[91]. AML1 expression is required for healthy hematopoiesis[67]. In contrast, ETO is not normally expressed in healthy hematopoietic progenitor cells[68-70]. Therefore, the factors which regulate AML1-ETO expression through the *ETO* portion of the chimeric transcript, including the 3'UTR, may be a unique sensitivity of t(8;21) leukemia cells compared to healthy hematopoietic cells.

The 3'UTR plays a crucial role in post-transcriptional gene expression by influencing the localization, stability, export, and translation efficiency of mRNA transcripts[95]. Sequence specific interactions between *cis*-elements within the 3'UTR and *trans*-factors, such as RNA binding proteins or microRNAs (miRNA), are major mediators of post-transcriptional regulation[95, 96]. miRNAs have also been shown to promote or suppress a variety of leukemic processes, including proliferation, apoptosis, differentiation, self-renewal, epigenetic regulation, and chemotherapy resistance[97-99]. The let-7 family of miRNAs are well described tumor suppressors in a variety of cancers, including leukemias[100-102]. Members of the let-7 miRNA family have demonstrated roles in sensitizing leukemic cells to chemotherapy[103-107]. Furthermore, the overexpression of let-7 miRNAs have also been shown to inhibit proliferation and promote differentiation in certain leukemic contexts[100, 108].

Since AML1-ETO expression is critical for t(8;21) AML leukemia, identifying factors that post-transcriptionally regulate AML1-ETO via the *ETO* 3'UTR may improve our understanding of how AML1-ETO expression is maintained and uncover suitable targets for t(8;21) AML therapy. Here, we demonstrate that *AML1-ETO* transcripts predominantly use the first 3.7 kb of the *ETO* 3'UTR, in both t(8;21) AML patients and

cell lines. Using a luciferase assay approach to identify regulatory elements within the 3.7 kb *AML1-ETO* 3' UTR, we found a fragment of the *AML1-ETO* 3'UTR between 2.8 and 3.4 kb which was negatively regulated, increased expression upon inhibition of miRNA biogenesis, and contained a putative miRNA let-7 target site. We further showed that let-7b targets and represses AML1-ETO expression through this site. Finally, exogenous let-7b miRNA transfection inhibited the proliferation of t(8;21) AML cell lines, rescued expression of AML1-ETO downregulated target genes, and promoted leukemia cell differentiation. Our findings establish that the let-7b miRNA is a post-transcriptional regulator of *AML1-ETO and* affects the leukemic phenotype of t(8;21) AML.

2.2 RESULTS

2.2.1 AML1-ETO transcripts primarily use the first 3.7 kb of the *ETO* 3'UTR in t(8;21) AML patients and cell lines.

To uncover post-transcriptional regulators of the *AML1-ETO* oncogene that target the *ETO* 3'UTR, we first sought to identify which regions of the 3'UTR are present in *AML1-ETO* transcripts. Alternative polyadenylation regulates 3'UTR length and consequently the availability of *cis*-acting elements that bind *trans*-acting post-transcriptional regulators[95]. Therefore, to identify t(8;21) AML relevant interactions, we analyzed the endogenous *AML1-ETO* 3'UTR usage in t(8;21) AML patients and cell lines.

We performed RNA-seq on peripheral blood derived CD34+ HSPCs from healthy donors and CD34+ enriched t(8;21) AML primary patients' blasts. The longest predicted *AML1-ETO* 3'UTR sequence is 5.2 kb in length. However, analysis of the

sequencing reads in the t(8;21) patients showed that the abundance of reads aligned within the first 3.7 kb of the *ETO* 3'UTR and only minor signal is detected up to the full 5.2 kb (**Fig. 1A**). Importantly, a validated poly(A) site is located at 3.7kb, suggesting that *AML1-ETO* transcripts terminate at this proximal poly(A) site resulting in the observed shorter 3'UTR in patients. Consistent with previous reports[68-70], wild type *ETO* expression was undetectable in the healthy HSPC samples and the *ETO* RNA-seq reads in t(8;21) patient samples only map to the exons present in the *AML1-ETO* fusion (**Fig. 1A, S1A,B**)[66]. To compare *AML1-ETO* 3'UTR usage to wild type *ETO* in a normal physiological context, we analyzed publicly available RNA-seq data of healthy brain cortex[109], which is known to express *ETO*[70]. The normal brain cortex RNA-seq reads included peaks in exons not involved in the *AML1-ETO* fusion and had a very similar pattern within the *ETO* 3'UTR, with the abundance of reads mapping within the first 3.7 kb of the *ETO* 3'UTR (**Fig. S1A,B**). We further performed RNA-seq using the t(8;21) AML cell lines Kasumi-1 and SKNO-1. Interestingly, nearly all the *AML1-ETO* 3'UTR reads aligned within the first 3.7 kb in these cell lines (**Fig. 1B**). Taken together, our data suggests that *AML1-ETO* fusion transcripts primarily use the first 3.7 kb of the *ETO* 3'UTR in t(8;21) patients and cell lines.

2.2.2 AML1-ETO 3'UTR *cis*-elements affect expression and are targeted by miRNAs.

We next sought to identify the relevant regulatory sequences within the *AML1-ETO* 3′UTR. Because within 5.2 kb of 3'UTR, *AML1-ETO* patient transcripts predominantly used the first 3.7 kb of the *ETO* 3'UTR, we focused on sequences within this region. To identify regions within the 3'UTR that contain *cis*-elements that regulate

AML1-ETO expression, we created a set of dual luciferase reporters that express *Renilla* luciferase with 3'UTRs containing progressive 600 bp fragments spanning the length of the first 3.7 kb of the *ETO* 3'UTR (with 200 bp overlaps between fragments) and firefly luciferase as an internal control (**Fig. 2A**). We mapped the effects of the *AML1-ETO* 3'UTR fragments on luciferase reporter expression compared to a control reporter through luciferase assays after transient transfection into the t(8;21)+ Kasumi-1 and SKNO-1 cell lines (**Fig. 2B**). The reporters containing *AML1-ETO* 3'UTR fragments had equal or lower expression compared to the control reporter, with some having up to 9-fold lower expression. We also observed up to 7-fold differences in luciferase activity between the reporters containing *AML1-ETO* 3'UTR fragments. Interestingly, reporters containing fragments near the 3' end of the *AML1-ETO* 3'UTR (#7 2400-3000 bp, #8 2800-3400 bp, and #9 3100-3741 bp) had the lowest expression levels in both Kasumi-1 and SKNO-1 cells, suggesting that there are negatively regulated *cis*-elements in this region.

miRNAs are major mediators of negative post-transcriptional regulation. Normal miRNA biogenesis requires a multi-step process involving the RNAse DICER[110]. To assess the contribution of miRNAs in the regulation of AML1-ETO, we made stable shRNA-mediated DICER knockdown or control shRNA transduced SKNO-1 cell lines. We observed significantly increased levels of AML1-ETO protein upon DICER knockdown, compared with controls (**Fig. 2C, S2A**). This result suggests that miRNAs regulate AML1-ETO protein levels and supports previous work that identified miR-193a, miR-9, and miR-29b as AML1-ETO regulators[111-113]. However, none of these miRNAs had predicted target sites within the 2600-3741bp negatively regulated fragments near

the end of the *AML1-ETO* 3'UTR[111-113]. To determine if miRNAs were involved specifically in the negative regulation of our *AML1-ETO* 3'UTR reporters, we transfected the lowest expressing 600 bp *AML1-ETO* 3'UTR reporters into the SKNO-1 shRNA control and shRNA DICER cell lines and performed luciferase assays (**Fig. 2D**). We observed significantly increased luciferase activity in both DICER knockdown cell lines transfected with the reporter containing the *AML1-ETO* 3'UTR fragment #8 (2800-3400 bp). Together, these results suggest that miRNAs are involved in the regulation of *AML1-ETO* and that at least one such miRNA specifically targets the *AML1-ETO* 3'UTR between 2800 and 3400 bp.

2.2.3 let-7b targets and down regulates AML1-ETO via the 3'UTR.

To find miRNAs which putatively target the *AML1-ETO* 3'UTR between 2800 and 3400 bp, we used a miRNA targeting prediction model, TargetScan 7.2[114]. We identified 6 families of miRNAs that were predicted to target this region: let-7, miR-33, miR-129, miR-153, miR-190, and miR-202 (**Fig. 3A**). We next tested the ability of all 6 candidate miRNA families to downregulate the AML1-ETO 3'UTR. We co-transfected miRNA "mimics" or non-targeting control mimics with a luciferase reporter containing the full 3.7 kb *AML1-ETO* 3'UTR in HEK293T cells (**Fig. 3B**). The let-7 family member mimic, let-7b, significantly decreased luciferase activity of the *AML1-ETO* 3'UTR reporter, suggesting that let-7b targets the *AML1-ETO* 3'UTR. Interestingly, among favorable-risk AML patients in the TCGA adult AML dataset[115], those with high expression of let-7b had significantly higher overall and disease-free survival (**Fig. S3A**); though direct correlation between let-7b expression and overall and disease-free

survival was only weakly positive (**Fig, S3B**). Based on the potential survival benefit and the *AML1-ETO* 3'UTR reporter results, we focused on let-7b for our further studies.

We investigated the effect of let-7b on regulating endogenous AML1-ETO by transfecting let-7b-5p or non-targeting control miRNA mimics into the Kasumi-1 and SKNO-1 cell lines (**Fig. 4A, S4A**). We observed significantly decreased AML1-ETO protein expression in both Kasumi-1 and SKNO-1 cells that were transfected with the let-7b-5p mimics compared to controls (**Fig. 4A**). To further test the role of let-7 miRNAs in regulating endogenous AML1-ETO expression, we made stable Kasumi-1 and SKNO-1 cell lines which expressed an anti-let-7 family member miRNA sponge[116]. Consistent with previous reports[117], we observed a modest decrease in mature let-7b-5p levels in the anti-let-7 miRNA sponge expressing cell lines because the major activity of bulged miRNA sponges is through miRNA decoy rather than miRNA decay (**Fig. S4B**). Both the Kasumi-1 and SKNO-1 cell lines which stably expressed let-7 miRNA sponges showed significantly increased AML1-ETO protein levels compared to control cell lines (**Fig. 4B**). Together, these results demonstrate that AML1-ETO protein is down-regulated upon the addition of exogenous let-7b miRNA and is up-regulated when endogenous let-7 family members are inhibited.

The *AML1-ETO* 3'UTR contains a seed sequence for let-7 miRNA family members at 2.85 kb. Therefore, we next examined whether the regulation of AML1-ETO expression by let-7b was due to direct targeting of the *AML1-ETO* 3'UTR at this site. Indeed, luciferase activity of the *AML1-ETO* 3'UTR fragment #8 (2,800-3,400 bp) luciferase reporter was significantly decreased in Kasumi-1 cells co-transfected with let-7b-5p miRNA mimics compared to non-targeting control (**Fig. 4C**). Next, we introduced

mutations of the putative let-7 target site (AE-MUT 3‘UTR) within the wild-type *AML1-ETO* 3’UTR #8 fragment luciferase reporter (AE-WT 3’UTR) (**Fig. 4D**). Luciferase assays in Kasumi-1 and SKNO-1 cells showed significantly increased activity in the reporters with the mutated let-7 target site compared to wild-type (**Fig. 4E**). Luciferase activity of the AE-WT 3’UTR reporter was also significantly greater in let-7 sponge expressing SKNO-1 and Kasumi-1 lines versus controls, whereas there was no significant difference in luciferase production by the AE-MUT 3’UTR reporter in these cellular contexts (**Fig. 4F**). Together, these results suggest that let-7b directly targets and down-regulates AML1-ETO via the 3’UTR.

2.2.4 Expression of let-7b inhibits cell growth in t(8;21) AML cell lines.

Having observed that let-7b-5p overexpression can reduce AML1-ETO protein expression, we next wondered whether the degree of AML1-ETO downregulation has potential therapeutic relevance. Therefore, we first measured the expression of known transcriptionally repressed AML1-ETO target genes, *CEBPA*[77] and *RASSF2*[118]*,* upon transfection of Kasumi-1 and SKNO-1 cells with the let-7b-5p miRNA mimic. In both cell lines, treatment with the miRNA mimic resulted in a significant increase of both transcripts in comparison to cells treated with a non-targeting control mimic (**Fig 5A**). These results suggest that down regulation of AML1-ETO by let-7b-5p can partially rescue expression of genes that are transcriptionally repressed directly by AML1-ETO. We next measured the phenotypic impact of let-7 restoration on t(8;21)+ AML cell lines. The AML1-ETO protein has been shown to impair myeloid differentiation and transiently silencing its expression reduces cell proliferation and induces differentiation[84, 85, 88-90]. Likewise, the restoration of let-7 expression has been shown to inhibit cell proliferation

and induce differentiation in cancers with low let-7 expression[119, 120]. Indeed, we observed significant inhibition of cell proliferation in the Kasumi-1 and SKNO-1 t(8;21) AML cell lines, but not in the HL-60 or THP-1 non-t(8;21) AML cell lines, after transfection with the let-7b-5p miRNA mimic versus the non-targeting control mimic (**Fig. 5B**). Additionally, both Kasumi-1 and SKNO-1 cells treated with the let-7b-5p mimic had significantly reduced cell surface expression of the hematopoietic stem cell marker, CD34 (**Fig. 5C, D**). Furthermore, let-7b-5p mimic treated cells had significantly increased cell surface expression of the CD38 progenitor marker, as well as the CD33 and CD13 myeloid markers (**Fig. 5C, D**). These results are indicative of a more differentiated cellular state, consistent with release of the AML1-ETO mediated myeloid differentiation block. Collectively, these results demonstrate that the restoration of let-7b levels rescues expression of repressed AML1-ETO target genes, impairs t(8;21) AML cell proliferation, and induces differentiation.

2.3 DISCUSSION

The AML1-ETO oncofusion protein impairs myeloid differentiation and is important for the initiation and maintenance of t(8;21) AML[84, 85, 88-94]. Thus, *AML1-ETO* 3'UTR is an appropriate target for t(8;21) AML therapies due to importance of AML1-ETO expression to t(8;21) AML and the lack of wild type *ETO* expression in healthy hematopoietic cells. However, the post-transcriptional regulation of AML1-ETO via its 3'UTR has not been well studied. We demonstrate that AML1-ETO transcripts primarily use a 3.7 kb isoform which is targeted and repressed by the let-7b miRNA. Furthermore, we show that the transient expression of let-7b in t(8;21) AML cell lines

confers a tumor-suppressive phenotype, partially rescues AML1-ETO target gene expression, and induces differentiation.

Our study is the first examination of *AML1-ETO* 3'UTR usage in t(8;21) AML patients and cell lines. Interestingly, the 3'UTR usage within our set of four t(8;21) AML patient samples was quite similar, with the majority of RNA-seq reads mapping within the first 3.7 kb of the 3'UTR. Based on these results, further studies of factors that may regulate AML1-ETO via the 3'UTR should focus on the first 3.7 kb of the 3'UTR. The role of *AML1-ETO* 3'UTR isoform usage in t(8;21) leukemogenesis is difficult to determine because wild type *ETO* expression is undetectable in healthy HSPCs. However, future studies to examine how modulation of *AML1-ETO* 3'UTR usage affects AML1-ETO expression would be of interest and may lead to novel therapeutic strategies.

Our study further analyzed the contribution of different regulatory regions within the *AML1-ETO* 3'UTR to AML1-ETO expression. Our luciferase assay experiments using progressive *AML1-ETO* 3′UTR fragments showed up to 7-fold differences in luciferase activity between the fragments, with the lowest expression in fragments near the 3' end of the UTR. These data suggest that the expression of AML1-ETO is controlled by negatively acting regulatory elements near the 3' end of the 3.7 kb 3'UTR isoform. Strikingly, both the Kasumi-1 and SKNO-1 t(8;21) AML cell lines shared this trend, suggesting that these regulatory elements may be important in controlling the dosage of AML1-ETO for t(8;21) leukemic maintenance. Our DICER knockdown experiments showed a ~3-fold increase in AML1-ETO levels, which is consistent with other reported miRNA regulated genes[121, 122] and may be even greater than observed

because DICER knockdown was incomplete. These results suggest that miRNAs are involved in the negative regulation of AML1-ETO, consistent with previous reports[111-113]. We further show that this miRNA-mediated regulation affects the *AML1-ETO* 3'UTR fragment between 2.8 and 3.4 kb. It is likely that additional *trans*-factors, such as RNA binding proteins, are also involved in the post-transcriptional regulation of *AML1-ETO*. Our luciferase reporter analysis of the *AML1-ETO* 3'UTR may be useful in further studies of *AML1-ETO* post-transcriptional regulation along this line.

Our study identifies let-7b as a direct regulator of the *AML1-ETO* oncogene. The let-7 family of miRNAs are well described tumor suppressors and are known to target several oncogenes including RAS, MYC and HMGA2[120, 123-125]. Indeed, we found that overall and disease-free survival was significantly higher in let-7b high expression patients within the favorable-risk AML category, of which t(8;21) AML belongs, in the TCGA adult AML dataset. We further demonstrate that transient expression of let-7b inhibits t(8;21) AML proliferation, rescues AML1-ETO target expression, and promotes differentiation. Although additional let-7b targets likely also contribute, these results agree with previous studies showing that directly silencing AML1-ETO with siRNA or shRNA releases the AML1-ETO mediated differentiation block of t(8;21) AML cells as evidenced by down-regulation of the hematopoietic stem cell marker CD34, and up-regulation of more mature myeloid markers such as CD38, CD33, and CD13[88-90, 92, 93]. Identifying endogenous miRNAs that regulate AML1-ETO, such as let-7b, offers a potential method to silence AML1-ETO beyond the direct delivery of exogenous synthetic siRNAs. For example, pre-clinical strategies have been used to upregulate let-

7 miRNA expression using small molecule inhibitors against the endogenous protein inhibitors of let-7 biogenesis, such as *LIN28A/LIN28B*[126-128]*, TUT4*[129, 130]*, or ADAR1*[131]*.*

Collectively, our study revealed the 3'UTR isoform usage of AML1-ETO in t(8;21) AML, examined regulatory regions throughout the AML1-ETO 3'UTR, and identified let-7b as a novel regulator of AML1-ETO. We further demonstrate that this regulation can inhibit t(8;21) AML cell line proliferation, partially reverse the AML1-ETO mediated differentiation block, and affect AML1-ETO transcriptional targets. Consequently, the post-transcriptional regulation of AML1-ETO through let-7b contributes to the leukemic phenotype of t(8;21) AML and may be important for t(8;21) leukemogenesis and maintenance.

2.4 METHODS

Patients Samples

t(8;21) AML samples were obtained from patients at UC San Diego Health. Following collection of peripheral blood or bone marrow from AML patients, cells were separated using Ficoll-Paque (VWR, Radnor, PA) and frozen until further use. Thawed products were diluted in 1x PBS supplemented with 1mg/mL DNAse I (Sigma-Aldrich, St. Louis, MO) and washed with 1x PBS supplemented with 2% FBS. Live, mononuclear cells were isolated by density gradient centrifugation using Ficoll-Paque (VWR). Magnetic bead CD34-enrichment was performed using a human CD34 MicroBead Kit (Miltenyi Biotec, Bergisch Gladbach, Germany), following the manufacturer's instructions. An aliquot of CD34-enriched leukemic blasts was analyzed by flow cytometry to confirm that cells were >95% CD34+. RNA was extracted from

patient blasts using Trizol reagent (ThermoFisher, Waltham, MA) according to the manufacturer's instructions.

CD34+ HSPCs from healthy donors were obtained from Fred Hutchinson Cooperative Center for Excellence in Hematology (Seattle, Washington). Cells were thawed quickly and serially diluted with 1x PBS supplemented with 2% FBS. Cells were resuspended in Trizol for RNA extraction.

RNA-sequencing

Total RNA from Kasumi-1 and SKNO-1 cells was isolated using Trizol reagent (ThermoFisher). Library preparation of total RNA from Kasumi-1, SKNO-1, healthy HSPCs and patient blasts was performed using the TruSeq Stranded mRNA kit (Illumina, San Diego, CA) followed by sequencing on an Illumina HiSeq4000. Available public data for normal brain samples (SRR5938419 and SRR5938420) was downloaded from the NCBI Gene Expression Omnibus (GEO) database[109]**.** Raw RNA-seq reads were aligned and mapped using HISAT2 using the usegalaxy public supercomputing platform[132].

Transfection

One to two million cells of THP-1, HL-60, Kasumi-1, SKNO-1, or associated cell lines were resuspended with plasmid DNA or miRNA mimics in 100 µL of transfection buffer [140 mM Na_2HPO_4/NaH_2PO_4 (pH 7.2), 5 mM KCl, 15 mM $MgCl_2$]. Cells were then transfected using programs P-19 (SKNO-1 and Kasumi-1), U-01 (THP-1), or Y-01 (HL-60) of the AMAXA II Nucleofector (Lonza; Basel, Switzerland) and were cultured in RPMI media plus 20% FBS in a 37°C incubator with 5% CO_2. After 24 h the media was

changed to RPMI plus 10% FBS and 100 U/mL penicillin-streptomycin for the indicated times. For the HEK293T reporter assay, HEK293T cells were plated in 96-well plates and transfected with 5 ng of the psiCHECK2 3.7kb AML1-ETO 3'UTR reporter plasmid DNA and 10 pmol of miRIDIAN™ microRNA Mimic negative control #2 or indicated miRIDIAN™ microRNA mimics (Dharmacon, Lafayette, CO), using DharmaFECT™ Duo transfection reagent (Dharmacon) according to manufacturer's instructions.

Proliferation Assay

miRIDIAN™ microRNA Mimic negative control #2 or hsa-let-7b-5p (Dharmacon) were transfected into the SKNO-1 (100 pmol), THP-1 (100 pmol), HL-60 (200 pmol), or Kasumi-1 (200 pmol) cell lines. Viable cells were counted via trypan blue exclusion using a TC20 Automated Cell Counter (Bio-Rad Laboratories, Hercules, CA) on indicated days and were initially cultured at a density of 2×10^5 cells per mL.

Western blot

Primary antibodies included a mouse anti-α-tubulin (1:10,000) antibody (12G10, Developmental Studies Hybridoma Bank, University of Iowa, Iowa City, IA) and a previously described rabbit anti-AML1 (1:500) antibody generated by Covance[83]. Licor (Lincoln, NE) IRDye 680RD goat anti-mouse IgG and IRDye 800CW goat anti-rabbit IgG secondary antibodies (1:10,000) were used for visualization on a LI-COR Odyssey Classic imager. Image analysis and densitometry were performed using the LI-COR Application Software Version 3.0.

Statistical analyses

All statistical analyses were performed using GraphPad Prism Software (Version 8.4.2). The specific tests used are documented in the corresponding figure legend. All t-tests were two-tailed. P values are denoted as follows: ns $p > 0.05$, * $p < 0.05$, ** $p < 0.01$, *** $p < 0.001$.

Plasmids

MSCV-Puro (Clontech Laboratories, Mountain View, CA) was used as a control for let-7 sponge experiments. MSCV-Puro let-7 sponge was a gift from Phil Sharp (Addgene plasmid # 29766). For shRNA knockdown, control scrambled shRNA (gift from David Sabatini, Addgene plasmid #1864) and human DICER shRNA #1 and #2 constructs TRCN0000051260 and TRCN0000051261 were used. The psiCHECK-2 dual luciferase reporter vector (Promega, Madison, WI) was utilized for all luciferase assays, and all 3'UTR sequences were subcloned into the Xho1 and Not1 sites. The full-length 5.2 kb ETO 3'UTR was amplified from KG-1a (ATCC CCL-246.1) genomic DNA using following primer pairs: forward (5'– ACGTGAACTCAGAACTGTCGGAG –3'), reverse (5'– CATGATTAGGCAAACACAAC –3'). All canonical poly-adenylation sites (AATAAA) were removed by overlap PCR. The series of 600 bp *ETO* 3'UTR fragments were amplified from the full-length 5.2 kb plasmid using the listed primers (**Table S2.1**). The psiCHECK-2 3.7kb AML1-ETO 3'UTR reporter was cloned from the full-length 5.2 kb plasmid using the ETO_3'UTR_#1 forward and ETO_3'UTR_#9 Reverse primers (**Table S2.1**). The let-7-5p seed sequence mutant 3'UTR reporters were created through overlap PCR using the listed primers (**Table S2.1**).

Cell Culture

Human AML cell lines Kasumi-1, SKNO-1, THP-1, and HL-60 were cultured in RPMI media supplemented with 10% FBS and 100U/mL PSQ. Although SKNO-1 cells were initially established as a GM-CSF-dependent cell line [133], over time in culture, they have lost their cytokine dependence. HEK293T cells were cultured in DMEM media supplemented with 10% FCS and 100U/mL PSQ. All cells were maintained in a 37°C incubator with 5% CO2.

Viral Transduction

For retroviral transduction experiments, retrovirus was produced in HEK293T cells. Transfections of HEK293T cells were conducted by combining 5 µg of MSCV-Puro or MSCV-puro let-7 vectors, 5 µg of packaging vector (pCL-10A1), and 40 µl of polyethylenimine (PEI) in 1 mL of Opti-MEM reduced serum medium (Thermo Fisher, Waltham, MA). Approximately 16 h post-transfection, media was aspirated, cells were washed once in PBS, and 7 mL of fresh RPMI media supplemented with 10% fetal bovine serum and 1% penicillin-streptomycin was added to each plate. 24 h after the media change, RPMI media containing retroviral particles was collected, passed through a 0.45 µm syringe filter, pooled, and supplemented with polybrene (4 µg/mL). Kasumi-1 or SKNO-1 cells were resuspended in retroviral media at a concentration of approximately 0.5 x 10^6cells/mL and were transduced in 6-well plates by centrifugation (2,000 x g) for 3 h at 32°C in an Allegra X-12R centrifuge (Beckman Coulter, Brea, CA) on two consecutive days. 24 h following the second transduction, cells were resuspended in fresh RPMI media supplemented with 1 µg/mL puromycin. After 48 h of puromycin selection, cells were diluted and maintained at 0.5 µg/mL puromycin until future analysis.

For DICER shRNA knockdown experiments, lentiviral transduction of shRNA constructs was performed. Transfection of HEK293T cells was conducted by combining 5 µg of psPAX2, 2.5 µg of pMD2.G, and 3 µg of respective pLKO.1-based shRNA vector, and 44 µl of polyethylenimine (PEI) in 1 mL of Opti-MEM reduced serum medium (Thermo Fisher, Waltham, MA). Approximately 16 h post-transfection, media was aspirated, cells were washed once in PBS, and 7 mL fresh RPMI supplemented with 10% fetal bovine serum and 1% penicillin-streptomycin was added to each plate. 24 h following media change, RPMI media containing lentiviral particles was collected, passed through a 0.45 µm syringe filter, pooled, and supplemented with polybrene (final working concentration: 4 µg/mL). Kasumi-1 or SKNO-1 cells were resuspended in lentiviral media at a concentration of approximately 0.5 x 10^6cells/mL and were transduced in 6-well plates by centrifugation (2,000 x g) for 3 h at 32°C in an Allegra X-12R centrifuge (Beckman Coulter, Brea, CA). 24 h following the transduction, cells were resuspended in fresh RPMI media supplemented with 1 µg/mL puromycin. After 48 h of puromycin selection, cells were diluted and maintained at 0.5 µg/mL puromycin until future analysis.

Luciferase Assays

For the 3'UTR 600 bp-scanning due luciferase reporter assay, 100 ng and 500 ng plasmid DNA were transfected into Kasumi-1 cells and SKNO-1 cells, respectively, and cell lysates were prepared 48 h later. For luciferase assays in SKNO-1 shRNA experiments, 0.5-1 µg of control luciferase reporter DNA was transfected in each sample and cell lysates were prepared 72 h later. For the miRNA mimic luciferase assays, Kasumi-1 cells were transfected with 100 ng of luciferase reporter plasmid

DNA, containing the 600 bp *ETO* 3'UTR fragment #8, and 100 pmol of negative control or hsa-let-7b-5p miRNA mimics; cell lysates were prepared 72 h later. For let-7 target site mutation luciferase assays experiments, Kasumi-1 or SKNO-1 cells were transfected with 0.5 or 2 µg of luciferase reporter plasmid DNA, containing the 600 bp *ETO* 3'UTR fragment #8 with or without let-7 target site mutation, and cell lysates were prepared 48 h later. For the let-7 sponge experiments, MSCV-Puro let-7 sponge and control MSCV-Puro expressing Kasumi-1 or SKNO-1 cell lines were transfected with 0.5 or 1 µg of luciferase reporter plasmid DNA, containing the 600 bp *ETO* 3'UTR fragment #8 with or without let-7 target site mutation, and cell lysates were prepared 48 h later. The Dual-Luciferase Reporter Assay System (Promega, Madison, WI) was used to make all cell lysates and firefly/*renilla* luciferase activities were measured using a Monolight 3010 luminometer (BD Biosciences, San Jose, CA) following manufacturer's instructions.

qPCR Analysis

For miRNA-qPCR, isolation of total RNA (including small RNAs) was performed using the mirVana™ miRNA isolation Kit (Thermo Fisher, Waltham, MA) according to the manufacturer's instructions. Universal polyadenylation and reverse transcription of miRNAs within total RNA was done using the miRCURY LNA RT system (Qiagen, Venlo, Holland) according to the manufacturer's instructions. Quantification of specific mature miRNAs was performed using technical triplicate miRCURY LNA miRNA PCR assays for hsa-let-7b-5p and hsa-miR-103a-3p with the miRCURY LNA SYBR Green PCR Kit (Qiagen, Venlo, Holland) run on the CFX Connect Real-Time PCR Detection System (Bio-Rad Laboratories, Hercules, CA) following the manufacturer's instructions.

Data analysis was performed using a standard delta-delta Ct method relative to the geometric-mean of hsa-miR-103a-3p.

For qPCR of *RASSF2* and *CEBPA*, isolation of total RNA (including small RNAs) was performed using the mirVana™ miRNA isolation Kit (Thermo Fisher, Waltham, MA) according to the manufacturer's instructions. For qPCR of *DICER*, cell lysis and RNA isolation were performed using Trizol reagent (Thermo Fisher, Waltham, MA) according to the manufacturer's instructions. cDNA preparation and quantitative PCR was performed as previously described[58], using the listed primers (**Table S2.1**). Data analysis was performed using a standard delta-delta Ct method relative to the geometric-mean of the *GAPDH* reference gene.

TCGA clinical and miRNA-sequencing dataset

Clinical information and pre-processed TCGA miRNA-sequencing data from AML patients in the favorable risk category (n = 36) was obtained through the TCGA data portal (https://tcga-data.nci.nih.gov/tcga)[115]. We used the "reads per million miRNA mapped" (RPMM) from the TCGA LAML miRNA quantification files as the miRNA expression values.

Flow Cytometry

Cells were stained with 7AAD (BD Biosciences, San Jose, CA) and PE-conjugated antibody against human CD34 (Miltenyi Biotec, AC136, Bergisch Gladbach, Germany), APC/Cy7-conjugated human CD13 (Biolegend, WM15, San Diego, CA), PE/Cy7-conjugated human CD33 (eBioscience, WM-53, San Diego, CA) or PE/Cy7-conjugated CD38 (Biolegend, HIT2) for flow cytometric analysis. Cells were analyzed

with a FACS Canto cytometer (BD Biosciences, San Jose, CA), non-viable 7AAD+ cells were excluded.

Ethics approval and consent to participate

Patient samples were obtained at UC San Diego Health with written consent, following ethics approval and consent in accordance with the university-approved Institutional Review Board protocol.

Competing Interests

The authors declare that they have no competing interests.

Funding

This work was supported by National Institutes of Health, National Cancer Institute grants R01CA104509 (D.E.Z), F31CA228324 (D.T.J), and T32CA009523 (D.T.J).

Author's contributions

Contribution: D.T.J. and D.E.Z. conceived of the study and designed the experimental plan. D.T.J. performed the *in-vitro* biological experiments and interpretation. J.H.Z. and E.D.B. collected, annotated, and provided clinical samples for the study. A.G.D. prepared clinical samples for RNA-sequencing. D.T.J. performed the bioinformatics and other data analyses. D.T.J, A.G.D., and D.E.Z prepared the manuscript. All authors approved of the final manuscript version.

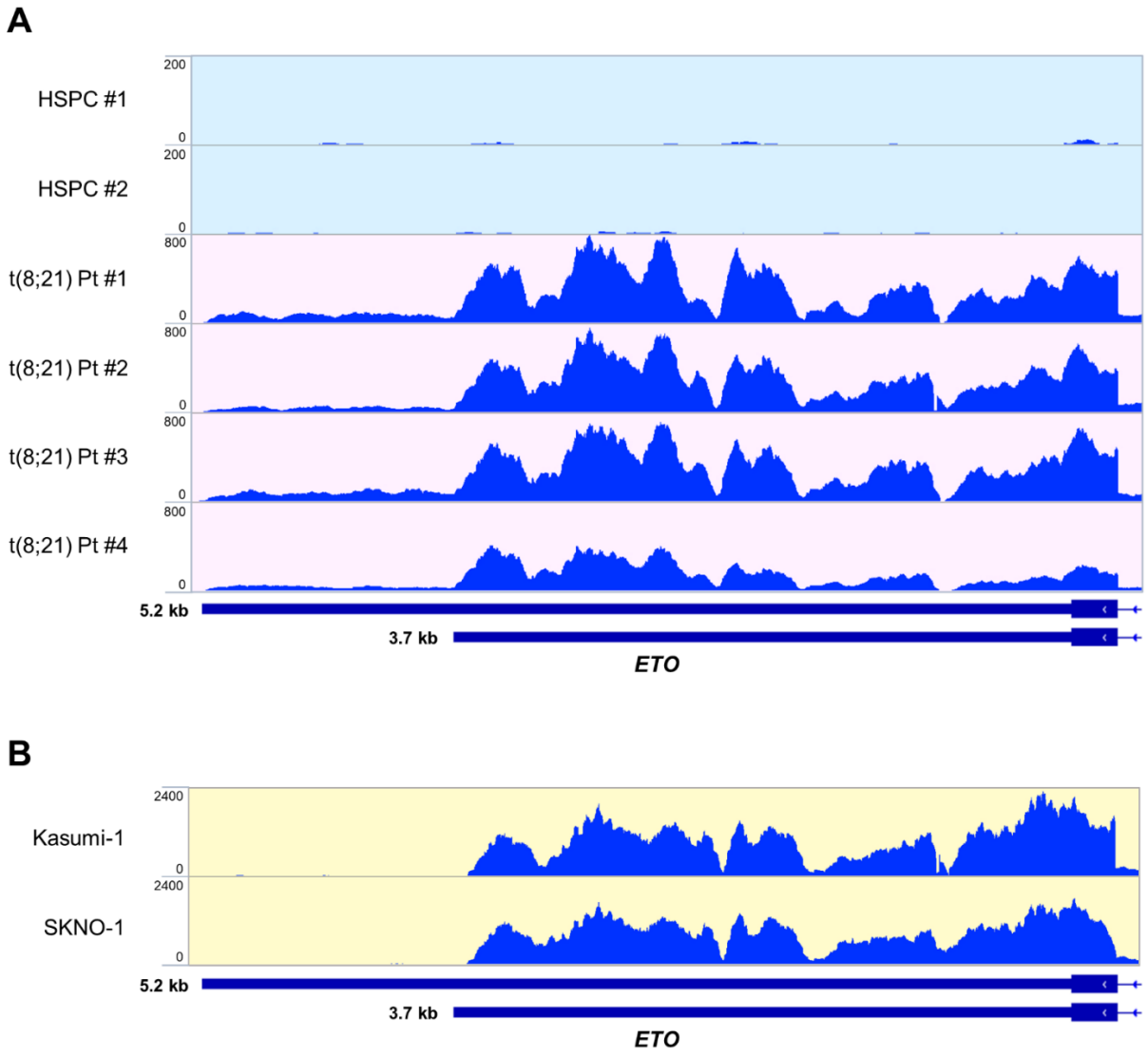

Figure 2.1. *AML1-ETO* transcripts primarily use a 3.7 kb isoform of the *ETO* 3'UTR in t(8;21) AML patients and cell lines. (A) Alignment of RNA-seq reads from healthy HSPCs (n = 2) and t(8;21) AML patient blasts (n = 4) to the final exon of *ETO*. Putative 3.7 kb and full-length 5.2 kb *ETO* 3'UTR isoforms are depicted below. (B) Alignment of RNA-seq reads from the t(8;21)+ Kasumi-1 and SKNO-1 cell lines to the final exon of *ETO*. Putative 3.7 kb and full-length 5.2 kb *ETO* 3'UTR isoforms are depicted below.

Figure 2.2. *AML1-ETO* 3'UTR *cis*-elements affect expression and are targeted by miRNAs. (A) Schematic of the dual luciferase reporters containing 600 bp fragments of the *AML1-ETO* 3'UTR. (B) Individual *AML1-ETO* 3'UTR dual luciferase reporters were transfected into Kasumi-1 and SKNO-1 cells and luciferase activity was measured. Assay results were normalized to an empty vector control. Values and error bars represent the average and SD of relative luciferase from three independent experiments. Significance is shown compared to empty vector control using one-way ANOVA with a post-hoc Tukey test. (C) Representative western blot and quantification of AML1-ETO protein in SKNO-1 DICER knockdown or control shRNA cell lines. Values and error bars represent the mean and SD of three independent experiments. (D) SKNO-1 cells expressing shRNAs targeting DICER or control shRNA were transfected with dual luciferase reporters expressing the indicated *AML1-ETO* 3'UTR fragments. Values and error bars represent the mean and SD of relative luciferase activity of shDICER compared to shCTRL from indicated number of independent experiments. Significance is shown compared to shCTRL control using unpaired t-tests corrected for multiple comparisons using the Holm-Sidak method.

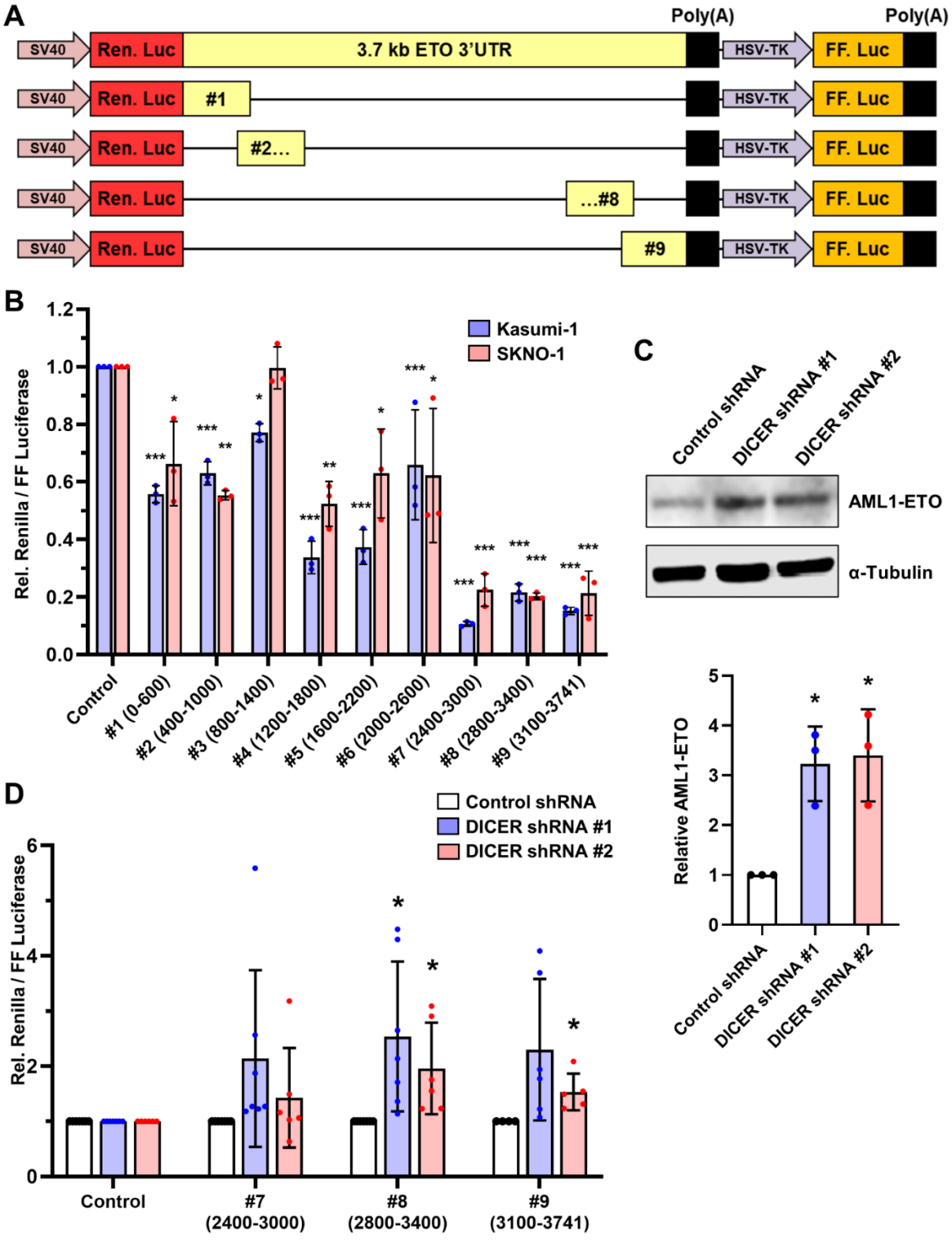
A
Poly(A)
Poly(A)
SV40
Ren. Luc
3.7 kb ETO 3'UTR
HSV-TK
FF. Luc
#1
#2…
…#8
#9
B
Kasumi-1
SKNO-1
Rel. Renilla / FF Luciferase
Control
#1 (0-600)
#2 (400-1000)
#3 (800-1400)
#4 (1200-1800)
#5 (1600-2200)
#6 (2000-2600)
#7 (2400-3000)
#8 (2800-3400)
#9 (3100-3741)
C
Control shRNA
DICER shRNA #1
DICER shRNA #2
AML1-ETO
α-Tubulin
Relative AML1-ETO
D
Control shRNA
DICER shRNA #1
DICER shRNA #2
Rel. Renilla / FF Luciferase
Control
#7 (2400-3000)
#8 (2800-3400)
#9 (3100-3741)

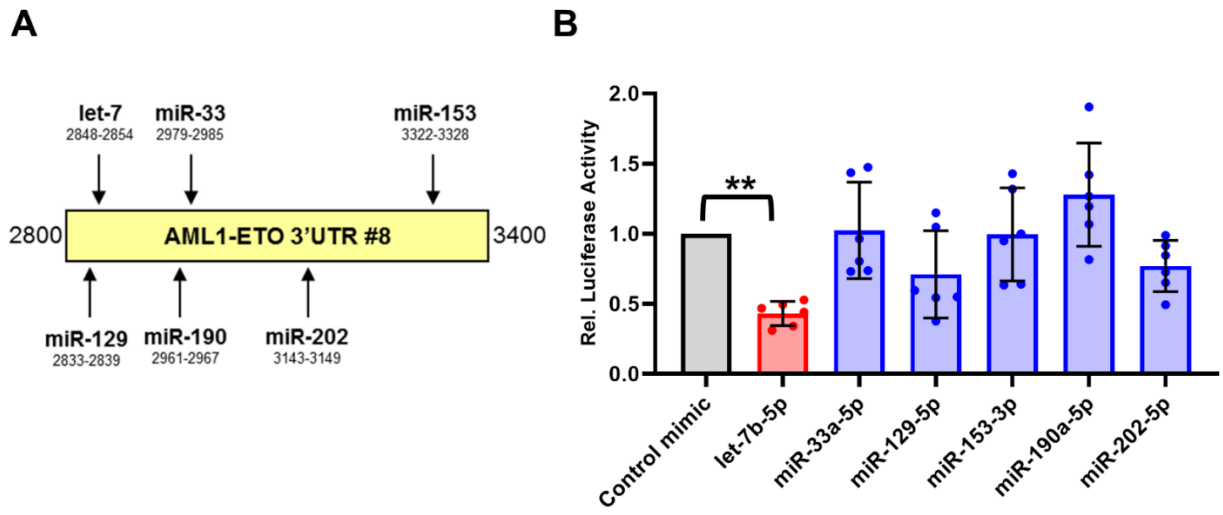

Figure 2.3. let-7b targets and down regulates an AML1-ETO 3'UTR reporter in HEK293T cells. (A) Schematic representation of miRNAs with predicted target sites within the 2800-3400 bp *AML1-ETO* 3'UTR fragment. Predictions were made using TargetScan 7.2. (B) miRNA mimics or non-targeting control mimic were co-transfected into HEK293T cells with the AML1-ETO 3.7 kb 3'UTR luciferase reporter and luciferase assays were performed 24 h post-transfection. Data is shown as relative luciferase activity normalized to non-targeting control mimic. Significance was determined using one-way ANOVA with a post-hoc Tukey test.

Figure 2.4. let-7b targets the 3'UTR and downregulates AML1-ETO in t(8;21) AML cells. (A,B) Representative western blots and protein quantification of Kasumi-1 and SKNO-1 whole cell lysates probed for endogenous AML1-ETO or α-Tubulin 48 h post-transfection with let-7b-5p or control miRNA mimics (A), or in cells stably expressing an anti-let-7 miRNA family sponge or control cells (B). (C) let-7b-5p or control miRNA mimics were co-transfected into Kasumi-1 cells with the AML1-ETO 3'UTR fragment #8 luciferase reporter and luciferase assays were performed 72 h post-transfection. Data is shown as relative luciferase activity normalized to control mimics. (D) Schematic of WT (AE-WT) and let-7 targeting mutant (AE-MUT) *AML1-ETO* 3'UTR fragment #8 luciferase reporters. (E) Luciferase assay results of AE-WT and AE-MUT reporters in Kasumi-1 or SKNO-1 cells 72 h post-transfection. (F) Kasumi-1 and SKNO-1 cell lines stably expressing either an anti-let-7 miRNA family sponge or control cells were transfected with the AE-WT or AE-MUT 3'UTR reporters and luciferase assays were performed 72 h later. Data is shown as relative luciferase activity normalized to control cell lines. All data in this figure is presented as the average and SD of the indicated number of individual experiments, unpaired t-tests with corrections for multiple tests using the Holm-Sidak method.

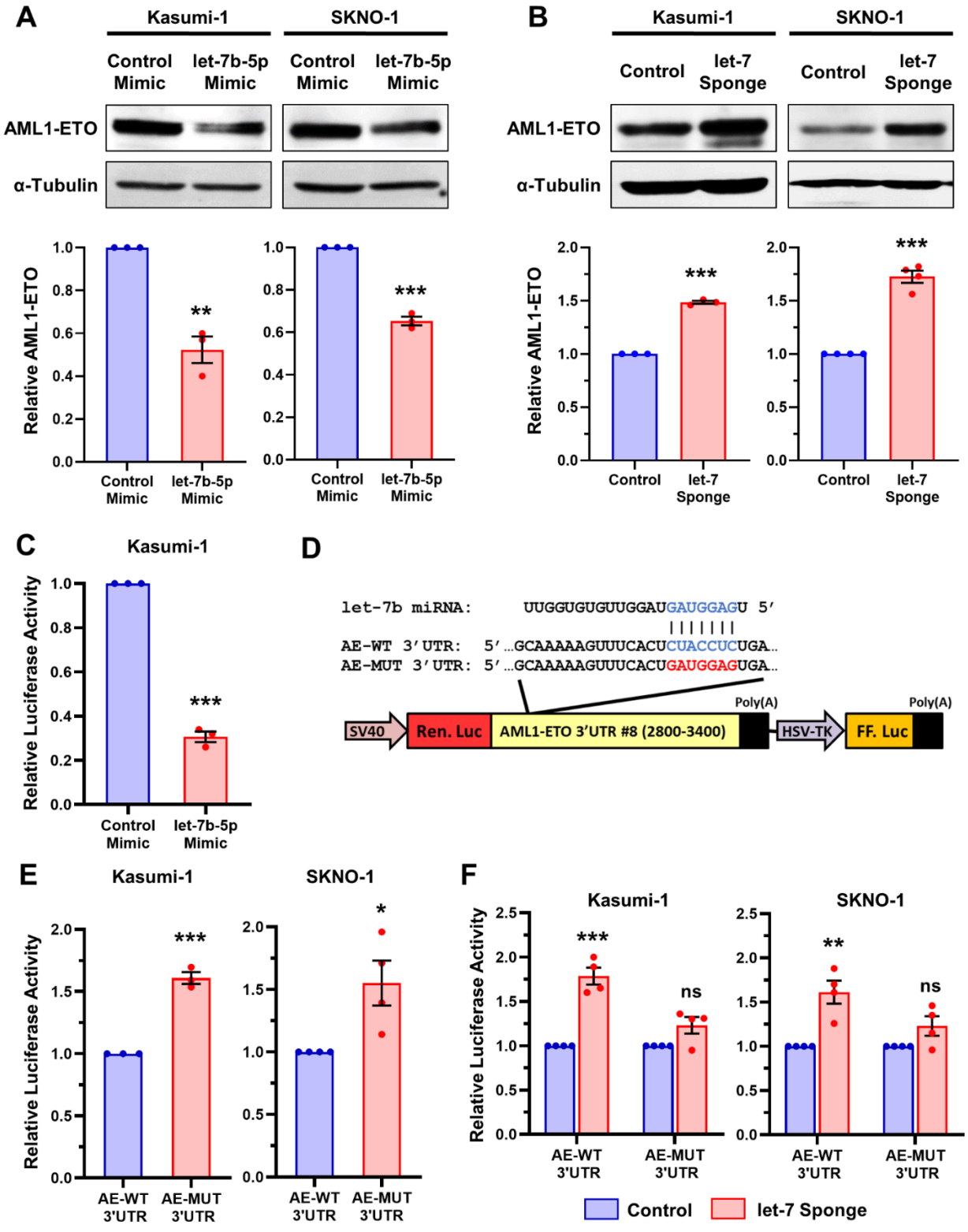
A
Kasumi-1
SKNO-1
Control Mimic
let-7b-5p Mimic
AML1-ETO
α-Tubulin
Relative AML1-ETO
B
Control
let-7 Sponge
C
Kasumi-1
Relative Luciferase Activity
D
let-7b miRNA: UUGGUGUGUUGGAUGAUGGAGU 5′
AE-WT 3′UTR: 5′…GCAAAAAGUUUCACUCUACCUCUGA…
AE-MUT 3′UTR: 5′…GCAAAAAGUUUCACUGAUGGAGUGA…
SV40
Ren. Luc
AML1-ETO 3′UTR #8 (2800-3400)
Poly(A)
HSV-TK
FF. Luc
E
Kasumi-1
SKNO-1
AE-WT 3'UTR
AE-MUT 3'UTR
F
Kasumi-1
SKNO-1
ns
Control
let-7 Sponge

Figure 2.5. Expression of let-7b inhibits cell growth in t(8;21) AML cell lines. (A) Either let-7b-5p or control miRNA mimics were transfected into Kasumi-1 or SKNO-1 cells at an amount of 200 or 100 pmol for each respective cell line. Relative expression of *CEBPA* and *RASSF2* were determined by qPCR 96 h post-transfection. Data is presented as let-7b-5p mimic fold change relative to control. Values represent mean and SD of three individual experiments. Significance was determined by unpaired t-tests. (B) Cell growth of the t(8;21) AML cell lines Kasumi-1 and SKNO-1 or the non-t(8;21) AML cell lines HL-60 and THP-1, after transfection with let-7b-5p or control miRNA mimics, was determined by cell counting on the indicated days. Values represent mean and SD of four individual experiments. Significance was determined by unpaired t-tests of individual timepoints assuming homoscedasticity and with a correction for multiple tests using the Holm-Sidak method. (C,D) Relative mean fluorescent intensity (MFI) of CD34, CD33, CD38, and CD13 in Kasumi-1 or SKNO-1 96 h post-transfection with let-7b-5p or control miRNA mimics was determined using flow-cytometry. Values represent MFI relative to control mimic from indicated number of individual experiments. Significance determined by unpaired t-tests corrected for multiple comparisons using the Holm-Sidak method. (D) Representative histograms depict the fluorescence distribution of indicated markers in the indicated cell populations.

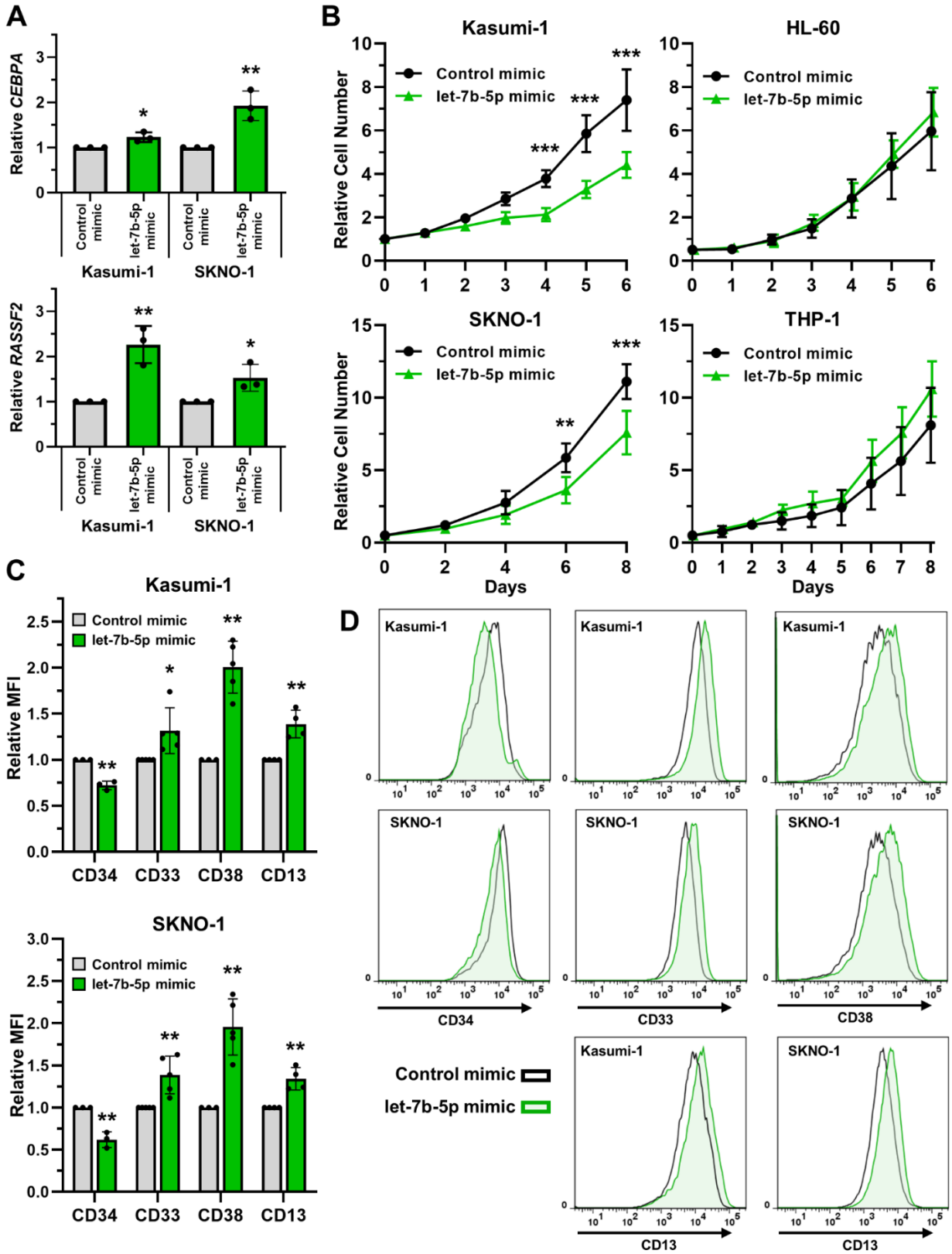
A
Relative CEBPA
Control mimic
let-7b-5p mimic
Kasumi-1
SKNO-1
Relative RASSF2
B
Kasumi-1
HL-60
SKNO-1
THP-1
Relative Cell Number
Control mimic
let-7b-5p mimic
Days
C
Kasumi-1
SKNO-1
Relative MFI
CD34
CD33
CD38
CD13
D
Kasumi-1
SKNO-1
CD34
CD33
CD38
CD13
Control mimic
let-7b-5p mimic

Supplementary Table 2.1. Primers used in this study.

Primer Name	Sequence 5'->3'	Purpose
ETO_3'UTR_#1_0-600-FWD-XhoI	TTTCGCTCGAGACGTGAACTCAGAACTGTCGGAG	Cloning into psiCheck2
ETO_3'UTR_#1_0-600-REV-NotI	TTTTTAGCGGCCGCACCGAACATCTGTGTCTCCTTCC	Cloning into psiCheck2
ETO_3'UTR_#2_400-1000-FWD-XhoI	TCCTCCTCGAGATATTAAAAGTCACAATGTTCTTTA	Cloning into psiCheck2
ETO_3'UTR_#2_400-1000-REV-NotI	TCTCTCGCGGCCGCATTTTTAAAATTATTTTTTTCAATAT	Cloning into psiCheck2
ETO_3'UTR_#3_800-1400-FWD-XhoI	TCCTCCTCGAGACACACACACACACACACACACACACACAAGTAAGAGACTCAGCCTGC	Cloning into psiCheck2
ETO_3'UTR_#3_800-1400-REV-NotI	ACGCTCGCGGCCGCCATGCTGGTTTTCAGGAAAAAAAAAAATCCTATAAGAG	Cloning into psiCheck2
ETO_3'UTR_#4_1200-1800-FWD-XhoI	TTCGCCTCGAGAGTTGGTGAGAAACCTGTATC	Cloning into psiCheck2
ETO_3'UTR_#4_1200-1800-REV-NotI	TTTTAAGCGGCCGCAATACTGTATAACCTGGCATTC	Cloning into psiCheck2
ETO_3'UTR_#5_1600-2200-FWD-XhoI	TTTGGCTCGAGTTTTTTAAATCATTATTAGGGAC	Cloning into psiCheck2
ETO_3'UTR_#5_1600-2200-REV-NotI	TACTGTGCGGCCGCGATACTTAAAAGCCACTTAAAACTG	Cloning into psiCheck2
ETO_3'UTR_#6_2000-2600-FWD-XhoI	TTTGGCTCGAGGTTGTGTGCTTTAGGAAAGTCAGC	Cloning into psiCheck2
ETO_3'UTR_#6_2000-2600-REV-NotI	TTTTTTGCGGCCGCTGGGTATGACATACCTCATTTTTGGG	Cloning into psiCheck2
ETO_3'UTR_#7_2400-3000-FWD-XhoI	TTAGACTCGAGACCTGCTTAAAGTGAAATGAAAG	Cloning into psiCheck2
ETO_3'UTR_#7_2400-3000-REV-NotI	ACGATCGCGGCCGCGTTTATGAGGTCTGCATTGTTACC	Cloning into psiCheck2
ETO_3'UTR_#8_2800-3400-FWD-XhoI	TTAGACTCGAGTCCTCTCCTCCTGTTTTGCTACATTCTCCTCAGTGGC	Cloning into psiCheck2
ETO_3'UTR_#8_2800-3400-REV-NotI	ACGATCGCGGCCGCTGTCCCTTGAGGAATTCGGACAACATGG	Cloning into psiCheck2
ETO_3'UTR_#9_3145-3747-FWD-XhoI	TTAGACTCGAGGATAGGAATAGGGCGTCCTCT	Cloning into psiCheck2
ETO_3'UTR_#9_3145-3747-REV-NotI	ACGATCGCGGCCGCTTTTTTTCAACTTTACACAGTAAAGAATACAACAATACC	Cloning into psiCheck2
ETO_3'UTR_let7MUT_overlap-FWD	CAGTGGCAAAAAGTTTCACTGATGGAGTGACAGCATGTATATTGCAC	Overlap PCR
ETO_3'UTR_let7MUT_overlap-REV	GTGCAATATACATGCTGTCACTCCATCAGTGAAACTTTTTGCCACTG	Overlap PCR
hRASSF2_qPCR_F1	CAGGAGGAAGAAGATCGGGAAGTAA	qPCR Primer
hRASSF2_qPCR_R2	GAAAGAAAGTGCCTAGCTTCCTGG	qPCR Primer
hCEBPA_qPCR_F1	AACCTTGTGCCTTGGAAATG	qPCR Primer
hCEBPA_qPCR_R1	CCCTATGTTTCCACCCCTTT	qPCR Primer
hGAPDH_qPCR_F1	TCGCTCAGACACCATGGGGAAG	qPCR Primer
hGAPDH_qPCR_R1	GCCTTGACGGTGCCATGGAATTTG	qPCR Primer
hDICER1_qPCR_F1	AAAGCCAAATGGGAAAGTCTGC	qPCR Primer
hDICER1_qPCR_R1	AAGGCAGTGAAGGCGATAAAGTAT	qPCR Primer

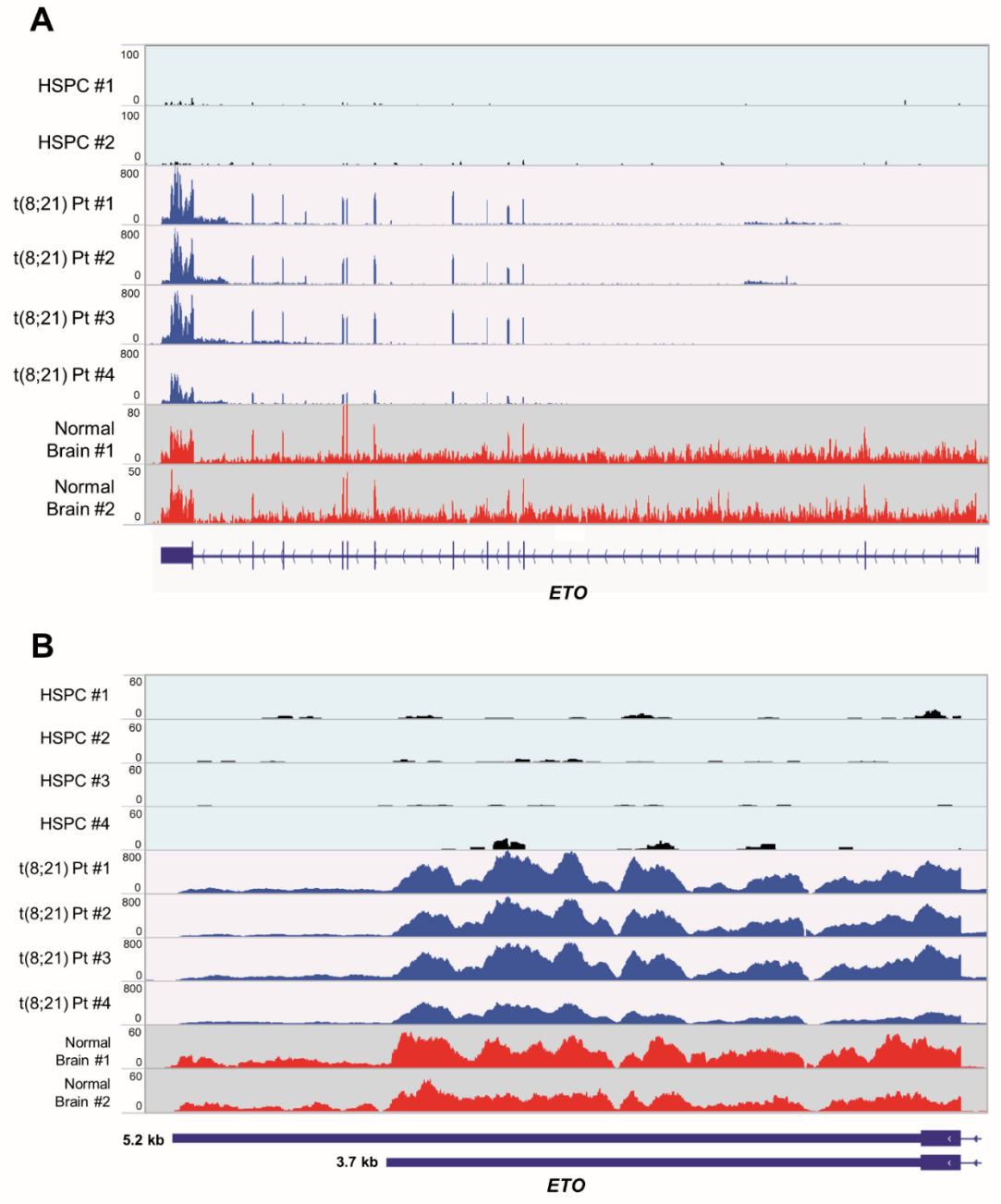

Supplementary Figure 2.1. Additional RNA-seq alignments. (A) Alignment of RNA-seq reads from healthy HSPCs (n = 2), t(8;21) AML patient blasts (n = 4), and public normal human brain data (n = 2) (SRR5938419 and SRR5938420) to the full *ETO* gene. Exons 1 and 2 are not involved in *AML1-ETO* translocation. (B) Alignment of RNA-seq reads from all healthy HSPCs (n = 4), t(8;21) AML patient blasts (n = 4), and public normal human brain data (n = 2) (SRR5938419 and SRR5938420) to the final exon of *ETO*. Putative 3.7 kb and full-length 5.2 kb *ETO* 3'UTR isoforms are depicted below.

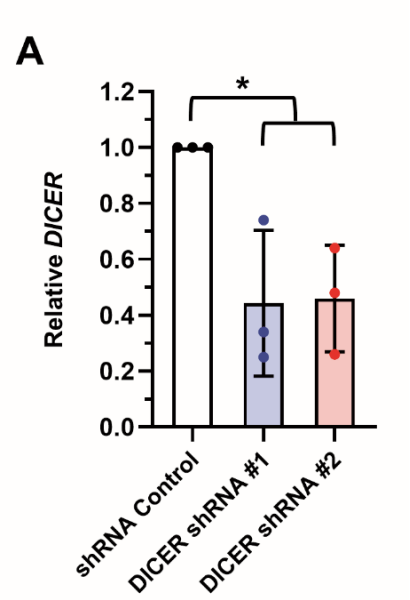

Supplementary Figure 2.2. *DICER* knockdown in SKNO-1 shRNA cell lines. (A) qPCR quantification of relative *DICER* expression in SKNO-1 shRNA cell lines from indicated number of independent experiments. p values indicated from unpaired t-test (* $p < 0.05$).

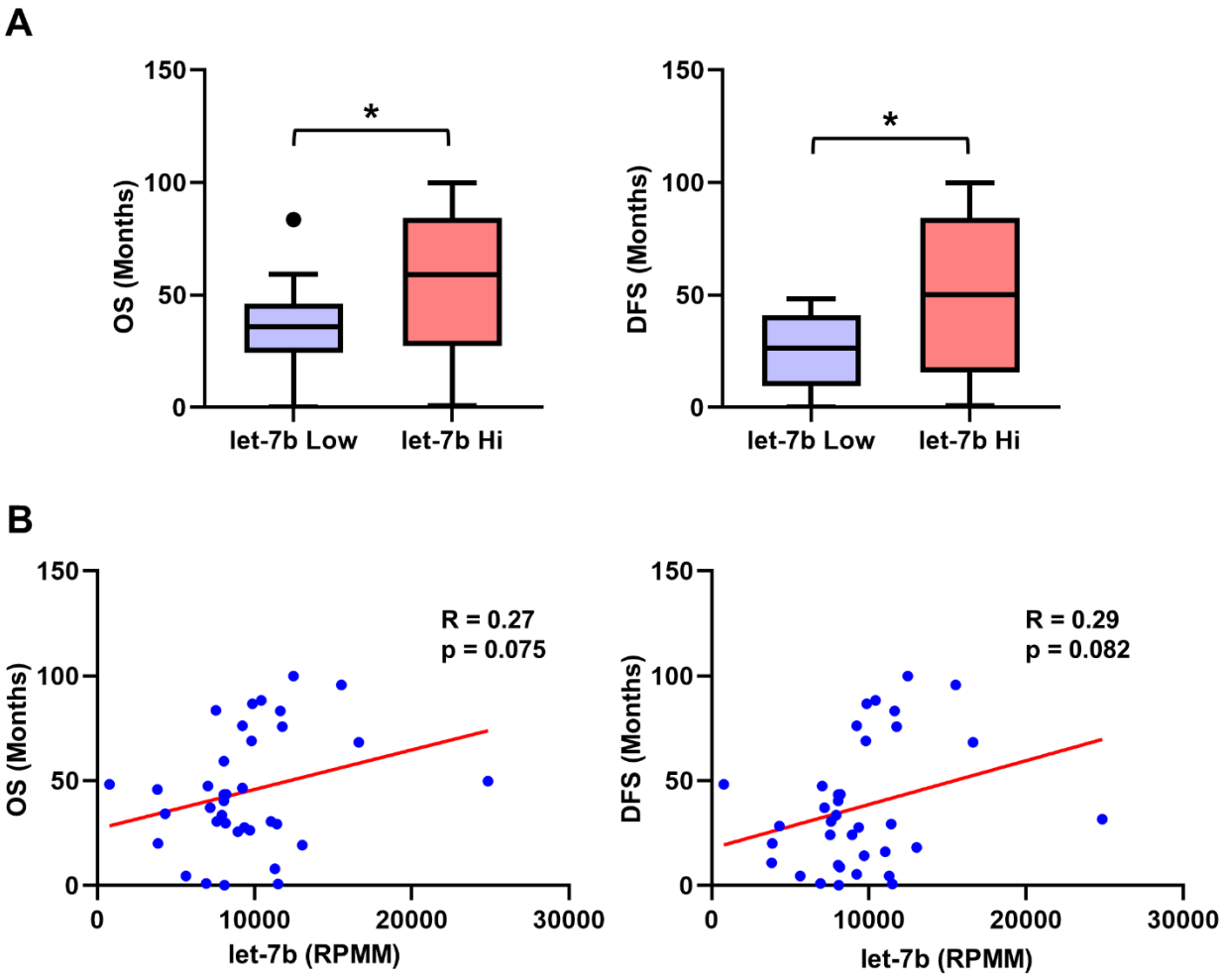

Supplementary Figure 2.3. Correlation of survival and let-7b expression in favorable-risk AML. (A) Overall survival (OS) and disease-free survival (DFS) of low (bottom 50%, n = 18) or high (top 50%, n = 18) let-7b expressing patients among favorable-risk AML samples in the TCGA cohort of adult AML samples. Significance determined by unpaired t-test. (B) Correlation of OS or DFS and let-7b normalized read counts per million mapped (RPMM) among favorable-risk AML samples in the TCGA cohort. Linear regression line is shown (red). Correlation determined using Pearson's correlation coefficient.

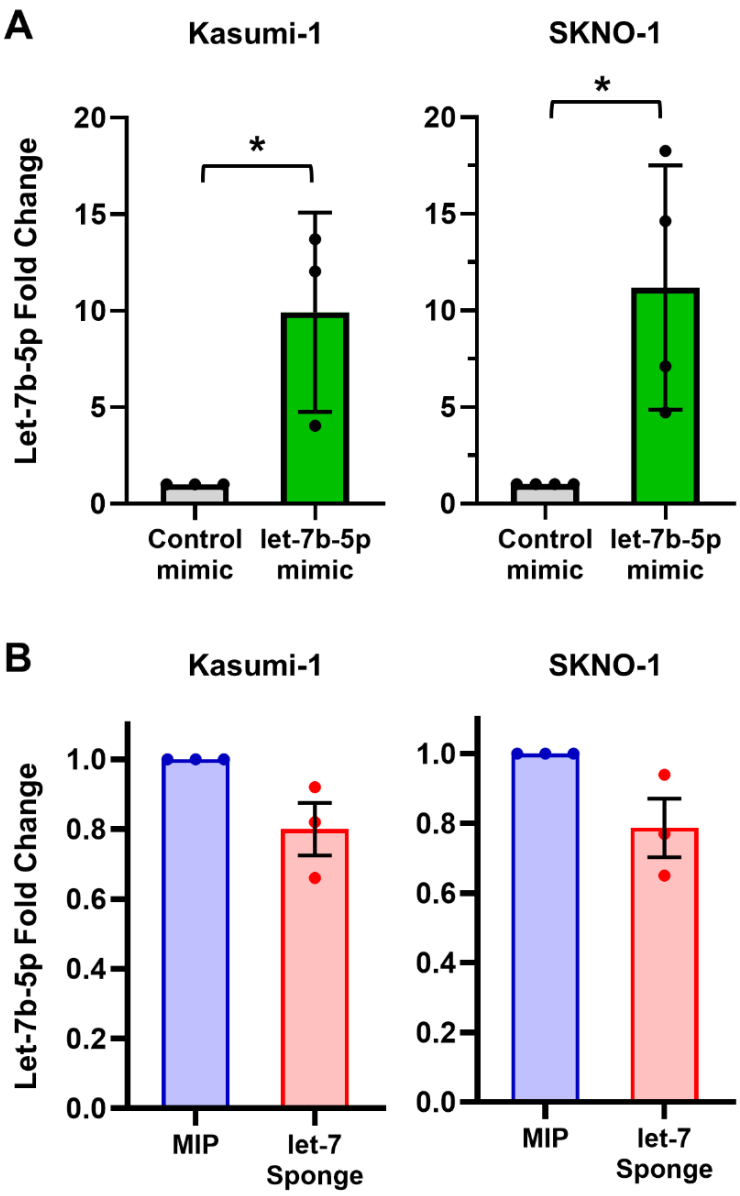

Supplementary Figure 2.4. Quantification of mature let-7b-5p change in associated experiments. (A) Kasumi-1 and SKNO-1 cell lines were treated with 200 or 100 pmol, respectively, of let-7b-5p or control miRNA mimics. Relative let-7b-5p expression levels compared to endogenous control miR-103a-3p were determined using microRNA qPCR. Data is presented as let-7b-5p fold change relative to control mimic transfection. (B) Relative let-7b-5p expression levels were determined using lysates from Kasumi-1 and SKNO-1 cell lines stably expressing an anti-let-7 miRNA family sponge or controls. Data is shown as let-7b-5p fold change relative to control lines. All data is presented as the average and SD of indicated number of individual experiments, unpaired t-test (* $p < 0.05$).

ACKNOWLEDGMENTS

This chapter is a modified version of a manuscript[134] published in *Experimental Hematology & Oncology* (BioMed Central, Springer Nature Group) and authored by Daniel T. Johnson, Amanda G. Davis, Jie-Hua Zhou, Edward D. Ball, and Dong-Er Zhang. The dissertation author was the primary investigator and author of this paper. We thank the UC San Diego Institute for Genomic Medicine (IGM) and their staff for sequencing the RNA-seq libraries.

Chapter 3. Summary and Recommendations for Future Research

Acute myeloid leukemia (AML) is a heterogeneous hematopoietic malignancy that is characterized by impaired myeloid differentiation and the clonal expansion of dysfunctional immature myeloid lineage progenitors, or “blasts”, in the bone marrow and peripheral blood[6]. AML is the most common and deadly leukemia in adults[6]. Although most AML patients respond to first-line chemotherapy, relapse is common and the five-year overall survive rate remains under 50%[135]. The high relapse rate of patients who achieve “complete remission” is largely due to the difficulties of eradicating minimal residual AML cells[3], using current therapeutic strategies. Thus, there is great need for the identification and development of additional therapeutic strategies to treat AML.

In Chapter 1, we report the development of a novel nanoparticle-based AML vaccination immunotherapy for the treatment of AML. Our vaccine platform utilizes AML cell membrane-coated nanoparticles (AMCNPs), in which immune stimulatory adjuvant-loaded nanoparticles are coated with leukemic cell membrane material. We used the C1498 AML mouse cell line model to demonstrate that AMCNPs are a promising strategy for AML vaccination immunotherapy, in principle. The AMCNP vaccination strategy offers the potential advantages of being multi-antigenic, fully personalized, and of obviating the need for neoantigen identification. Our research establishes the feasibility and benefit of this novel AML vaccination strategy, using mouse AML models. However, before moving the AMCNP strategy toward clinical application several outstanding important pre-clinical questions should be addressed. Experiments should examine whether AMCNP vaccination benefits from combination therapy with immune

checkpoint inhibitors, what the ideal adjuvant the AMCNPs should be loaded with, and if the AMCNP method works using primary human AML cells.

The efficacy of AMCNP vaccination might be improved when combined with other immune-activating therapies, such as checkpoint inhibition. Immune cell function is tightly controlled through the interactions of co-stimulatory and co-inhibitory molecules[13]. Chronic exposure of T cells to their targets can result in a dysfunctional T cell state, known as “T cell exhaustion”[136]. The cytotoxic T-lymphocyte–associated antigen 4 (CTLA-4) and programmed death 1 (PD-1) receptors are among the most well studied regulators of T cell exhaustion[47, 137]. Inhibition of these negative regulators of T cell function can overcome the T cell exhaustion state and result in increased T cell activation as a treatment for various cancers[137]. Thus, further study of the AMCNP method should examine the potential benefits of combination therapies using AMCNPs and inhibitors of PD-1 or CTLA-4.

The AMCNP method may be further improved through loading of different adjuvants into the nanoparticles. Immunostimulatory adjuvants primarily consist of molecules that mimic pathogen-associated molecular patterns that engage Toll-like receptors (TLRs) on antigen presenting cells (APCs)[55]. In our study, we used the TLR9 agonist, CpG. CpG adjuvant has been used in many preclinical models[14], however, there are many additional immunostimulatory adjuvants[55]. Further studies using AMCNPs should evaluate which immunostimulatory agents, such as GM-CSF and TLR ligands, can stimulate the most robust CD8 T cell activation in combination with AMCNPs.

Demonstration of the AMCNP method using human AML cells will be required prior to translation from pre-clinical to clinical use. My studies utilized the C1498 mouse AML model. However, future studies should move toward the use of human AML cells. First, human immortalized AML cell lines could be used to assess human AMCNPs using similar *in vitro* assays as we used with the C1498 mouse AML cell line. Ultimately, primary patient cells could be used to formulate AMCNPs, with assays using patient derived dendritic cells or CD8 T cells to evaluate the immunostimulatory properties of the primary patient AMCNPs. These experiments would enhance the feasibility of moving the AMCNP method from pre-clinical to clinical use.

In Chapter 2, we report the identification of the let-7b microRNA as a novel regulator of the AML1-ETO fusion gene in t(8;21) AML. Chromosomal translocations, and their resulting fusion genes, drive oncogenesis in many types of cancer, but occur particularly frequently in hematologic disorders. One of the most common genetic abnormalities in AML is the translocation between chromosome 8q22 and chromosome 21q22 [t(8;21)(q22;q22)], which gives rise to the *AML1-ETO* fusion gene. AML1-ETO is a transcription factor whose expression blocks normal myeloid differentiation and is critical to t(8;21) leukemogenesis, leading to the proliferation of immature leukemic blast cells. Because *AML1-ETO* uses the 3'UTR of the *ETO* gene, which is not normally expressed in hematopoietic cells, factors that regulate AML1-ETO expression via the 3'UTR are attractive therapeutic targets. Our research identified the let-7b microRNA as a novel regulator of AE via targeting its 3'UTR and provides evidence that let-7 based therapeutics may be suitable for treating t(8;21) AML.

There are several advantages in the application of let-7 based therapies to t(8;21) AML. The let-7 family of microRNAs are downregulated in many cancers and restoration of let-7 expression has been shown, in principle, to be an effective pre-clinical therapeutic strategy[102, 116, 119, 123, 138-141]. We demonstrated that transient elevation of let-7b expression inhibits t(8;21) AML proliferation, rescues AML1-ETO target expression, and promotes differentiation. A variety of pre-clinical strategies to deliver synthetic let-7 miRNA mimics have been developed, including packaging within nanoparticles[142], carrying by nanoassemblies[143], and tethering to nucleic acid aptamers[144]. These let-7 based therapeutics can more easily establish clinical safety and efficacy profiles due to their broad usage in various cancers, as compared to t(8;21) specific therapies. Therefore, future studies examining the utility of broadly used let-7 based therapies in t(8;21) AML would be appropriate. Furthermore, beyond direct delivery of synthetic miRNA, additional pre-clinical strategies have been developed to restore endogenous let-7 expression by using small molecule inhibitors to target the proteins that inhibit let-7 biogenesis, such as LIN28A/LIN28B[126-128], TUT4[129, 130], or ADAR1[131]. Future experiments should examine whether these molecules are also effective against t(8;21) AML because it may be easier to successfully target these proteins, which will indirectly increase endogenous let-7 expression, than it is to successfully deliver additional synthetic let-7 microRNA.

Collectively, my dissertation research establishes the feasibility of the novel AMCNP vaccination immunotherapy strategy to AML and identifies let-7b as a regulator of AML1-ETO with possible therapeutic potential in t(8;21) AML. In summary, my

research has increased knowledge of the regulation of a critical oncogene and has added potential new therapeutic strategies for AML, which are greatly needed.

References

1. National Cancer Institue Surveillance, Epidemiology, and End Results Program. [cited 2020 June]. Available from: https://seer.cancer.gov/.

2. Buchner T, Schlenk RF, Schaich M, Dohner K, Krahl R, Krauter J, Heil G, Krug U, Sauerland MC, Heinecke A, Spath D, Kramer M, Scholl S, Berdel WE, Hiddemann W, Hoelzer D, Hehlmann R, Hasford J, Hoffmann VS, Dohner H, Ehninger G, Ganser A, Niederwieser DW, Pfirrmann M. Acute Myeloid Leukemia (AML): different treatment strategies versus a common standard arm--combined prospective analysis by the German AML Intergroup. J Clin Oncol. 2012;30(29):3604-10.

3. Hourigan CS, Karp JE. Minimal residual disease in acute myeloid leukaemia. Nat Rev Clin Oncol. 2013;10(8):460-71.

4. Schuurhuis GJ, Heuser M, Freeman S, Bene MC, Buccisano F, Cloos J, Grimwade D, Haferlach T, Hills RK, Hourigan CS, Jorgensen JL, Kern W, Lacombe F, Maurillo L, Preudhomme C, van der Reijden BA, Thiede C, Venditti A, Vyas P, Wood BL, Walter RB, Dohner K, Roboz GJ, Ossenkoppele GJ. Minimal/measurable residual disease in AML: a consensus document from the European LeukemiaNet MRD Working Party. Blood. 2018;131(12):1275-91.

5. Dohner H, Estey E, Grimwade D, Amadori S, Appelbaum FR, Buchner T, Dombret H, Ebert BL, Fenaux P, Larson RA, Levine RL, Lo-Coco F, Naoe T, Niederwieser D, Ossenkoppele GJ, Sanz M, Sierra J, Tallman MS, Tien HF, Wei AH, Lowenberg B, Bloomfield CD. Diagnosis and management of AML in adults: 2017 ELN recommendations from an international expert panel. Blood. 2017;129(4):424-47.

6. Dohner H, Weisdorf DJ, Bloomfield CD. Acute Myeloid Leukemia. N Engl J Med. 2015;373(12):1136-52.

7. Yang X, Wang J. Precision therapy for acute myeloid leukemia. J Hematol Oncol. 2018;11(1):3.

8. Lai C, Doucette K, Norsworthy K. Recent drug approvals for acute myeloid leukemia. J Hematol Oncol. 2019;12(1).

9. Avigan D, Rosenblatt J. Vaccine therapy in hematologic malignancies. Blood. 2018;131(24):2640-50.

10. Van Acker HH, Versteven M, Lichtenegger FS, Roex G, Campillo-Davo D, Lion E, Subklewe M, Van Tendeloo VF, Berneman ZN, Anguille S. Dendritic Cell-Based Immunotherapy of Acute Myeloid Leukemia. J Clin Med. 2019;8(5).

11. Hawiger D, Inaba K, Dorsett Y, Guo M, Mahnke K, Rivera M, Ravetch JV, Steinman RM, Nussenzweig MC. Dendritic cells induce peripheral T cell unresponsiveness under steady state conditions in vivo. J Exp Med. 2001;194(6):769-79.

12. Fischer NO, Rasley A, Corzett M, Hwang MH, Hoeprich PD, Blanchette CD. Colocalized Delivery of Adjuvant and Antigen Using Nanolipoprotein Particles Enhances the Immune Response to Recombinant Antigens. J Am Chem Soc. 2013;135(6):2044-7.

13. Coffman RL, Sher A, Seder RA. Vaccine adjuvants: putting innate immunity to work. Immunity. 2010;33(4):492-503.

14. Steinhagen F, Kinjo T, Bode C, Klinman DM. TLR-based immune adjuvants. Vaccine. 2011;29(17):3341-55.

15. van der Lee DI, Reijmers RM, Honders MW, Hagedoorn RS, de Jong RC, Kester MG, van der Steen DM, de Ru AH, Kweekel C, Bijen HM, Jedema I, Veelken H, van Veelen PA, Heemskerk MH, Falkenburg JHF, Griffioen M. Mutated nucleophosmin 1 as immunotherapy target in acute myeloid leukemia. J Clin Invest. 2019;129(2):774-85.

16. Tubb VM, Schrikkema DS, Croft NP, Purcell AW, Linnemann C, Freriks MR, Chen F, Long HM, Lee SP, Bendle GM. Isolation of T cell receptors targeting recurrent neoantigens in hematological malignancies. J Immunother Cancer. 2018;6(1):70.

17. Sahin U, Derhovanessian E, Miller M, Kloke BP, Simon P, Lower M, Bukur V, Tadmor AD, Luxemburger U, Schrors B, Omokoko T, Vormehr M, Albrecht C, Paruzynski A, Kuhn AN, Buck J, Heesch S, Schreeb KH, Muller F, Ortseifer I, Vogler I, Godehardt E, Attig S, Rae R, Breitkreuz A, Tolliver C, Suchan M, Martic G, Hohberger A, Sorn P, Diekmann J, Ciesla J, Waksmann O, Bruck AK, Witt M, Zillgen M, Rothermel A, Kasemann B, Langer D, Bolte S, Diken M, Kreiter S, Nemecek R, Gebhardt C, Grabbe S, Holler C, Utikal J, Huber C, Loquai C, Tureci O. Personalized RNA mutanome vaccines mobilize poly-specific therapeutic immunity against cancer. Nature. 2017;547(7662):222-6.

18. Ott PA, Hu Z, Keskin DB, Shukla SA, Sun J, Bozym DJ, Zhang W, Luoma A, Giobbie-Hurder A, Peter L, Chen C, Olive O, Carter TA, Li S, Lieb DJ, Eisenhaure T, Gjini E, Stevens J, Lane WJ, Javeri I, Nellaiappan K, Salazar AM, Daley H, Seaman M, Buchbinder EI, Yoon CH, Harden M, Lennon N, Gabriel S, Rodig SJ, Barouch DH, Aster JC, Getz G, Wucherpfennig K, Neuberg D, Ritz J, Lander ES, Fritsch EF, Hacohen N, Wu CJ. An immunogenic personal neoantigen vaccine for patients with melanoma. Nature. 2017;547(7662):217-21.

19. Keskin DB, Anandappa AJ, Sun J, Tirosh I, Mathewson ND, Li S, Oliveira G, Giobbie-Hurder A, Felt K, Gjini E, Shukla SA, Hu Z, Li L, Le PM, Allesoe RL, Richman AR, Kowalczyk MS, Abdelrahman S, Geduldig JE, Charbonneau S, Pelton K, Iorgulescu JB, Elagina L, Zhang W, Olive O, McCluskey C, Olsen LR, Stevens J, Lane WJ, Salazar AM, Daley H, Wen PY, Chiocca EA, Harden M, Lennon NJ, Gabriel S, Getz G, Lander ES, Regev A, Ritz J, Neuberg D, Rodig SJ, Ligon KL, Suva ML, Wucherpfennig KW, Hacohen N, Fritsch EF, Livak KJ, Ott PA, Wu CJ, et al. Neoantigen vaccine generates intratumoral T cell responses in phase Ib glioblastoma trial. Nature. 2019;565(7738):234-9.

20. Lee JJ, Kook H, Park MS, Nam JH, Choi BH, Song WH, Park KS, Lee IK, Chung IJ, Hwang TJ, Kim HJ. Immunotherapy using autologous monocyte-derived dendritic cells pulsed with leukemic cell lysates for acute myeloid leukemia relapse after autologous peripheral blood stem cell transplantation. J Clin Apher. 2004;19(2):66-70.

21. Fujii S, Shimizu K, Fujimoto K, Kiyokawa T, Tsukamoto A, Sanada I, Kawano F. Treatment of post-transplanted, relapsed patients with hematological malignancies by infusion of HLA-matched, allogeneic-dendritic cells (DCs) pulsed with irradiated tumor cells and primed T cells. Leuk Lymphoma. 2001;42(3):357-69.

22. Kitawaki T, Kadowaki N, Fukunaga K, Kasai Y, Maekawa T, Ohmori K, Itoh T, Shimizu A, Kuzushima K, Kondo T, Ishikawa T, Uchiyama T. Cross-priming of CD8(+) T cells in vivo by dendritic cells pulsed with autologous apoptotic leukemic cells in immunotherapy for elderly patients with acute myeloid leukemia. Exp Hematol. 2011;39(4):424-33 e2.

23. Li L, Giannopoulos K, Reinhardt P, Tabarkiewicz J, Schmitt A, Greiner J, Rolinski J, Hus I, Dmoszynska A, Wiesneth M, Schmitt M. Immunotherapy for patients with acute myeloid leukemia using autologous dendritic cells generated from leukemic blasts. Int J Oncol. 2006;28(4):855-61.

24. Roddie H, Klammer M, Thomas C, Thomson R, Atkinson A, Sproul A, Waterfall M, Samuel K, Yin J, Johnson P, Turner M. Phase I/II study of vaccination with dendritic-like leukaemia cells for the immunotherapy of acute myeloid leukaemia. Br J Haematol. 2006;133(2):152-7.

25. Dong M, Liang D, Li Y, Kong D, Kang P, Li K, Ping C, Zhang Y, Zhou X, Zhang Y, Hong L. Autologous dendritic cells combined with cytokine-induced killer cells synergize low-dose chemotherapy in elderly patients with acute myeloid leukaemia. J Int Med Res. 2012;40(4):1265-74.

26. Rosenblatt J, Stone RM, Uhl L, Neuberg D, Joyce R, Levine JD, Arnason J, McMasters M, Luptakova K, Jain S, Zwicker JI, Hamdan A, Boussiotis V, Steensma DP, DeAngelo DJ, Galinsky I, Dutt PS, Logan E, Bryant MP, Stroopinsky D, Werner L, Palmer K, Coll M, Washington A, Cole L, Kufe D, Avigan D. Individualized vaccination of AML patients in remission is associated with induction of antileukemia immunity and prolonged remissions. Sci Transl Med. 2016;8(368).

27. Huber A, Dammeijer F, Aerts J, Vroman H. Current State of Dendritic Cell-Based Immunotherapy: Opportunities for in vitro Antigen Loading of Different DC Subsets? Front Immunol. 2018;9:2804.

28. Ho VT, Vanneman M, Kim H, Sasada T, Kang YJ, Pasek M, Cutler C, Koreth J, Alyea E, Sarantopoulos S, Antin JH, Ritz J, Canning C, Kutok J, Mihm MC, Dranoff G, Soiffer R. Biologic activity of irradiated, autologous, GM-CSF-secreting leukemia cell vaccines early after allogeneic stem cell transplantation. Proc Natl Acad Sci U S A. 2009;106(37):15825-30.

29. Ho VT, Kim HT, Bavli N, Mihm M, Pozdnyakova O, Piesche M, Daley H, Reynolds C, Souders NC, Cutler C, Koreth J, Alyea EP, Antin JH, Ritz J, Dranoff G, Soiffer RJ. Vaccination with autologous myeloblasts admixed with GM-K562 cells in patients with advanced MDS or AML after allogeneic HSCT. Blood Adv. 2017;1(24):2269-79.

30. van de Loosdrecht AA, van Wetering S, Santegoets S, Singh SK, Eeltink CM, den Hartog Y, Koppes M, Kaspers J, Ossenkoppele GJ, Kruisbeek AM, de Gruijl TD. A novel allogeneic off-the-shelf dendritic cell vaccine for post-remission treatment of elderly patients with acute myeloid leukemia. Cancer Immunol Immunother. 2018;67(10):1505-18.

31. Fang RH, Kroll AV, Gao W, Zhang L. Cell Membrane Coating Nanotechnology. Adv Mater. 2018;30(23):e1706759.

32. Zhou J, Kroll AV, Holay M, Fang RH, Zhang L. Biomimetic Nanotechnology toward Personalized Vaccines. Adv Mater. 2020;32(13):e1901255.

33. Kroll AV, Fang RH, Jiang Y, Zhou J, Wei X, Yu CL, Gao J, Luk BT, Dehaini D, Gao W, Zhang L. Nanoparticulate Delivery of Cancer Cell Membrane Elicits Multiantigenic Antitumor Immunity. Adv Mater. 2017;29(47).

34. Law LW. Characterization of an Influence Affecting Growth of Transplantable Leukemias in Mice. Cancer Res. 1944(4):257-60.

35. Nakajima H, Oka Y, Tsuboi A, Tatsumi N, Yamamoto Y, Fujiki F, Li Z, Murao A, Morimoto S, Hosen N, Shirakata T, Nishida S, Kawase I, Isaka Y, Oji Y, Sugiyama H. Enhanced tumor immunity of WT1 peptide vaccination by interferon-beta administration. Vaccine. 2012;30(4):722-9.

36. Curran E, Chen X, Corrales L, Kline DE, Dubensky TW, Jr., Duttagupta P, Kortylewski M, Kline J. STING Pathway Activation Stimulates Potent Immunity against Acute Myeloid Leukemia. Cell Rep. 2016;15(11):2357-66.

37. Zhang L, Chen X, Liu X, Kline DE, Teague RM, Gajewski TF, Kline J. CD40 ligation reverses T cell tolerance in acute myeloid leukemia. J Clin Invest. 2013;123(5):1999-2010.

38. Karttunen J, Sanderson S, Shastri N. Detection of rare antigen-presenting cells by the lacZ T-cell activation assay suggests an expression cloning strategy for T-cell antigens. Proc Natl Acad Sci U S A. 1992;89(13):6020-4.

39. Iwasaki A, Medzhitov R. Toll-like receptor control of the adaptive immune responses. Nat Immunol. 2004;5(10):987-95.

40. Askew D, Chu RS, Krieg AM, Harding CV. CpG DNA induces maturation of dendritic cells with distinct effects on nascent and recycling MHC-II antigen-processing mechanisms. J Immunol. 2000;165(12):6889-95.

41. Kamala T. Hock immunization: a humane alternative to mouse footpad injections. J Immunol Methods. 2007;328(1-2):204-14.

42. Nahas MR, Rosenblatt J, Lazarus HM, Avigan D. Anti-cancer vaccine therapy for hematologic malignancies: An evolving era. Blood Rev. 2018;32(4):312-25.

43. Osada T, Woo CY, McKinney M, Yang XY, Lei G, LaBreche HG, Hartman ZC, Niedzwiecki D, Chao N, Amalfitano A, Morse MA, Lyerly HK, Clay TM. Induction of Wilms' Tumor Protein (WT1)-Specific Antitumor Immunity Using a Truncated WT1-Expressing Adenovirus Vaccine. Clin Cancer Res. 2009;15(8):2789-96.

44. Gokbuget N, Canaani J, Nagler A, Bishop M, Kroger N, Avigan D. Prevention and treatment of relapse after stem cell transplantation with immunotherapy. Bone Marrow Transplant. 2018;53(6):664-72.

45. Nahas MR, Stroopinsky D, Rosenblatt J, Cole L, Pyzer AR, Anastasiadou E, Sergeeva A, Ephraim A, Washington A, Orr S, McMasters M, Weinstock M, Jain S, Leaf RK, Ghiasuddin H, Rahimian M, Liegel J, Molldrem JJ, Slack F, Kufe D, Avigan D. Hypomethylating agent alters the immune microenvironment in acute myeloid leukaemia (AML) and enhances the immunogenicity of a dendritic cell/AML vaccine. Br J Haematol. 2019;185(4):679-90.

46. Hsu JL, Bryant CE, Papadimitrious MS, Kong B, Gasiorowski RE, Orellana D, McGuire HM, Groth BFS, Joshua DE, Ho PJ, Larsen S, Iland HJ, Gibson J, Clark GJ, Fromm PD, Hart DN. A blood dendritic cell vaccine for acute myeloid leukemia expands anti-tumor T cell responses at remission. Oncoimmunology. 2018;7(4):e1419114.

47. Haroun F, Solola SA, Nassereddine S, Tabbara I. PD-1 signaling and inhibition in AML and MDS. Ann Hematol. 2017;96(9):1441-8.

48. Jia B, Wang L, Claxton DF, Ehmann WC, Rybka WB, Mineishi S, Rizvi S, Shike H, Bayerl M, Schell TD, Hohl RJ, Zheng H. Bone marrow CD8 T cells express high frequency of PD-1 and exhibit reduced anti-leukemia response in newly diagnosed AML patients. Blood Cancer J. 2018;8(3):34.

49. Zhang L, Gajewski TF, Kline J. PD-1/PD-L1 interactions inhibit antitumor immune responses in a murine acute myeloid leukemia model. Blood. 2009;114(8):1545-52.

50. Berlin C, Kowalewski DJ, Schuster H, Mirza N, Walz S, Handel M, Schmid-Horch B, Salih HR, Kanz L, Rammensee HG, Stevanovic S, Stickel JS. Mapping the HLA ligandome landscape of acute myeloid leukemia: a targeted approach toward peptide-based immunotherapy. Leukemia. 2015;29(3):647-59.

51. Moyer TJ, Zmolek AC, Irvine DJ. Beyond antigens and adjuvants: formulating future vaccines. J Clin Invest. 2016;126(3):799-808.

52. Schlosser E, Mueller M, Fischer S, Basta S, Busch DH, Gander B, Groettrup M. TLR ligands and antigen need to be coencapsulated into the same biodegradable

microsphere for the generation of potent cytotoxic T lymphocyte responses. Vaccine. 2008;26(13):1626-37.

53. Heit A, Schmitz F, Haas T, Busch DH, Wagner H. Antigen co-encapsulated with adjuvants efficiently drive protective T cell immunity. Eur J Immunol. 2007;37(8):2063-74.

54. Zhao L, Seth A, Wibowo N, Zhao CX, Mitter N, Yu C, Middelberg AP. Nanoparticle vaccines. Vaccine. 2014;32(3):327-37.

55. Vermaelen K. Vaccine Strategies to Improve Anti-cancer Cellular Immune Responses. Front Immunol. 2019;10:8.

56. Peterson LF, Wang Y, Lo MC, Yan M, Kanbe E, Zhang DE. The multi-functional cellular adhesion molecule CD44 is regulated by the 8;21 chromosomal translocation. Leukemia. 2007;21(9):2010-9.

57. Ehst BD, Ingulli E, Jenkins MK. Development of a novel transgenic mouse for the study of interactions between CD4 and CD8 T cells during graft rejection. Am J Transplant. 2003;3(11):1355-62.

58. Stoner SA, Yan M, Liu KTH, Arimoto KI, Shima T, Wang HY, Johnson DT, Bejar R, Jamieson C, Guan KL, Zhang DE. Hippo kinase loss contributes to del(20q) hematologic malignancies through chronic innate immune activation. Blood. 2019;134(20):1730-44.

59. Pear WS, Miller JP, Xu L, Pui JC, Soffer B, Quackenbush RC, Pendergast AM, Bronson R, Aster JC, Scott ML, Baltimore D. Efficient and rapid induction of a chronic myelogenous leukemia-like myeloproliferative disease in mice receiving P210 bcr/abl-transduced bone marrow. Blood. 1998;92(10):3780-92.

60. Golde WT, Gollobin P, Rodriguez LL. A rapid, simple, and humane method for submandibular bleeding of mice using a lancet. Lab Anim (NY). 2005;34(9):39-43.

61. Dolton G, Tungatt K, Lloyd A, Bianchi V, Theaker SM, Trimby A, Holland CJ, Donia M, Godkin AJ, Cole DK, Straten PT, Peakman M, Svane IM, Sewell AK. More tricks with tetramers: a practical guide to staining T cells with peptide-MHC multimers. Immunology. 2015;146(1):11-22.

62. Byrd JC, Mrozek K, Dodge RK, Carroll AJ, Edwards CG, Arthur DC, Pettenati MJ, Patil SR, Rao KW, Watson MS, Koduru PRK, Moore JO, Stone RM, Mayer RJ, Feldman EJ, Davey FR, Schiffer CA, Larson RA, Bloomfield CD. Pretreatment cytogenetic abnormalities are predictive of induction success, cumulative incidence of relapse, and overall survival in adult patients with de novo acute myeloid leukemia: results from Cancer and Leukemia Group B (CALGB 8461). Blood. 2002;100(13):4325-36.

63. Suvajdzic N, Novkovic A, Djunic I, Virijevic M, Colovic N, Vidovic A, Kraguljac-Kurtovic N, Djordjevic V, Elezovic I, Tomin D. Prognostic Factors and Outcome of Core Binding Factor Acute Myeloid Leukemia Patients. Haematologica. 2012;97:274-5.

64. Bhatt VR, Kantarjian H, Cortes JE, Ravandi F, Borthakur G. Therapy of core binding factor acute myeloid leukemia: incremental improvements toward better long-term results. Clin Lymphoma Myeloma Leuk. 2013;13(2):153-8.

65. Kurosawa S, Miyawaki S, Yamaguchi T, Kanamori H, Sakura T, Moriuchi Y, Sano F, Kobayashi T, Yasumoto A, Hatanaka K, Yanada M, Nawa Y, Takeuchi J, Nakamura Y, Fujisawa S, Shibayama H, Miura I, Fukuda T. Prognosis of patients with core binding factor acute myeloid leukemia after first relapse. Haematologica. 2013;98(10):1525-31.

66. Lam K, Zhang DE. RUNX1 and RUNX1-ETO: roles in hematopoiesis and leukemogenesis. Front Biosci (Landmark Ed). 2012;17:1120-39.

67. Sood R, Kamikubo Y, Liu P. Role of RUNX1 in hematological malignancies. Blood. 2017;129(15):2070-82.

68. Ibanez V, Sharma A, Buonamici S, Verma A, Kalakonda S, Wang JX, Kadkol SH, Sauntharajah Y. AML1-ETO decreases ETO-2 (MTG16) interactions with nuclear receptor corepressor, an effect that impairs granulocyte differentiation. Cancer Res. 2004;64(13):4547-54.

69. Lindberg SR, Olsson A, Persson AM, Olsson I. The Leukemia-associated ETO homologues are differently expressed during hematopoietic differentiation. Exp Hematol. 2005;33(2):189-98.

70. Migasa AA, Mishkova OA, Ramanouskaya TV, Ilyushonak IM, Aleinikova OV, Grinev VV. RUNX1T1/MTG8/ETO gene expression status in human t(8;21)(q22;q22)-positive acute myeloid leukemia cells. Leukemia Res. 2014;38(9):1102-10.

71. Okumura AJ, Peterson LF, Okumura F, Boyapati A, Zhang DE. t(8;21)(q22;q22) Fusion proteins preferentially bind to duplicated AML1/RUNX1 DNA-binding sequences to differentially regulate gene expression. Blood. 2008;112(4):1392-401.

72. Gelmetti V, Zhang J, Fanelli M, Minucci S, Pelicci PG, Lazar MA. Aberrant recruitment of the nuclear receptor corepressor-histone deacetylase complex by the acute myeloid leukemia fusion partner ETO. Mol Cell Biol. 1998;18(12):7185-91.

73. Lutterbach B, Westendorf JJ, Linggi B, Patten A, Moniwa M, Davie JR, Huynh KD, Bardwell VJ, Lavinsky RM, Rosenfeld MG, Glass C, Seto E, Hiebert SW. ETO, a target of t(8;21) in acute leukemia, interacts with the N-CoR and mSin3 corepressors. Mol Cell Biol. 1998;18(12):7176-84.

74. Amann JM, Nip J, Strom DK, Lutterbach B, Harada H, Lenny N, Downing JR, Meyers S, Hiebert SW. ETO, a target of t(8;21) in acute leukemia, makes distinct contacts with multiple histone deacetylases and binds mSin3A through its oligomerization domain. Molecular and Cellular Biology. 2001;21(19):6470-83.

75. Wang L, Gural A, Sun XJ, Zhao XY, Perna F, Huang G, Hatlen MA, Vu L, Liu F, Xu HM, Asai T, Xu H, Deblasio T, Menendez S, Voza F, Jiang YW, Cole PA, Zhang JS,

Melnick A, Roeder RG, Nimer SD. The Leukemogenicity of AML1-ETO Is Dependent on Site-Specific Lysine Acetylation. Science. 2011;333(6043):765-9.

76. Shia WJ, Okumura AJ, Yan M, Sarkeshik A, Lo MC, Matsuura S, Komeno Y, Zhao X, Nimer SD, Yates JR, 3rd, Zhang DE. PRMT1 interacts with AML1-ETO to promote its transcriptional activation and progenitor cell proliferative potential. Blood. 2012;119(21):4953-62.

77. Pabst T, Mueller BU, Harakawa N, Schoch C, Haferlach T, Behre G, Hiddemann W, Zhang DE, Tenen DG. AML1-ETO downregulates the granulocytic differentiation factor C/EBP alpha in t(8;21) myeloid leukemia. Nat Med. 2001;7(4):444-51.

78. Vangala RK, Heiss-Neumann MS, Rangatia JS, Singh SM, Schoch C, Tenen DG, Hiddemann W, Behre G. The myeloid master regulator transcription factor PU.1 is inactivated by AML1-ETO in t(8;21) myeloid leukemia. Blood. 2003;101(1):270-7.

79. Klampfer L, Zhang J, Zelenetz AO, Uchida H, Nimer SD. The AML1/ETO fusion protein activates transcription of BCL-2. P Natl Acad Sci USA. 1996;93(24):14059-64.

80. Zhang JS, Kalkum M, Yamamura S, Chait BT, Roeder RG. E protein silencing by the leukemogenic AML1-ETO fusion protein. Science. 2004;305(5688):1286-9.

81. Ptasinska A, Assi SA, Martinez-Soria N, Imperato MR, Piper J, Cauchy P, Pickin A, James SR, Hoogenkamp M, Williamson D, Wu MC, Tenen DG, Ott S, Westhead DR, Cockerill PN, Heidenreich O, Bonifer C. Identification of a Dynamic Core Transcriptional Network in t(8;21) AML that Regulates Differentiation Block and Self-Renewal. Cell Rep. 2014;8(6):1974-88.

82. DeKelver RC, Lewin B, Lam K, Komeno Y, Yan M, Rundle C, Lo MC, Zhang DE. Cooperation between RUNX1-ETO9a and novel transcriptional partner KLF6 in upregulation of Alox5 in acute myeloid leukemia. PLoS Genet. 2013;9(10):e1003765.

83. Yan M, Kanbe E, Peterson LF, Boyapati A, Miao Y, Wang Y, Chen IM, Chen ZX, Rowley JD, Willman CL, Zhang DE. A previously unidentified alternatively spliced isoform of t(8;21) transcript promotes leukemogenesis. Nat Med. 2006;12(8):945-9.

84. Burel SA, Harakawa N, Zhou LM, Pabst T, Tenen DG, Zhang DE. Dichotomy of AML1-ETO functions: Growth arrest versus block of differentiation. Molecular and Cellular Biology. 2001;21(16):5577-90.

85. Tonks A, Tonks AJ, Pearn L, Pearce L, Hoy T, Couzens S, Fisher J, Burnett AK, Darley RL. Expression of AML1-ETO in human myelomonocytic cells selectively inhibits granulocytic differentiation and promotes their self-renewal. Leukemia. 2004;18(7):1238-45.

86. Yuan YZ, Zhou LM, Miyamoto T, Iwasaki H, Harakawa N, Hetherington CJ, Burel SA, Lagasse E, Weissman IL, Akashi K, Zhang DE. AML1-ETO expression is directly

involved in the development of acute myeloid leukemia in the presence of additional mutations. P Natl Acad Sci USA. 2001;98(18):10398-403.

87. Higuchi M, O'Brien D, Kumaravelu P, Lenny N, Yeoh EJ, Downing JR. Expression of a conditional AML1-ETO oncogene bypasses embryonic lethality and establishes a murine model of human t(8;21) acute myeloid leukemia. Cancer Cell. 2002;1(1):63-74.

88. Heidenreich O, Krauter J, Riehle H, Hadwiger P, John M, Heil G, Vornlocher HP, Nordheim A. AML1/MTG8 oncogene suppression by small interfering RNAs supports myeloid differentiation of t(8;21)-positive leukemic cells. Blood. 2003;101(8):3157-63.

89. Martinez N, Drescher B, Riehle H, Cullmann C, Vornlocher HP, Ganser A, Heil G, Nordheim A, Krauter J, Heidenreich O. The oncogenic fusion protein RUNX1-CBFA2T1 supports proliferation and inhibits senescence in t(8;21)-positive leukaemic cells. BMC Cancer. 2004;4:44.

90. Dunne J, Cullmann C, Ritter M, Soria NM, Drescher B, Debernardi S, Skoulakis S, Hartmann O, Krause M, Krauter J, Neubauer A, Young BD, Heidenreich O. siRNA-mediated AML1/MTG8 depletion affects differentiation and proliferation-associated gene expression in t(8;21)-positive cell lines and primary AML blasts. Oncogene. 2006;25(45):6067-78.

91. Martinez Soria N, Tussiwand R, Ziegler P, Manz MG, Heidenreich O. Transient depletion of RUNX1/RUNX1T1 by RNA interference delays tumour formation in vivo. Leukemia. 2009;23(1):188-90.

92. Ptasinska A, Assi SA, Mannari D, James SR, Williamson D, Dunne J, Hoogenkamp M, Wu M, Care M, McNeill H, Cauchy P, Cullen M, Tooze RM, Tenen DG, Young BD, Cockerill PN, Westhead DR, Heidenreich O, Bonifer C. Depletion of RUNX1/ETO in t(8;21) AML cells leads to genome-wide changes in chromatin structure and transcription factor binding. Leukemia. 2012;26(8):1829-41.

93. Spirin PV, Lebedev TD, Orlova NN, Gornostaeva AS, Prokofjeva MM, Nikitenko NA, Dmitriev SE, Buzdin AA, Borisov NM, Aliper AM, Garazha AV, Rubtsov PM, Stocking C, Prassolov VS. Silencing AML1-ETO gene expression leads to simultaneous activation of both pro-apoptotic and proliferation signaling. Leukemia. 2014;28(11):2222-8.

94. Link KA, Lin S, Shrestha M, Bowman M, Wunderlich M, Bloomfield CD, Huang G, Mulloy JC. Supraphysiologic levels of the AML1-ETO isoform AE9a are essential for transformation. Proc Natl Acad Sci U S A. 2016;113(32):9075-80.

95. Mayr C. Regulation by 3'-Untranslated Regions. Annu Rev Genet. 2017;51:171-94.

96. Hammond SM. An overview of microRNAs. Adv Drug Deliv Rev. 2015;87:3-14.

97. Lin SB, Gregory RI. MicroRNA biogenesis pathways in cancer. Nat Rev Cancer. 2015;15(6):321-33.

98. Rupaimoole R, Slack FJ. MicroRNA therapeutics: towards a new era for the management of cancer and other diseases. Nat Rev Drug Discov. 2017;16(3):203-22.

99. Wallace JA, O'Connell RM. MicroRNAs and acute myeloid leukemia: therapeutic implications and emerging concepts. Blood. 2017;130(11):1290-301.

100. Nishi M, Eguchi-Ishimae M, Wu Z, Gao W, Iwabuki H, Kawakami S, Tauchi H, Inukai T, Sugita K, Hamasaki Y, Ishii E, Eguchi M. Suppression of the let-7b microRNA pathway by DNA hypermethylation in infant acute lymphoblastic leukemia with MLL gene rearrangements. Leukemia. 2013;27(2):389-97.

101. Xu WQ, Huang YM, Xiao HF. [Expression Analysis and Epigenetics of MicroRNA let-7b in Acute Lymphoblastic Leukemia]. Zhongguo Shi Yan Xue Ye Xue Za Zhi. 2015;23(6):1535-41.

102. Balzeau J, Menezes MR, Cao SY, Hagan JP. The LIN28/let-7 Pathway in Cancer. Front Genet. 2017;8:1-16.

103. Chen Y, Jacamo R, Konopleva M, Garzon R, Croce C, Andreeff M. CXCR4 downregulation of let-7a drives chemoresistance in acute myeloid leukemia. J Clin Invest. 2013;123(6):2395-407.

104. Dai CW, Bai QW, Zhang GS, Cao YX, Shen JK, Pei MF, Yin CC. MicroRNA let-7f is down-regulated in patients with refractory acute myeloid leukemia and is involved in chemotherapy resistance of adriamycin-resistant leukemic cells. Leuk Lymphoma. 2014;55(7):1645-8.

105. Huang Y, Hong X, Hu J, Lu Q. Targeted regulation of MiR-98 on E2F1 increases chemosensitivity of leukemia cells K562/A02. Onco Targets Ther. 2017;10:3233-9.

106. Zhou H, Li Y, Liu B, Shan Y, Li Y, Zhao L, Su Z, Jia L. Downregulation of miR-224 and let-7i contribute to cell survival and chemoresistance in chronic myeloid leukemia cells by regulating ST3GAL IV expression. Gene. 2017;626:106-18.

107. Cao YX, Wen F, Luo ZY, Long XX, Luo C, Liao P, Li JJ. Downregulation of microRNA let-7f mediated the Adriamycin resistance in leukemia cell line. J Cell Biochem. 2019.

108. Pelosi A, Careccia S, Lulli V, Romania P, Marziali G, Testa U, Lavorgna S, Lo-Coco F, Petti MC, Calabretta B, Levrero M, Piaggio G, Rizzo MG. miRNA let-7c promotes granulocytic differentiation in acute myeloid leukemia. Oncogene. 2013;32(31):3648-54.

109. Wright C, Shin JH, Rajpurohit A, Deep-Soboslay A, Collado-Torres L, Brandon NJ, Hyde TM, Kleinman JE, Jaffe AE, Cross AJ, Weinberger DR. Altered expression of histamine signaling genes in autism spectrum disorder. Transl Psychiat. 2017;7.

110. Hutvagner G, McLachlan J, Pasquinelli AE, Balint E, Tuschl T, Zamore PD. A cellular function for the RNA-interference enzyme Dicer in the maturation of the let-7 small temporal RNA. Science. 2001;293(5531):834-8.

111. Li YH, Gao L, Luo XF, Wang LL, Gao XN, Wang W, Sun JZ, Dou LP, Li JX, Xu CW, Wang LX, Zhou MH, Jiang MM, Zhou JH, Caligiuri MA, Nervi C, Bloomfield CD, Marcucci G, Yu L. Epigenetic silencing of microRNA-193a contributes to leukemogenesis in t(8;21) acute myeloid leukemia by activating the PTEN/PI3K signal pathway. Blood. 2013;121(3):499-509.

112. Fu L, Shi J, Liu A, Zhou L, Jiang M, Fu H, Xu K, Li D, Deng A, Zhang Q, Pang Y, Guo Y, Hu K, Zhou J, Wang Y, Huang W, Jing Y, Dou L, Wang L, Xu K, Ke X, Nervi C, Li Y, Yu L. A minicircuitry of microRNA-9-1 and RUNX1-RUNX1T1 contributes to leukemogenesis in t(8;21) acute myeloid leukemia. Int J Cancer. 2017;140(3):653-61.

113. Zaidi SK, Perez AW, White ES, Lian JB, Stein JL, Stein GS. An AML1-ETO/miR-29b-1 regulatory circuit modulates phenotypic properties of acute myeloid leukemia cells. Oncotarget. 2017;8(25):39994-40005.

114. Agarwal V, Bell GW, Nam JW, Bartel DP. Predicting effective microRNA target sites in mammalian mRNAs. Elife. 2015;4.

115. Ley TJ, Miller C, Ding L, Raphael BJ, Mungall AJ, Robertson AG, Hoadley K, Triche TJ, Laird PW, Baty JD, Fulton LL, Fulton R, Heath SE, Kalicki-Veizer J, Kandoth C, Klco JM, Koboldt DC, Kanchi KL, Kulkarni S, Lamprecht TL, Larson DE, Lin L, Lu C, McLellan MD, McMichael JF, Payton J, Schmidt H, Spencer DH, Tomasson MH, Wallis JW, Wartman LD, Watson MA, Welch J, Wendl MC, Ally A, Balasundaram M, Birol I, Butterfield Y, Chiu R, Chu A, Chuah E, Chun HJ, Corbett R, Dhalla N, Guin R, He A, Hirst C, Hirst M, Holt RA, Jones S, et al. Genomic and Epigenomic Landscapes of Adult De Novo Acute Myeloid Leukemia. New Engl J Med. 2013;368(22):2059-74.

116. Kumar MS, Erkeland SJ, Pester RE, Chen CY, Ebert MS, Sharp PA, Jacks T. Suppression of non-small cell lung tumor development by the let-7 microRNA family. Proc Natl Acad Sci U S A. 2008;105(10):3903-8.

117. Ebert MS, Neilson JR, Sharp PA. MicroRNA sponges: competitive inhibitors of small RNAs in mammalian cells. Nat Methods. 2007;4(9):721-6.

118. Stoner SA, Liu KTH, Andrews ET, Liu MD, Arimoto KI, Yan M, Davis AG, Weng S, Dow M, Xian S, DeKelver RC, Carter H, Zhang DE. The RUNX1-ETO target gene RASSF2 suppresses t(8;21) AML development and regulates Rac GTPase signaling. Blood Cancer Journal. 2020;10(2).

119. Johnson CD, Esquela-Kerscher A, Stefani G, Byrom N, Kelnar K, Ovcharenko D, Wilson M, Wang XW, Shelton J, Shingara J, Chin L, Brown D, Slack FJ. The let-7 MicroRNA represses cell proliferation pathways in human cells. Cancer Res. 2007;67(16):7713-22.

120. Schultz J, Lorenz P, Gross G, Ibrahim S, Kunz M. MicroRNA let-7b targets important cell cycle molecules in malignant melanoma cells and interferes with anchorage-independent growth. Cell Research. 2008;18(5):549-57.

121. Schmitter D, Filkowski J, Sewer A, Pillai RS, Oakeley EJ, Zavolan M, Svoboda P, Filipowicz W. Effects of Dicer and Argonaute down-regulation on mRNA levels in human HEK293 cells. Nucleic Acids Res. 2006;34(17):4801-15.

122. Suarez Y, Fernandez-Hernando C, Pober JS, Sessa WC. Dicer dependent microRNAs regulate gene expression and functions in human endothelial cells. Circ Res. 2007;100(8):1164-73.

123. Sampson VB, Rong NH, Han J, Yang QY, Aris V, Soteropoulos P, Petrelli NJ, Dunn SP, Krueger LJ. MicroRNA let-7a down-regulates MYC and reverts MYC-induced growth in Burkitt lymphoma cells. Cancer Res. 2007;67(20):9762-70.

124. Johnson SM, Grosshans H, Shingara J, Byrom M, Jarvis R, Cheng A, Labourier E, Reinert KL, Brown D, Slack FJ. RAS is regulated by the let-7 MicroRNA family. Cell. 2005;120(5):635-47.

125. Lee YS, Dutta A. The tumor suppressor microRNA let-7 represses the HMGA2 oncogene. Gene Dev. 2007;21(9):1025-30.

126. Roos M, Pradere U, Ngondo RP, Behera A, Allegrini S, Civenni G, Zagalak JA, Marchand JR, Menzi M, Towbin H, Scheuermann J, Neri D, Caflisch A, Catapano CV, Ciaudo C, Hall J. A Small-Molecule Inhibitor of Lin28. Acs Chem Biol. 2016;11(10):2773-81.

127. Lim D, Byun WG, Park SB. Restoring Let-7 microRNA Biogenesis Using a Small-Molecule Inhibitor of the Protein-RNA Interaction. Acs Med Chem Lett. 2018;9(12):1181-5.

128. Wang LF, Rowe RG, Jaimes A, Yu CX, Nam Y, Pearson DS, Zhang J, Xie XY, Marion W, Heffron GJ, Daley GQ, Sliz P. Small-Molecule Inhibitors Disrupt let-7 Oligouridylation and Release the Selective Blockade of let-7 Processing by LIN28. Cell Rep. 2018;23(10):3091-101.

129. Lin SB, Gregory RI. Identification of small molecule inhibitors of Zcchc11 TUTase activity. Rna Biol. 2015;12(8):792-800.

130. Yu CX, Wang LF, Rowe RG, Han A, Ji WY, McMahon C, Baier AS, Huang YC, Marion W, Pearson DS, Kruse AC, Daley GQ, Wu H, Sliz P. A nanobody targeting the LIN28:let-7 interaction fragment of TUT4 blocks uridylation of let-7. P Natl Acad Sci USA. 2020;117(9):4653-63.

131. Zipeto MA, Court AC, Sadarangani A, Delos Santos NP, Balaian L, Chun HJ, Pineda G, Morris SR, Mason CN, Geron I, Barrett C, Goff DJ, Wall R, Pellecchia M, Minden M, Frazer KA, Marra MA, Crews LA, Jiang QF, Jamieson CHM. ADAR1 Activation

Drives Leukemia Stem Cell Self-Renewal by Impairing Let-7 Biogenesis. Cell Stem Cell. 2016;19(2):177-91.

132. Kim D, Langmead B, Salzberg SL. HISAT: a fast spliced aligner with low memory requirements. Nat Methods. 2015;12(4):357-60.

133. Matozaki S, Nakagawa T, Kawaguchi R, Aozaki R, Tsutsumi M, Murayama T, Koizumi T, Nishimura R, Isobe T, Chihara K. Establishment of a myeloid leukaemic cell line (SKNO-1) from a patient with t(8;21) who acquired monosomy 17 during disease progression. Br J Haematol. 1995;89(4):805-11.

134. Johnson DT, Davis AG, Zhou JH, Ball ED, Zhang DE. MicroRNA let-7b downregulates AML1-ETO oncogene expression in t(8;21) AML by targeting its 3'UTR. Exp Hematol Oncol. 2021;10(1):8.

135. Roboz GJ. Current treatment of acute myeloid leukemia. Curr Opin Oncol. 2012;24(6):711-9.

136. Blank CU, Haining WN, Held W, Hogan PG, Kallies A, Lugli E, Lynn RC, Philip M, Rao A, Restifo NP, Schietinger A, Schumacher TN, Schwartzberg PL, Sharpe AH, Speiser DE, Wherry EJ, Youngblood BA, Zehn D. Defining 'T cell exhaustion'. Nat Rev Immunol. 2019;19(11):665-74.

137. Curran MA, Glisson BS. New Hope for Therapeutic Cancer Vaccines in the Era of Immune Checkpoint Modulation. Annu Rev Med. 2019;70:409-24.

138. Torrisani J, Bournet B, du Rieu MC, Bouisson M, Souque A, Escourrou J, Buscail L, Cordelier P. let-7 MicroRNA Transfer in Pancreatic Cancer-Derived Cells Inhibits In Vitro Cell Proliferation but Fails to Alter Tumor Progression. Hum Gene Ther. 2009;20(8):831-44.

139. Esquela-Kerscher A, Trang P, Wiggins JF, Patrawala L, Cheng AG, Ford L, Weidhaas JB, Brown D, Bader AG, Slack FJ. The let-7 microRNA reduces tumor growth in mouse models of lung cancer. Cell Cycle. 2008;7(6):759-64.

140. Akao Y, Nakagawa Y, Naoe T. let-7 microRNA functions as a potential growth suppressor in human colon cancer cells. Biol Pharm Bull. 2006;29(5):903-6.

141. Aslan D, Garde C, Nygaard MK, Helbo AS, Dimopoulos K, Hansen JW, Severinsen MT, Treppendahl MB, Sjo LD, Gronbaek K, Kristensen LS. Tumor suppressor microRNAs are downregulated in myelodysplastic syndrome with spliceosome mutations. Oncotarget. 2016;7(9):9951-63.

142. Yang HW, Huang CY, Chih-Wen L, Liu HL, Huang CW, Liao SS, Chen PY, Lu YJ, Wei KC, Ma CCM. Gadolinium-functionalized nanographene oxide for combined drug and microRNA delivery and magnetic resonance imaging. Biomaterials. 2014;35(24):6534-42.

143. Dai X, Fan W, Wang YZ, Huang LJ, Jiang Y, Shi L, Mckinley D, Tan W, Tan C. Combined Delivery of Let-7b MicroRNA and Paclitaxel via Biodegradable Nanoassemblies for the Treatment of KRAS Mutant Cancer. Mol Pharmaceut. 2016;13(2):520-33.

144. Esposito CL, Cerchia L, Catuogno S, De Vita G, Dassie JP, Santamaria G, Swiderski P, Condorelli G, Giangrande PH, de Franciscis V. Multifunctional Aptamer-miRNA Conjugates for Targeted Cancer Therapy. Mol Ther. 2014;22(6):1151-63.